High Temperature Superconducting Thin Films:
Sputter Deposition and Fast Optical Switching

by

Paul H. Ballentine

Curriculum Vitae

The author was born in Ellenville, New York, on October 3, 1957. He received a
B.A. in Physics at Siena College, Loudonville, New York in 1979, and went on to
obtain a M.S. in Mechanical Engineering at the Massachusetts Institute of Technology
in 1982. From 1982 to 1986 he worked as a research engineer for Carrier Corporation
in Syracuse, New York. He came to the University of Rochester in the fall of 1986 and
began graduate studies in Electrical Engineering. He was a graduate teaching assistant
in 1986-87, a Link Foundation Fellow in 1987-88, and a Laser Lab Fellow in 1988-89.
He received his M.S. in Electrical Engineering from the University of Rochester in
1987, and began research in high-temperature superconducting films under the
direction of Professor Alan Kadin. In 1990 he began working full-time at CVC
Products, Inc. of Rochester, becoming Vice President for Research and Development in
1991. He has completed his Ph.D. thesis at UR part-time. He and his wife Andrea are
the parents of three sons.

Acknowledgments

First, I would like to express my thanks to the many people at UR who made this thesis possible. In particular, I owe a major debt of gratitude to Professor Alan Kadin, who introduced me to the science and technology of thin film deposition, which has led directly to my career as a technical manager with CVC Products, Inc. Without Dr. Kadin's wide-ranging knowledge and stubborn determination, I never would have completed this thesis. I would also like to thank many others at UR who assisted me in various stages of my graduate work, including Dr. William Donaldson, Professor Mark Bocko, Dr. Roman Sobolewski, and my fellow graduate students Derek Mallory, Michael Fisher, and Noshir Dubash. In addition, I would also like to thank the three EE Department Chairmen who never gave up hope that I would eventually finish my Ph.D.: Professors Sidney Shapiro, Edwin Kinnen, and Kevin Parker.

Second, I would like to thank my present and former colleagues at CVC Products for their assistance with what was from a beginning a collaborative university-industry venture. These include Christine Whitman, now President of CVC, who initiated the collaboration, together with James Argana and Robert Rath, as well as others who assisted in later stages, including Kelly Truman, John Allen, Loretta Fendrock, and Patrick Borrelli.

Third, financial assistance is always appreciated, and came from a wide variety of sources in my time as a graduate student. These include the University of Rochester, CVC Products, Inc., the Link Foundation, the Laser Fusion Feasibility Project at UR, the National Science Foundation, the New York State Institute on Superconductivity, DARPA, and NASA Jet Propulsion Lab.

Finally, I would like to acknowledge my wife, Andrea, and our three wonderful children, Alex, Peter, and Andrew. Their continuing love and support helped me to withstand the combined pressures of job and school over so many years, and ultimately to complete this thesis.

Abstract

A sputtering process for the *in-situ* deposition of high temperature superconducting $YBa_2Cu_3O_7$ (YBCO) thin films with uniformly good properties over several square inches was developed. These films along with others deposited by electron-beam evaporation were used to study the electrical response of YBCO to pulsed laser irradiation. The possibility of using high T_c thin films as the active element in an optically triggered fast opening switch was investigated.

RF magnetron sputtering from a single 8-inch diameter oxide target was used to deposit the films. By heating the substrates to 700-800 °C during deposition and by adding oxygen to the sputter gas, highly oriented superconducting thin films were formed *in-situ* without the need for a high temperature post deposition anneal. Special precautions were taken to avoid resputtering by negative ions and thus produce films having the desired composition and structure. Films on a variety of substrates, including yttria-stabilized ZrO_2 (YSZ), MgO, $LaAlO_3$, and $SrTiO_3$, had T_cs up to 90 K and critical currents above 10^6 A/cm^2 at 77 K. Scanning electron microscopy, energy dispersive x-ray analysis, and x-ray diffraction were used to study the surface morphology, composition, and crystal structure respectively. The deposition process and equipment developed in this work are described in detail.

The optoelectronic response of the sputter deposited films as well as some co-evaporated films was investigated with a 150 psec pulsed YAG laser. The temperature, bias current, and laser fluence were varied and the signal voltage rise time, amplitude, and fall time were recorded in order to determine whether the response was due to heating (i.e., bolometric) or if there was a direct, non-thermal component present. The magnitude and decay time of the signal were consistent with a bolometric response. Fast (1 nsec) switching from the superconducting to the normal state of current densities up to 10^6 A/cm^2 could be obtained in optically thin films and for thicker films

biased close to the critical current. At temperatures below about 20 K a fast rise time could also be observed for optically thick films biased well below the critical current, indicating non-equilibrium energy transport from the surface to the bottom of the film. The prospects for switching large currents in thick films for pulsed power applications is discussed.

Table of Contents

List of Tables

List of Figures

Chapter 1

Introduction

The discovery by Bednorz and Mueller in 1986 of high temperature superconductors (HTS) based on copper oxides[1] initiated a tremendous amount of research into the nature and potential applications of these novel materials. The subsequent discovery by Chu and co-workers[2] of the HTS compound $YBa_2Cu_3O_7$ (YBCO), with a critical temperature $T_c = 93$ K, created the possibility of superconducting devices that operate at or above the boiling point of liquid nitrogen (77 K). Attempts to fabricate bulk structures such as wire for large scale applications have suffered from the ceramic nature and anisotropic electrical properties of high temperature superconducting (HST) materials. On the other hand, much more progress has been made over the past six years in the area of thin film fabrication for electronic applications. High quality films of $YBa_2Cu_3O_{7-x}$ (YBCO) have been made with zero resistance temperatures above 90 K and critical current densities above 10^6 A/cm^2 at 77 K. Microwave surface resistance well below that of copper has been achieved in HTS thin films.[3]

With these properties the high T_c materials are good candidates for a number of applications, including high-speed digital interconnects and passive microwave devices. In addition, these materials exhibit some unique optical properties for a conductor (i.e. they are strongly absorbing) and are thus potentially useful in optoelectronic applications. In the remainder of this chapter, some background information on HTS materials is given and potential applications are discussed.

1.1 HTS Properties

In order to understand the requirements for thin film fabrication, and to assess the potential for applications of HTS, it is useful to review some of the basic properties of these unique and interesting materials. While a complete understanding of the mechanism for high temperature superconductivity remains to be established, much has been learned of the electrical and material properties. The superconducting copper oxides are based on a class of materials known as perovskites which have a general chemical formula ABO_3.[4] Perovskites are interesting in their own right, and are known to exhibit such diverse behavior as dielectric, ferroelectric, piezoelectric and electro-optic, as well as superconductive properties.

There are five main families of HTS copper oxide compounds; La-Sr-Cu-O, Y-Ba-Cu-O, Bi-Sr-Ca-Cu-O, Tl-Ba-Ca-Cu-O, and very recently, Hg-Ba-Ca-Cu-O. Table 1.1 lists the critical temperatures for some members of these families, and compares them to some other high-temperature superconductors. While this thesis deals with the $YBa_2Cu_3O_7$ compound, some of the more general findings will apply to the other copper-oxide materials as well. There are also several known families of superconducting oxides which do not contain Cu; in fact the first superconducting perovskite, $BaPb_{0.7}Bi_{0.3}O_3$, was discovered in 1972.[5] However, most of the current research is now focused on the copper-oxide-based materials.

The most important properties from an applications point of view are the high critical parameters, with T_c as high as 123 K for the 2223 phase of the Tl-Ba-Ca-Cu-O material, and up to 133 K for the Hg compound. Single crystal c-axis oriented thin films of YBCO have been produced with J_c as high as 10^7 A/cm^2 at 77 K and upper critical magnetic field H_{c2} as high as 30 T. On the other hand, the normal state resistivity is fairly high, on the order of 300 $\mu\Omega$-cm for YBCO in the a-b planes. This

property is related to the low carrier density, on the order of $5 \times 10^{21}/cm^3$.

Table 1.1 Critical temperatures for copper-based high T_c oxide superconductors (From Ref. 6) and other HTS materials.

Material	T_c(K)
$(La\text{-}Sr)_2CuO_4$	40
$YBa_2Cu_3O_7$	93
$Bi_2Sr_2CuO_6$	12
$Bi_2Sr_2CaCu_2O_8$	90
$Bi_2Sr_2Ca_2Cu_3O_{10}$	110
$Tl_2Ba_2CuO_6$	90
$Tl_2Ba_2CaCu_2O_8$	110
$Tl_2Ba_2Ca_2Cu_3O_{10}$	122
$HgBa_2CaCu_2O_6$	117
$HgBa_2Ca_2Cu_3O_8$	133
$Ba_{0.6}K_{0.4}BiO_3$	30
$Cs_2Rb_1C_{60}$	33

The periodicity of flux quantization in the HTS materials is $\Phi_0 = h/2e$, indicating the formation of Cooper pairs as in conventional superconducting materials. In the normal state, the materials appear to be p-type and it is believed that the superconducting phenomena are associated with transport of hole pairs. The HTS materials are type-II superconductors. The coherence length ξ is extremely short and is anisotropic, on the order of 20 Å in the a-b directions (i.e., in the CuO planes) and a mere 3-5 Å along the c-axis. This property has profound ramifications for practical applications, as we discuss below. The magnetic penetration depth λ for YBCO is approximately 2000 Å at low T. There is as yet no widely accepted value for the energy gap, although it too is believed to be anisotropic. Measurements of the gap by the usual tunneling method are made difficult by the poor surface quality of most materials. The most widely accepted values for the 2Δ of YBCO fall around 24 meV,[7] or about $5kT_c$ which is near the BCS value of $3.52\,kT_c$.

The high T_c superconductors are multi-component materials and practical applications require thin films to be deposited with uniform atomic composition across the entire substrate. This is perhaps the most important aspect of our present work. Figure 1.1 shows the phase diagram for the Y_2O_3 - BaO - CuO system. The thermodynamically stable phases are points on the Y-Ba-Cu plane and are thus referred to as point compounds. To be more precise, the superconducting phase is a line compound along the oxygen content (out of the page in Fig. 1.1). There is only one phase, $YBa_2Cu_3O_7$, that is superconducting.

Slight shifts in metallic composition must be accomodated by the formation of secondary (non-superconducting) phases, the amount of which depends on both overall composition and the composition of the secondary phases that are formed. For example, consider a film having the average composition 17% Y, 37% Ba, and 46%

Cu, slightly Ba-rich (and Cu-poor) compared to the ideal 1-2-3 stoichiometry. If the competing phase had composition $YBa_3Cu_2O_6$, then about 22% of the film (on an atomic basis) would be in a secondary phase. However, if the only other oxides to form were Y_2O_3 and BaO, then only about 8% of the atoms would form secondary phases. Off-stoichiometric material may also get pushed to grain boundaries which form weak links with greatly depressed critical currents. Our work, as described in Chapter 3, indicates it is better to be slightly Cu-rich or Y-rich than Ba-rich.
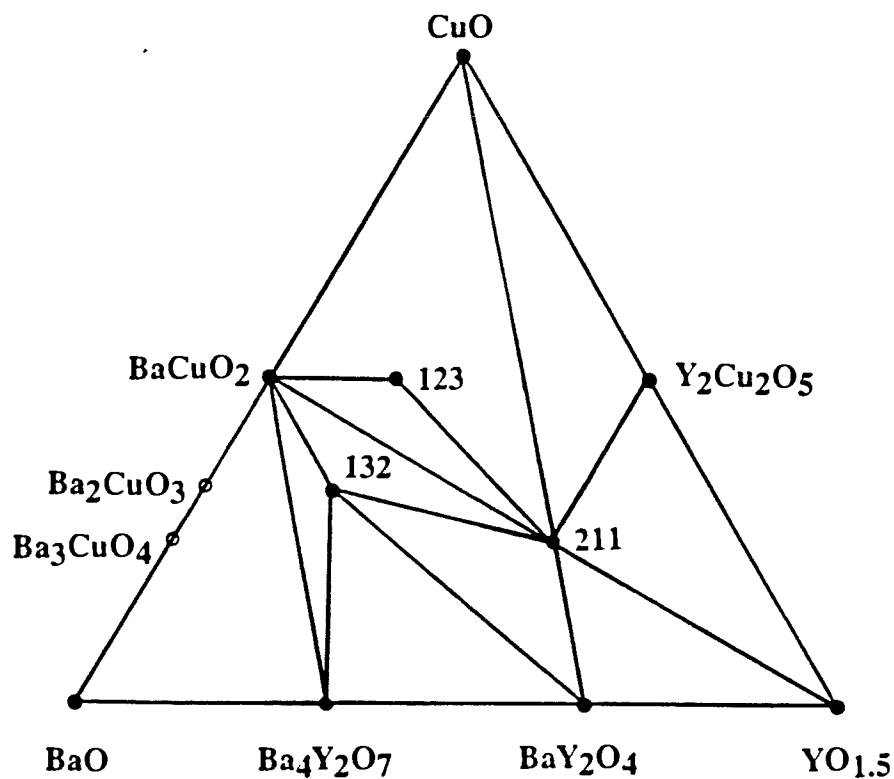
Fig. 1.1. Phase diagram of the Y_2O_3 - BaO - CuO system. (From Ref. 8)

The structural and electrical properties of HTS materials are highly anisotropic. The crystalline structures for the three most popular high T_c superconducting oxides are shown in Fig. 1.2. A common feature of these materials is the presence of one or more Cu-O planes separated by a layer of rare-earth atoms. It is customary to identify the a and b crystalline directions as falling in the CuO planes and the c-axis perpendicular to the planes. It is now fairly well established that the superconducting phenomena occurs in the Cu-O planes. As can be seen from Table 1.1, a general trend is the greater the number of CuO planes per unit cell, the higher the T_c. For example, the highest T_c of 123 K for the Tl-based superconductors found in the 2223 (3-layer) phase. This crystalline anistropy results in a highly anisotropic critical current. For single crystal YBCO at 77 K, $J_c \approx 10^7$ A/cm^2 in the a-b planes and only 5 x 10^5

A/cm^2 along the c-axis. The anisotropy, along with the short coherence length and the tendency to form off-stoichiometric material at grain boundaries, has profound effects on applications and places stringent requirements on materials processing. For many microelectronic applications, including passive microwave devices and high speed interconnects, the current flow is in the plane of the substrate. In Chapter 2 we discuss methods for obtaining c-axis oriented HTS films.

The oxygen content is also known to strongly affect the superconducting properties of YBCO. Above a temperature of approximately 600 °C, the thermodynamically stable composition is $YBa_2Cu_3O_6$. This material is a semiconductor with a tetragonal crystal structure (a=b≠c) and a room temperature resistivity above 10 mΩ-cm. As the material is cooled in the presence of oxygen, a tetragonal-to-orthorhombic transition occurs between 600 and 400 °C. Below about 400 °C the composition is $YBa_2Cu_3O_7$ with the extra oxygen providing the hole for conductivity (and superconductivity). A plot of the equilibrium oxygen content versus temperature for $YBa_2Cu_3O_y$ is shown in Fig. 1.3.

(a)

(b)

(c)
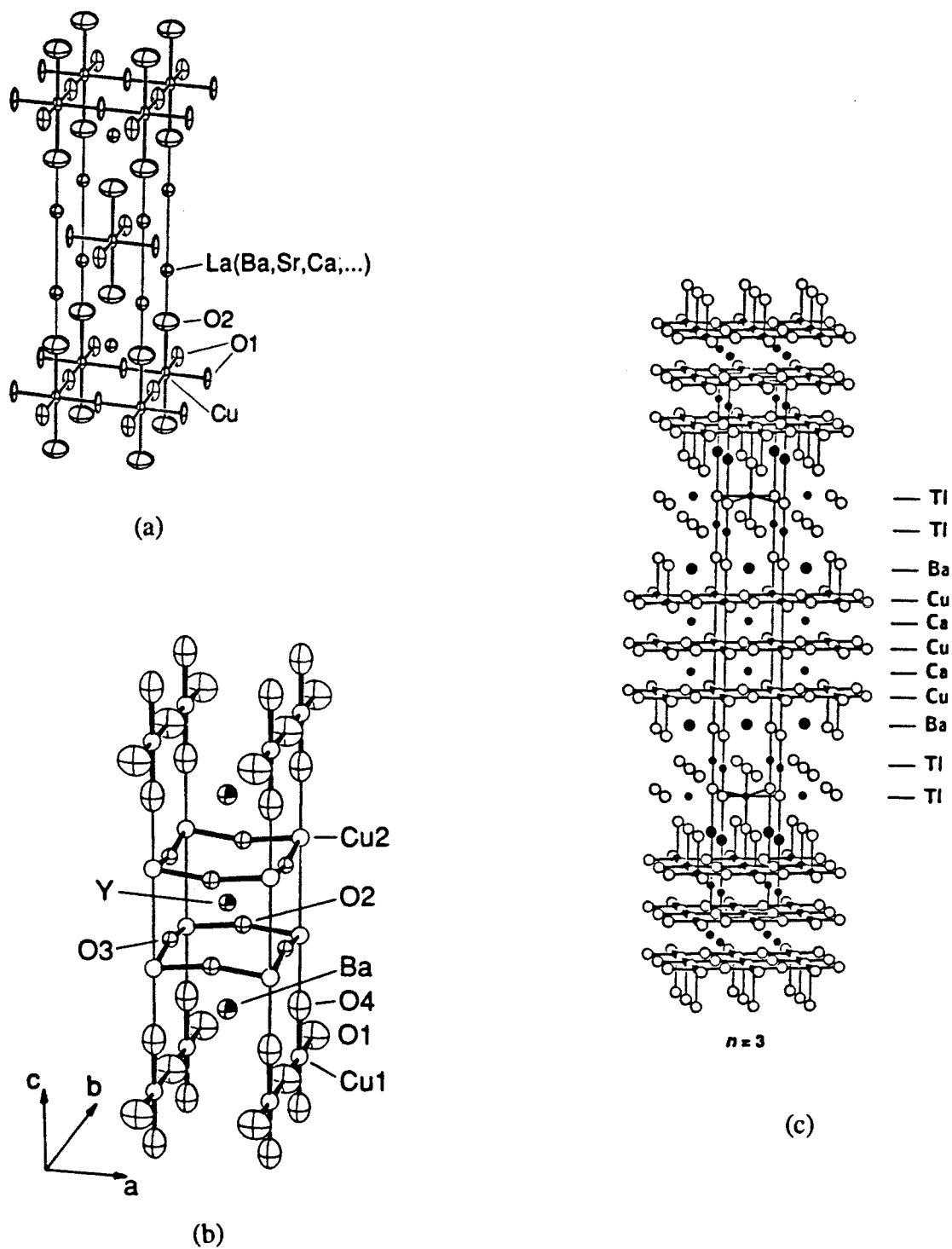
Figure 1.2. Crystal structure for (a) $(La\text{-}Sr)_2Cu_2O_4$, (b) $YBa_2Cu_3O_7$, and (c) $Tl_2Ba_2Ca_2Cu_3O_{10}$ (from Ref. 9).
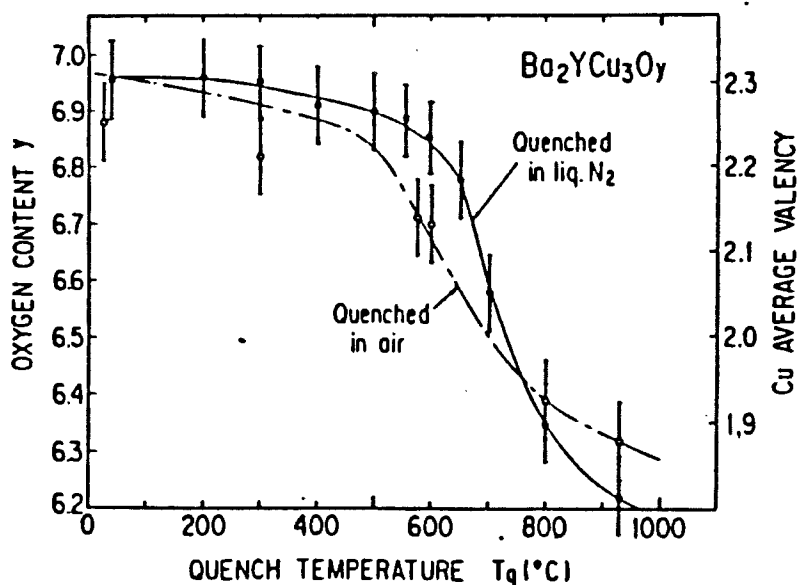
Fig. 1.3. Oxygen content versus quench temperature for $YBa_2Cu_3O_y$ (From Ref. 10).

Accompanying this transition are changes in the lattice constants, resistivity, and T_c.[11] Fig. 1.4 is a plot of the a, b, and c-axis lattice parameters as a function of oxygen content for $YBa_2Cu_3O_y$. Note in particular the contraction of the c-axis as y is increased from 6.3 to 7. Figure 1.5 shows the variation in T_c and room temperature resistivity with oxygen content. As can be seen in the figure, there is a range in oxygen content around 6.7 for which the resistivity is a local minimum and the T_c is fairly constant at 60 K. This is thought to be associated with a second superconducting phase of YBCO which is sometimes referred to as orthorhombic-II.

In addition to the unique electrical and material properties, HTS materials have some interesting optical properties as well. While most good conductors reflect incident radiation, the high T_c superconductors are strongy absorbing at near-infrared and visible wavelenths (i.e., they are black!). The low reflection coefficient is a result of the low carrier density while the absorption is thought to be due to interband

transitions.[12]   For optical wavelengths less than about 1 μm, most of the incident

radiation on a YBCO film is absorbed in a distance of order 1000Å, comparable to the

film thickness.
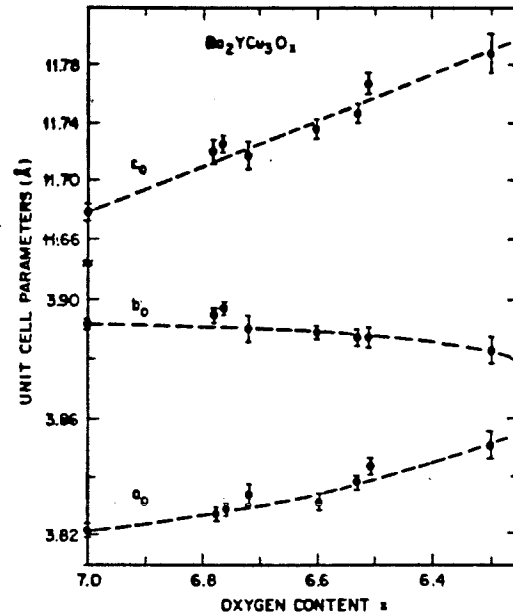
Fig. 1.4. Relation between oxygen content and lattice parameters of $YBa_2Cu_3O_x$ (From Ref. 11).
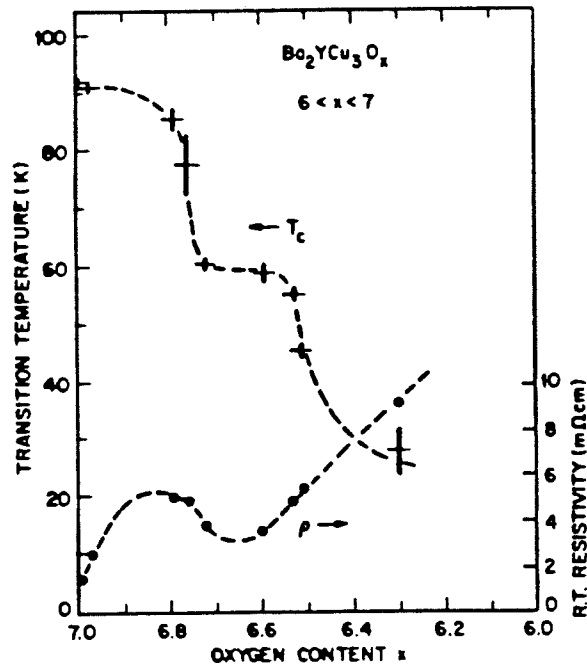
Fig. 1.5. Relation between oxygen content, resistivity, and T_c for $YBa_2Cu_3O_x$ (from Ref. 11).

1.2 Potential Applications

Applications for HTS materials are usually classified as either large-scale or small-scale. Large scale applications include power transmission, high-field magnets, and motor windings. These applications require the superconductor to be formed into a wire or cable, a difficult task with these materials. Small-scale applications, of which this thesis is concerned, include sensors, high speed interconnects, passive microwave devices, and digital devices. These applications require thin films and are more likely to be achieved in the next several years. Most of the small-scale or microelectronic applications require high quality films with c-axis orientation, high T_cs and J_cs, and low noise. Passive microwave devices, which are likely to be among the first practical applications, require films with low surface resistance. These electrical requirements are satisfied by only the highest quality films. Even with high-quality films, direct substitution of high T_c materials in electronic applications that have evolved for conventional superconductors is not a straightforward matter. For example, the short coherence length and poor interfacial properties of these materials make fabrication of Josephson tunnel junctions a formidable task.

One area of promising new applications for HTSC is in optoelectronics. The inherent high speed capability of superconducting devices coupled with the unique optical properties of the new high T_c materials make several applications appear possible. Examples include sensitive detectors of far infrared radiation ($\lambda > 20$ μm), fast photodetectors for integrated optical electronic circuits, and optically triggered fast opening switches for pulsed power sources. Development of these applications requires an understanding of the nature of the interaction between light and the superconducting materials.

In order to further explore the nature of the photoresponse of high T_c

superconductors and to evaluate the potential use of high T_c thin films for fast opening switches, we initiated a series of experiments at the University of Rochester's Laboratory for Laser Energetics. Using a pulsed YAG laser with 100 psec pulses, we measured the transient photoresponse of a current-biased strip of superconducting $YBa_2Cu_3O_{7-x}$ thin film. Our results[13] show that while the energy is deposited into the film in a nonequilibrium manner, the voltage across the sample corresponds to simple heating. This result has potential significance for the optical switching of higher currents in thicker (>1 μm) films for pulsed power applications.

This thesis has two parts, reflecting the two major thrusts of the research. In the first, a sputtering process for the deposition YBCO thin films was developed. This portion was done in close collaboration with CVC Products, Inc. of Rochester, NY, a manufacturer of sputtering equipment. The goal was to deposit films with uniformly good properties, in particular high T_c and J_c, smooth surfaces, and low microwave losses, over several square inches. These films have been used in this and other research efforts aimed at understanding the basics of HTS superconductors and exploring applications. Extensive material and electrical characterization of these films have been carried out, and the results have been correlated to deposition conditions to optimize the process. The focus has been on an *in-situ* process that would not require the use of a high temperature post-deposition anneal.

In the second part of this thesis, these films (as well as some others that were deposited by co-evaporation) were used to study the nature of the electrical response to pulsed laser irradiation. One main objective was to determine whether the response was purely thermal, or if there was a nonequilibrium component to the response, as has been claimed in the literature. In addition, the possible application of high T_c films as the active element in a laser-activated fast opening switch is discussed.

Chapter 2 is a survey of HTS thin film fabrication techniques. Chapter 3 describes the sputter deposition process developed by CVC Products and UR and gives the results of film characterization. Chapter 4 describes the optoelectronic switching experiments and presents our findings on the nature of the optical response. The final chapter summarizes this work and offers some prospects for future development of HTS materials and devices. Appendix A lists the technical publications that came out of this thesis research.

Chapter 2
Overview of HTS Thin Film Deposition

Based on the discussion of high T_c materials in the preceding chapter, it is evident that the production of thin films with high critical currents and temperatures requires excellent control over composition and crystalline structure. In addition, applications will require that these properties be maintained uniformly over several square inches. Furthermore the substrate must be compatible with these applications. In this chapter we discuss the general aspects of high T_c thin film growth and review the various deposition techniques being developed.

2.1 Key Issues

Control of composition is perhaps the most challenging aspect of high T_c thin film growth. As discussed in Chapter 1, composition can strongly effect superconducting properties. Most of the commonly used deposition techniques were developed for single component or at most two-component materials like Si, GaAs, SiO_2, and Al. While it is a relatively straightforward matter to mix desired amounts of materials for bulk preparations, it is not so easy to fabricate a thin film with the desired composition uniformly across a substrate of several inches in diameter. The process of transferring atoms from a source or group of sources to a substrate does not necessarily occur with a well defined rate for each constituent species. In Section 2.2 we describe each of the common HTS film deposition techniques and how they achieve compositional control.

Formation of the proper crystal structure is another key issue that must be addressed in any thin film process. Bulk fabrication of these ceramic materials requires temperatures on the order of 850 to 1000 °C. These temperatures are incompatible with many applications and, in the case of YBCO, cause severe reactions between the film and such common substrates as Si and Al_2O_3.

There have been two routes used to form crystalline high T_c thin films. The easiest route, and the one first used, is to deposit onto unheated substrates, with temperatures generally remaining below 300 °C (some heating does occur due to the deposition process itself). These films are amorphous and have to be crystallized by a post deposition anneal at 850 to 900 °C. For YBCO the anneals are done in oxygen while for the Bi- and Tl-based materials, anneals can be in air. Alternatively, crystallization can be done during deposition by heating substrates above 500 °C. This method, referred to as *in-situ* processing, is more difficult but results in higher quality films and reduces the maximum processing temperature required to obtain good films.

Most of the early work in high T_c thin film fabrication involved deposition of amorphous films onto unheated substrates followed by a high temperature anneal. Formation of the crystal structure from the solid phase results in a polycrystalline film with random orientation, except for the case of epitaxial substrates (see below). The critical current densities of these granular films are of the same order as for the bulk materials: a few hundred A/cm^2 at 77 K and a few thousand A/cm^2 at 4.2 K in the best cases. The low critical current densities are due probably to presence of grain boundaries in conjunction with short coherence lengths (on the order of a few Å in the c-direction) and the anisotropic transport properties of the high T_c superconductors. In addition to low critical current densities, granular films are found to have higher microwave losses than do the epitaxial films. This is a major problem for an important class of applications, such as high speed interconnects and high Q microwave resonators, where low losses are essential.

It is possible to produce crystalline films *in situ* without the need for a high temperature anneal by depositing at elevated temperatures of 600 to 700 °C.[14] A

relatively high pressure (1 mTorr) of oxygen is required and improvements are seen if the oxygen is in an excited state, such as created by a plasma discharge. These films tend to be c-axis oriented on a wide range of substrates and can be highly c-axis oriented on substrates with good lattice match with the HTS film. Most of the work being done today with HTS films utilizes *in-situ* crystallization.

Not only must the proper crystalline structure be obtained, but for most applications, the films must be highly oriented. The crystal structures of the $La_{2x}Sr_xCuO_4$, $YBa_2Cu_3O_{7-x}$, and $Tl_2Ca_2Ba_2Cu_3O_8$ compounds are shown in Fig. 1.2. They all consist of Cu-O planes perpendicular to the c-axis, which carry the supercurrent, separated by weakly superconducting or insulating layers. It is essential to produce films that are highly oriented with the c-axis perpendicular to the plane of the substrate. The easiest way of doing this is to use substrates having the same perovskite structure as the HTS film, such as $SrTiO_3$ or $LaAlO_3$, which also have a good lattice match with YBCO and promote epitaxial growth in the c- direction. Other substrates, such as MgO and ZrO_2, have also been used to produce c-axis oriented films. With these the mechanism of orietntation appears to be growth-driven instead of epitaxy with the substrate. Crystal growh appears to be fastest in the a-b planes, so during the early stages of film nucleation and coalescence, those nuclei with c-axis normal to the substrate expand laterally to cover most of the substrate. This mechanism, however, may be affected by growth conditions and is therefore less robust than epitaxy. In addition, the orientation within the plane may not be well defined, leading to grain boundaries between c-axis crystallites.

The effect of these grain boundaries on the critical current density was graphically demonstrated by a series of experiments at IBM[15]. Specially prepared substrates of $SrTiO_3$ were used to grow epitaxial films of YBCO having artificial grain boundaries with various degrees of misalignment between the grains. The critical current density

was measured both in the grain and across the grain boundary and it was found that J_c dropped by almost two orders of magnitude below the intragrain value for a misalignment angle of 35°.

From the above discussion it is obvious that substrate choice greatly affects HTS film quality. Table 2.1 lists the more commonly used substrates for HTS films along with some properties.[16] One of the most popular substrates used for obtaining films with high critical currents is $SrTiO_3$ which has lattice parameter of 3.92 Å closely matatching the 3.89 Å for the a-axis of YBCO. However, $SrTiO_3$ is expensive, available in only small sizes, and has high dielectric constant and loss tangent, making it unsuitable for microwave applications.

Table 2.1: Commonly used substrates for HTS films (From Ref. 16).

Material		Si	ZrO_2:Y	Al_2O_3	MgO	$SrTiO_3$	$LaAlO_3$	$LaGaO_3$
Unit Cell		Cubic	Cubic	Hexag.	Cubic	Cubic	Rhombo	Ortho
	a(nm)	0.543	0.524	0.476	0.421	0.3905	0.5357	0.5519
Lattice const.	b(nm)						$\alpha=$	0.5494
	c(nm)			1.299			60°6'	0.777
Lattice mismatch with YBCO (%)		40.6	35.5	21.0	9.0	1.2	1.8	1.6
Dielectric Properties at given f (GHz)		300	300	500	300	300	700	500
Dielectric	ε'(300K)	11.6	26	9.3	9.9	310	20 26
Const. ε'(100K)	11.4	25		9.7	2200		25
Loss (300K)		$1x10^{-3}$	$2x10^{-2}$	$1x10^{-3}$	$1x10^{-3}$	$3x10^{-2}$	$5x10^{-3}$	$8x10^{-3}$
Tangent (100K)		$4x10^{-4}$	$8x10^{-3}$		$5x10^{-4}$	$6x10^{-2}$		$6x10^{-3}$

Two new substrate materials have been introduced for growing epitaxial high T_c thin films, $LaGaO_3$ and $LaAlO_3$[17], both of which have less than a 2% lattice mismatch with YBCO. Both of these are of the perovskite family and they have superior dielectric properties to $SrTiO_3$. $LaGaO_3$ can be grown by the Czochralski method and can therefore be made in larger sizes, and $LaAlO_3$ has also recently become available in wafers as large as 3 inches in diameter.

The above developments not withstanding, it is still of interest to be able to use some of the more common substrate materials for HTS applications. At temperatures above 600 °C YBCO reacts with both Si and Al_2O_3 substrates. Rutherford back scattering and Auger depth profile experiments have demonstrated that Ba diffuses deeply into the substates and Si or Al diffuses into the film.[18] Thin films of YBCO on Si or Al_2O_3 heated above 800 °C are either insulating or semiconducting. In some cases the films crack and peel off the substrate. One approach to avoiding substrate reaction has been to introduce a buffer layer between the superconductor and the substrate[19]. In Chapter 3 we discuss some of our work with ZrO_2 barrier layers on Al_2O_3 substrates. Even if substrate reaction can be avoided, however, it is still desirable to reduce the maximum processing temperature to make high T_c thin films more compatible with existing integrated circuit technologies.

A final complicating factor in producing high-quality high T_c thin films is the need for oxygen to be present during the growth process. In order to form the oxide, the partial pressure of oxygen must be in the range of 10^{-3} to 10^{-4} Torr. This is not so much a problem for sputtering because this process can operate at high relatively high pressures. For evaporation, however, the presence of oxygen makes controlling the rates of individual sources difficult. Various attempts have been made to get around this problem as will be discussed below.

2.2 High T_c Thin Film Deposition Processes

All of the common techniques of thin film deposition, such as evaporation, sputtering, chemical vapor deposition (CVD), and molecular beam epitaxy (MBE), have been used, with varying degrees of success, to make high-T_c thin films. In addition some relatively lesser known thin film techniques have also been used, such as laser ablation and spin-on pyrolysis of metal-organic precursors. A brief summary of the various techniques, and how they address the above mentioned issues, is given below.

2.2.1 Evaporation

The first reported fabrication of high T_c thin films was by Laibowitz et al. [20] who used electron beam co-evaporation from three metal sources to produce YBCO and La-Sr-Cu-O thin films. Since that time numerous groups have used evaporation and it continues to be a common techniques for high T_c thin film deposition.

Evaporation from a single alloy source is not practical because, in general, each component will have different vapor pressures and evaporation rates.[21] The molten metal will therefore continually change in composition as the evaporation proceeds. Evaporation from three different sources can be either sequential or coevaporation. Mogro-Campero et al.[22] have shown that compositional control is easier with sequential evaporation although it is not clear that this technique can be used for with in-situ growth; all four atomic species may have to be coincident at the surface to allow for crystal growth. Coevaporation from multiple sources is accomplished by using individual rate monitoring with real time feedback control.[23]

Most of the earlier work with evaporation involved deposition of amorphous metal films with little or no oxygen present followed by an oxygen anneal at 850 - 950 °C. When $SrTiO_3$ was used as the substrate, it was found that the critical current densities could be as high as 10^6 A/cm^2 at 77 K. Mankiewich et al. [24] found that the film properties of YBCO could be improved by using BaF_2 as the Ba source and introducing some water vapor with the oxygen during the initial stages of annealing to extract the F atoms. A further improvement of this method was recently made by carrying out the post-anneal at reduced oxygen pressures and reduced temperatures.

Rate monitoring of the individual sources is complicated by the high oxygen partial pressures needed for *in situ* growth. Ion gauge detectors and mass spectrometers cannot be operated above 10^{-5} Torr. High pressure causes scattering of the evaporated materials resulting in cross-talk between the various sources and rate monitors. In addition, crystal quartz rate monitors lose calibration because oxygen is incorporated into the film growing on the sensor head. In order to get around this drawback of evaporation, a number of approaches have been pursued. The Stanford group[25] has used an atomic absorption rate monitor which uses optical absorption to measure the atomic vapor density of each component in front of the substrate. Although interference between species is eliminated, this monitor measures atomic gas density instead of flux, so differences in atomic velocity and sticking coefficients among components would lead to error in the mass ratio in the film.

Multi-source rate control can be improved by using a differentially pumped chamber to isolate the oxygen from the metal sources[26]. Alternatively, the oxygen partial pressure necessary to form the perovskite structure can be reduced by using activated oxygen, either from an atomic source[25] or an ozone source.[27]

Films produced by multi-source evaporation have a phase spread across the substrate plane unless the substrates (or sources) are rotated or moved in some fashion. This is because evaporation is a "line of sight" process and the sources appear as points. A phase spread may have advantages in early stages of research when a range of compositions are to be investigated, but is not suitable to commercial production or development of large area applications.

2.2.2 Sputtering

Sputtering is the most common commercial technique for thin film deposition and is normally chosen for multicomponent materials[28]. Fig. 2.1 is a schematic drawing of the sputtering process. A target of the material to be deposited is placed on a cathode in a vacuum chamber containing a low pressure, typically 1 - 10 mTorr, of an inert gas, usually Ar. A negative dc bias of several hundred volts is applied to the cathode to create a plasma discharge. Positive ions are attracted to the target and strike the surface with the full cathode potential, knocking off atoms which traverse the discharge region and condense on the substrate and surrounding surfaces. Secondary electrons are also generated at the cathode and accelerate into the plasma, colliding with gas atoms and thus creating more ions which sustain the plasma. The return to ground is provided through the anode which forms most of the remaining walls of the sputtering chamber. Once the power level and gas flow have been set and the plasma has stabilized, the rates for sputtering tend to be very stable. Furthermore, rates are reproducible from run to run so long as the target does not change (usually true for hundreds of microns of film deposition). This is an advantage over evaporation where rate monitoring and control are necessary.

There are many different configurations that can be used in sputtering. The

power can be either dc (for metallic targets), or rf (usually reserved for insulating targets). When rf power is used, a negative dc "self bias" is created at the target due to the difference in mobility between the electrons and ions in the plasma. The plasma can be confined close to the target and enhanced by having a magnetic field adjacent to the target to trap the electrons. This technique is known as magnetron sputtering.
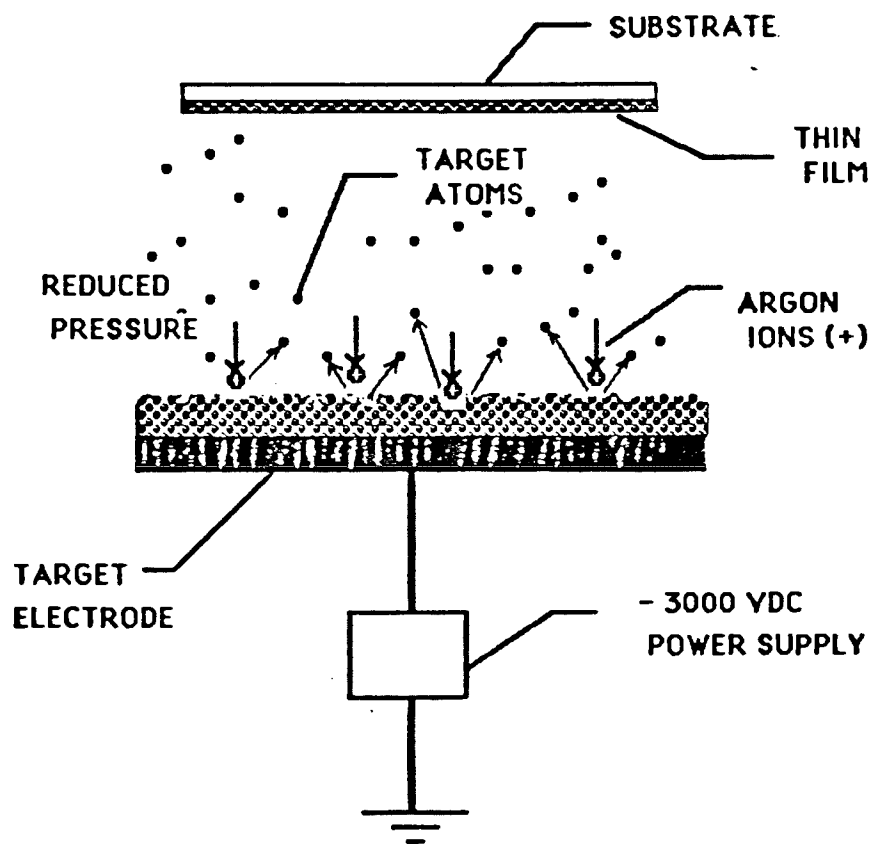
Figure 2.1. Schematic of the sputtering process.

Oxide films can be deposited either from metal targets or oxide targets. With metal targets, oxygen may be introduced in the film during sputtering, a process known as reactive sputtering, or the films may be oxidized after deposition. With oxide targets additional oxygen may be introduced during deposition to make up for a reduced sticking coefficient.

Multicomponent materials can be sputtered either from a single composite target or from multiple targets with independent power control. If a single target is used, the film normally attains the same composition as the target, even though each species may have different sputtering yields. Initially the sputtered flux is rich in the high sputter rate component. After an initial conditioning period, however, an "altered layer", which is depleted in the high sputter rate component, forms on the surface of the target. This acts to keep the composition of the sputtered atoms the same as that of the bulk.[28]

Formation of the altered layer is controlled by a balance between preferential sputtering at the surface and various diffusion processes in the target. For metal alloy targets the altered layer is only a few tens of angstroms thick and forms in less than one hour. For oxide targets, however, the altered layer can be much thicker. We have observed the formation of the altered layer in a loose powder target of YBCO and the results are presented in Section 3.3.

Once the altered layer is established, one might expect the composition of the film to accurately reflect the bulk composition of the target. This however has not been the case with YBCO; several groups[29-32], including our own, have found significant compositional deviation in the form of Cu and, to a lesser extent, Ba deficiency. There are a number of processes taking place at the substrate which may cause this effect. One possibility is that the sticking coefficient of the various species may not all be unity. This is likely to occur with oxygen which has to be compensated for by adding oxygen to the sputter gas. Metal atoms may also have low sticking coefficients, particularly at high temperatures.

Another process that causes the film to have a different composition than the target is the bombardment of the film by energetic particles which cause resputtering. It

is well known that negative oxygen ions are formed at a YBCO target due to the large difference in electronegativities between oxygen and barium.[33] These ions are accelerated away from the cathode, undergo charge stripping collisions in traversing the plasma, and strike the substrate as energetic neutrals.[34] The high sputter rate component is removed from the film and no bulk diffusion mechanism is present to make up for the lost material.

To avoid the negative ion resputtering effect, some groups have enriched the targets in one or more of the components, for example using a $Y_1Ba_2Cu_{4.5}$ composition. The problem with this approach is that the resputtering rate, and hence the required compositional adjustment, is sensitive to process parameters such as power and gas pressure. This tends to make the process more difficult to control and less repeatable. Other groups have tended to work at very high pressures, from 300 mTorr to 3 Torr[36], so that the energetic particles are scattered before they strike the substrate. High pressure sputtering has been used for *in situ* production and has yielded some of the best sputtering results so far.

Another way of avoiding the negative ion effect is to use an off-axis geometry (Fig. 2.2) in order to remove the film from the region of negative ion flux.[37] A variation on this approach[38] has been to use a facing target arrangement where both anode and cathode are made of YBCO and the substrate is placed off to the side. In our work we have avoided resputtering by using a large target and working in the magnetron mode. Further details of this process are given in Chapter 3.
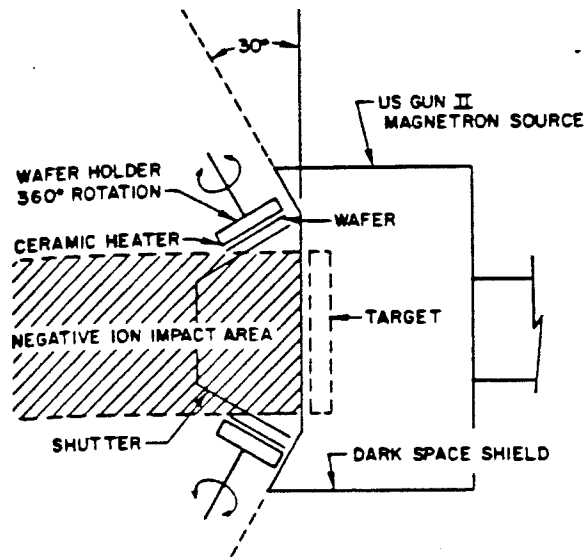
Fig. 2.2 Off-axis sputtering technique (from Ref. 37).

An alternative to oxide targets and the problems associated with negative ions is to use metal targets. For YBCO a single alloy metal target having the correct 1-2-3 composition is not possible because the three metals are immiscible even in the liquid state. Three metal targets[39] or two alloy targets made of $Ba_{.5}Cu_{.5}$ and $Y_{.5}Cu_{.5}$[40] have been used in the reactive mode. As in all reactive sputtering, the rates must be maintained such that the targets do not oxidize faster than metal atoms are removed. If multiple metal targets are used, the materials can be deposited either sequentially or simultaneously. Another approach is to sputter-deposit amorphous metal films and anneal the films in O_2 at high temperatures[41]. While this provides for finer compositional control the high temperature required for the anneal is unattractive for the reasons described above.

2.2.3 Laser Ablation

One of the more interesting and promising techniques for high T_c thin film deposition is laser ablation[42]. A pulsed excimer laser is used to ablate a solid target and the resulting plume gets deposited on the substrate (Fig. 2.3). High quality films as thin as 200 Å were found to be superconducting without the need for post deposition annealing. By placing a +300 volt ring between the target and the substrate, Witanachchi et al.[43] claimed to get in situ growth with a substrate temperature as low as 450 °C.

One of the reasons that laser ablation works well with multicomponent oxides like YBCO, is that it is very effective at transferring the composition of the target (normally a ceramic YBCO pellet) to the thin film. In this respect, it is more like single-target sputtering, in that individual atoms and small clusters are ejected from the target surface at high energies. Furthermore, it can have a very high deposition rate, up to 1000 Å per minute, if the laser pulse fluence and repetition rate are large enough. Finally, pulsed laser deposition does not have a problem with negative ion bombardment (in contrast to sputtering), since the excitation at the target is not electrical. For these reasons, laser deposition has become one of the leading methods for YBCO deposition on the research level.

Despite all of these advantages, pulsed laser deposition does have some shortcomings. First, it only works well with ultraviolet photons, since these have a very short absorption depth and can break chemical bonds holding atoms in place. It is for this reason that excimer lasers (e.g., KrF with $\lambda = 250$ nm) are generally used, although frequency-tripled Nd:YAG laser pulses have also been used effectively. Secondly, the laser plume that transfers the proper composition is very narrow, perhaps

10 ° in angle. Outside this angle, there is still some deposition, but the composition may be shifted somewhat. This makes it very difficult to get good uniformity over large areas, particularly since the source (the focused beam on the target) is typically only a few mm across. Finally, the laser ablation process tends to lead to large numbers of small particles in the film, which originate in part in the mini-explosions that take place on the surface of the target.

Given these various deposition methods, we decided to focus on sputtering for the fabrication of YBCO films. Apart from the problems associated with negative ion bombardment, sputtering is generally able to transfer target compositions accurately, and give good control and good uniformity. Finally, sputtering is the leading industrial method for physical vapor deposition, and is amenable to scale-up to commercial production. It is for these reasons that early on, we teamed up with CVC Products, Inc., of Rochester, a manufacturer of sputtering equipment, to determine how to use sputtering most effectively to produce high-quality, high temperature superconducting films.
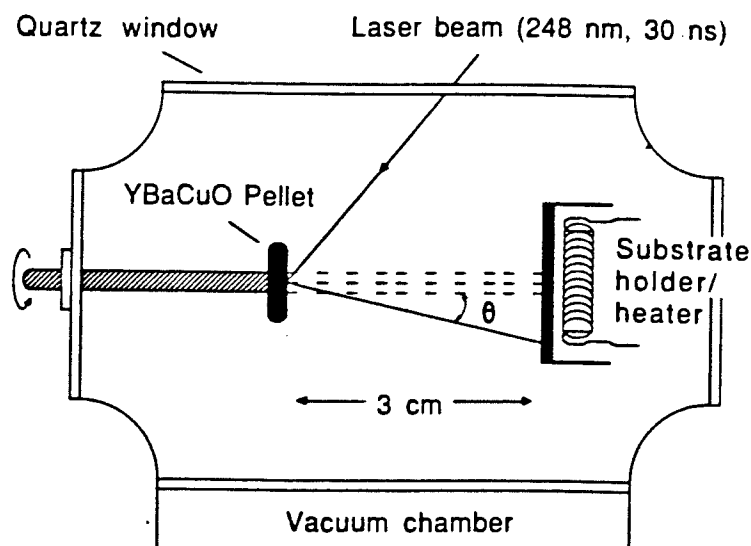
Fig. 2.3. Schematic of pulse laser deposition method (from ref. 42).

Chapter 3

Rochester Process for Sputtering YBCO Films

In this chapter we describe a sputtering process for fabricating high quality YBCO thin films that has been developed in a collaborative effort between CVC Products and the Department of Electrical Engineering at the University of Rochester. The primary goal of this effort was to develop a reproducible process for fabricating high quality HTS thin films on large area substrates (up to 2 inches in diameter) which could be used in this and other research efforts. The focus has been on developing an *in-situ* process that would not require a high temperature post-deposition anneal. We chose to use sputtering, as opposed to one of the other deposition techniques, because of our proximity to CVC, which makes the sputtering equipment, and because sputtering is a logical choice for reactive deposition of multi-component materials.

One of the unique features of this effort, as compared to the many other high T_c thin film deposition processes that have been developed in laboratories around the world over the past several years, has been the use of a relatively large target which provides for increased substrate size and better uniformity, as well as higher deposition rate. This capability will be important as applications for high T_c thin films are developed in the coming years.

The properties we were aiming for were a sharp superconducting transition at close to 93 K (for the YBCO material), critical currents of order 10^6 A/cm^2 at 77 K, compatibility with a wide range of substrates, and low microwave losses. This last requirement is particularly important for the development of passive microwave devices and high speed interconnects, both of which are being studied at the U of R.

3.1 Deposition Hardware

3.1.1 Systems

Two different sputtering systems have been used for depositing the YBCO films used in this research. In the early stages of our work the films were prepared on a CVC-601 sputtering system at CVC, (Fig. 3.1.) This system has four deposition locations, each of which is capable of accepting an 8-inch diameter sputtering target. The substrates are placed on an annular substrate holder which can be rotated during deposition (to improve film uniformity), indexed from station to station for multi-layer films, or held static. In our work we used a single target mounted in the baseplate and held the substrate in a fixed position above the center of the target. A heater was located in the chamber lid which opens as a clam shell to access the substrates. The chamber is cryopumped to a base pressure of 1×10^{-7} Torr.
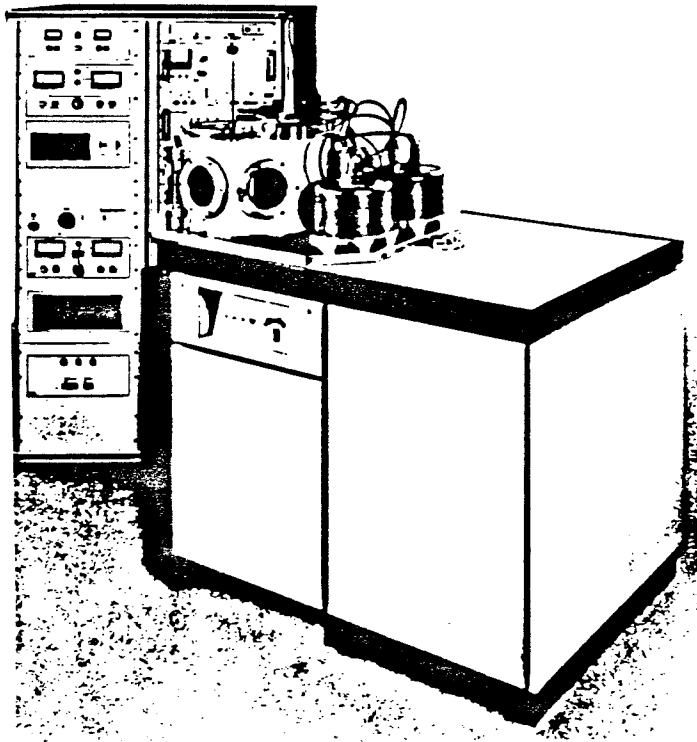
Fig. 3.1. Photo of CVC-601 used for much of the early deposition of YBCO.

During this research project a new sputtering system, the SC-4000, was developed by CVC with the aid of U of R researchers (Fig. 3.2). The system was developed specifically with high T_c thin film deposition in mind. One of these systems has been installed at the U of R and is currently being used to produce HTS thin films for microwave and pulsed laser switching experiments. Operating instructions for the SC-4000 are included as Appendix B for reference. The system has a 21" diameter water-cooled stainless steel chamber with several 2 3/4" and 6" Conflat^{TM} flanges for feedthroughs and 2 view ports. The U of R system has a single 8-inch target in the baseplate but can be equipped with three 2-inch sputter sources if desired. The system is pumped by a CTI-8 cryopump to a base pressure of 5×10^{-8} and is equipped with an MKS capacitance manometer and a 4-channel mass flow controller. At the present time, two gasses (Ar and O_2) are used. Power is supplied to the target by a 2.5 kW rf generator connected to a matching network. A high temperature substrate heater is installed in the lid. The substrate is placed on a stainless steel table which has the capability of being rotated during deposition, although all of our work was done with a static substrate. The substrate can be either electrically floated or grounded.
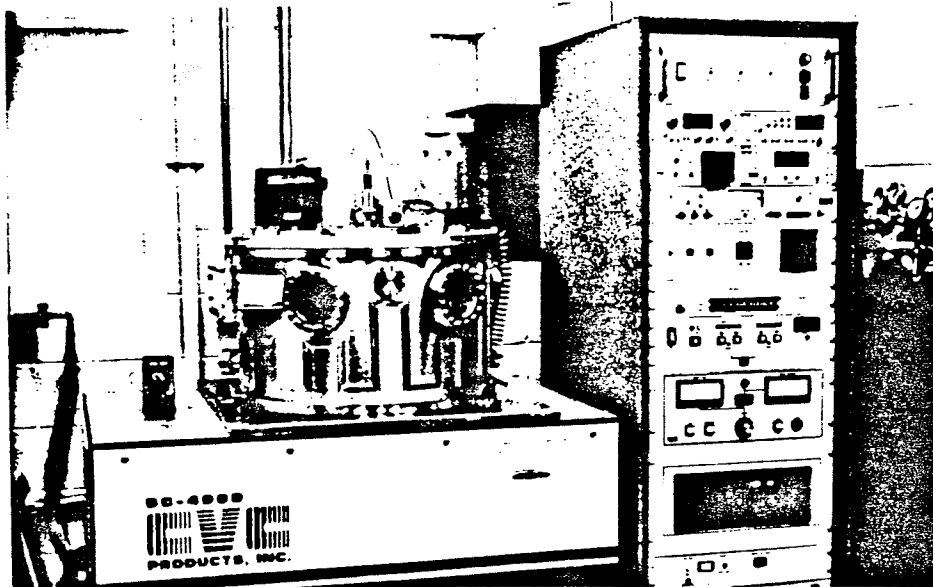
Fig. 3.2. Photo of the CVC SC-4000 sputtering system installed at the U of R.

3.1.2 Targets

We have used 8-inch diameter sputtering targets throughout this work. This size target is commonly used for commercial deposition of metals and dielectrics but has not been used widely in the development of HTS films. We began our work using loose powder targets and we continue to use these although we have also used 8-inch sintered targets. A photograph of one 8-inch diameter powder target is shown in Fig. 3.3.
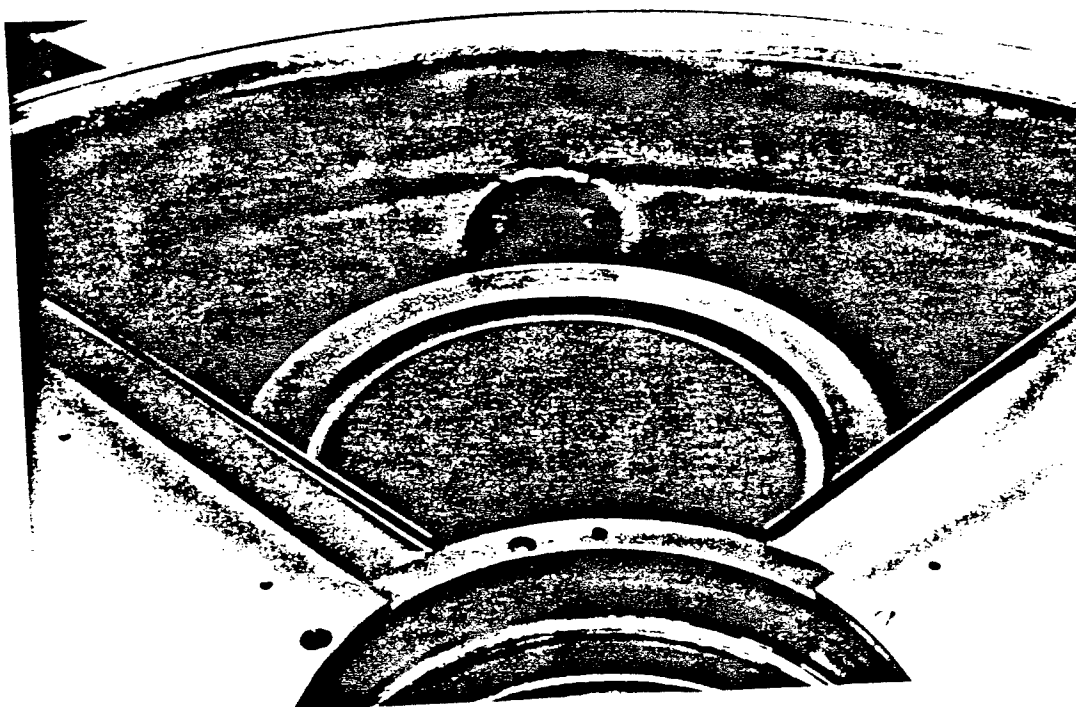
Fig. 3.3. Photograph of a 8-inch diameter YBCO powder sputtering target.

The advantages of powder targets are low cost, ease of fabrication, and potential for scaling up for large area substrates. The disadvantages are the tendency to absorb and desorb gas during vent cycles and the possibility of spreading particles around the vacuum chamber. Note that loose powder targets must be used on the sputter-up geometry. During the course of this work several different compositions of YBCO powder targets were used, as well as one BSCCO powder target. About 200 g

of the powder were spread over a copper backing plate to a thickness of 2-3 mm and tamped down to be smooth and slightly compacted. The target and copper plate were placed on a water-cooled cathode in the vacuum chamber. A ground shield located around the edge of the target to keep the plasma from sputtering the sides of the cathode reduced the effective target diameter to 7 inches.

The targets are made by mixing the desired amounts of commercially available CuO, $BaCO_3$, and Y_2O_3 powders (typically 99.9% pure) [44], firing the mixture at 950 °C in air overnight and regrinding into powder. This is followed by a second firing at 900 °C in O_2 for four hours and a final grinding with the resulting particle size typically less than 10 μm. Pellets pressed from stoichiometric YBCO powder showed superconducting transitions at around 90 K, typical of bulk preparations. The effect of target particle size on the properties of the resulting films has not been studied in detail, although we have seen variations from target to target which could be due to particle size. We have therefore attempted to use a consistent preparation proceedure.

In addition to the powdered targets, we have worked with two manufacturers of sputtering targets to develop solid 8-inch diameter YBCO targets.[45,46] This is one area that needs further work if large area high T_c thin films are to be commercialized. It is difficult to fabricate these large area targets and, once made, they are prone to cracking because of the low thermal conductivity and poor mechanical strength of YBCO. Thermal cracking is made worse by the high substrate temperatures used to deposit HTS films. Our first solid target cracked after only a few sputtering runs. To avoid thermal cracking, our second target had a criss-cross pattern of grooves cut partway down to the backing plate (Fig. 3.4)[46]. We used this target for approximately 20 runs to deposit YBCO onto substrates heated as high as 750 °C before the target failed. We also noticed evidence of arcing between the sections of this target.
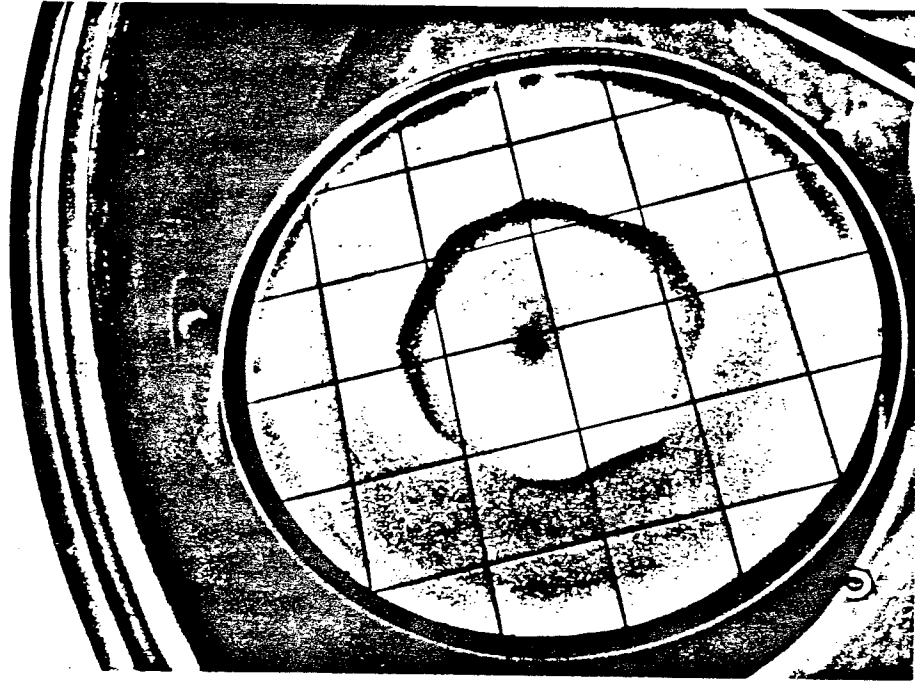
Figure 3.4. Photograph of an 8-inch diameter $YBa_2Cu_3O_{7-\delta}$ solid segmented sputtering target.

3.1.3. Cathodes

The targets are placed on a water cooled backing plate which are mounted on the cathode assembly. In this work we used both rf diode and rf magnetron cathodes. Figure 3.5 shows schematically an rf magnetron sputtering cathode. Note the confinement of the plasma to the racetrack region. This is to be contrasted with the diode sputtering arrangement shown in Fig. 2.3. The change from diode to magnetron is made simply by inserting a set of 8 magnets in a keeper ring.

3.1.4 Substrate Heaters

One of the challenging aspects of high T_c thin film growth is to heat the substrate during deposition to high temperatures (some researchers claim to need as much as 900 °C). The substrate temperature should be uniform (on the order of +/- 10 °C) in order that film properties be uniform across the substrate. In addition, the

substrate heater must be compatible with the high oxygen partial pressures used in high T_c deposition (on the order of 100 mTorr) and, in the case of sputtering, should be capable of providing rf or dc substrate bias during deposition. Our initial work used a quartz heater bank to provide up to 650 °C substrate temperature. The unit, however, was not designed for use at these high temperatures and required 3 kW of power, which caused overheating of the chamber lid. Subsequently we designed an inconel heater using a swaged heater cable brazed to a 5-inch diameter block. (Fig. 3.6) The development of this heater is described in Appendix C.
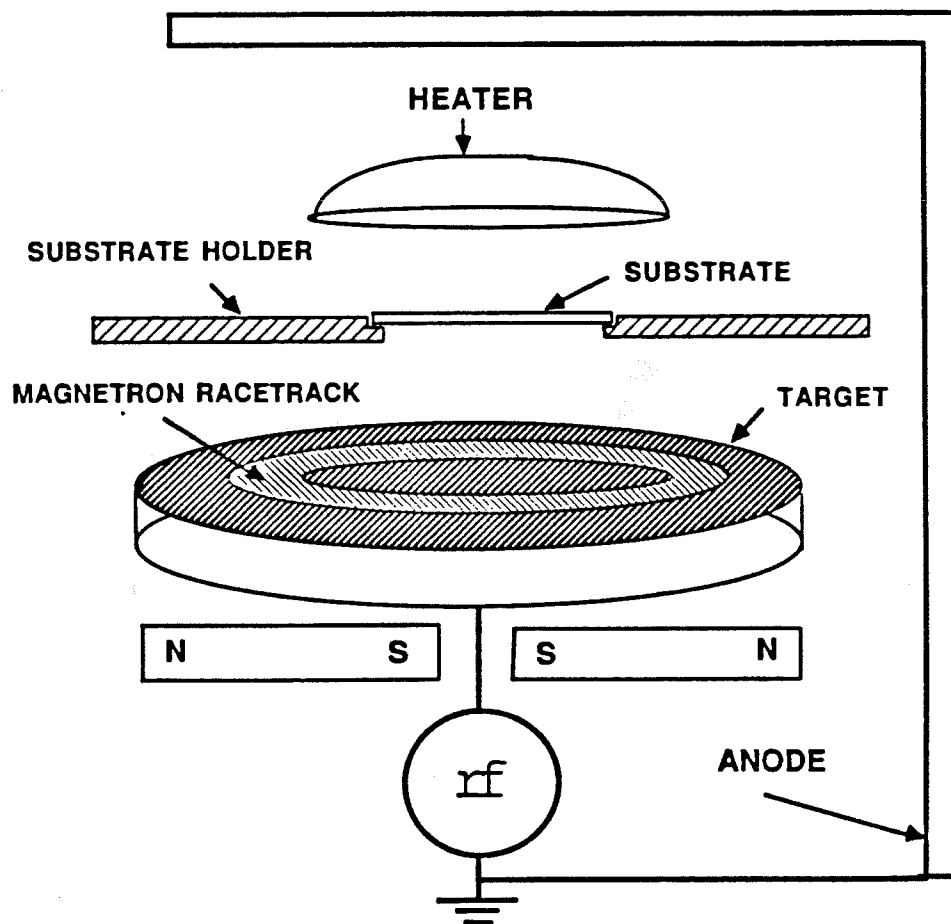
Figure 3.5. Schematic diagram of rf magnetron sputtering setup.

The substrate temperatures are measured using a chromel-alumel thermocouple sandwiched between two pieces of sapphire. We believe this gives an accuracy of ± 10 °C, although no calibration has been done. The temperature of the inconel block is also measured, and fed back to a P-I-D controller (West Instruments model 705) which drives a SCR power supply. At 700 W power, the heater temperature is 740 °C while the substrate is 700 °C. These numbers depend on the sputtering power, gas pressures, and type of target used. In fact, one advantage of the powder target is that less heater power is required becuase the target surface heats up (it has been observed to glow red) and re-radiates more heat back on to the substrate. One issue that may be of concern is that the absorption characteristics of the substrate changes during initial stages of nucleation and film growth, causing the substrate temperature to change as well.[47]

Because of the closed geometry we are using, with a reflecting "ion shield" (see below) beneath the substrate and a hot target surface, the substrate should be in equilibrium with its surroundings, even when it is transparent.
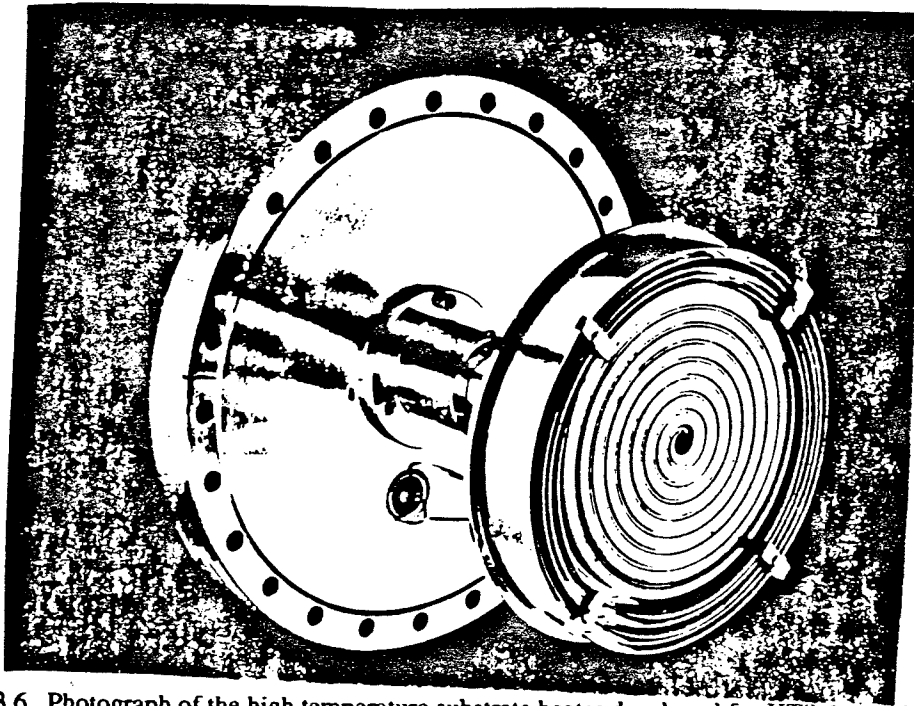
Fig. 3.6. Photograph of the high temperature substrate heater developed for HTS deposition.

3.1.5 Post Deposition Annealing and Patterning.

In our work, we employed post deposition annealing and we investigated two methods of patterning HTS films. Films that were deposited at low or intermediate temperatures were not superconducting as deposited and had to be given a post deposition high temperature anneal in flowing oxygen. For this work we used the tube furnaces located in the U of R Electrical Engineering clean room. Samples were placed on an alumina carrier and annealed at temperatures ranging from 600 to 1000 °C for 1 to 8 hours.

Patterning of the HTS films was required for measurement of the high critical current densities achieved in some of our later films, and for doing the laser driven switching experiments described in Chapter 4. We used two approaches: conventional photolithography followed by wet etching, and laser ablation using the same YAG laser as was used in the switching experiments. The details of this work are described in Appendix D.

3.2 Characterization of HTS Films

Before going into the process development and optimization for the HTS films, it is useful to describe the analytical techniques used to characterize the films.

3.2.1 Materials Characterization Techniques

Compositional measurement was a key aspect of this project, especially since we were trying to produce films with good uniformity over several square inches. For routine compositional analysis we used energy dispersive x-ray analysis (EDXA) on a scanning electron microscope. Normally the EDXA process can only be used for qualitative or semi-quantitative compsition measurement. In thin film work there are artifacts relating to film thickness, substrate type, and surface roughness that make quatitative analysis difficult. By holding the film thickness and substrate type constant,

and by using a calibration proceedure, we have been able to use EDXA to provide accuracy of 2-3 atomic %. An important aspect of the EDXA is that it provides a local measurement, so that the composition of a film can be mapped out as a function of position. In addition, EDXA, in combination with imaging by the SEM, can be used to identify roughly the composition of secondary phases and precipitates that often form on the surface of HTS films during deposition. A description of the EDXA process is given in Appendix E. The calibration for the EDXA was done by inductively coupled plasma atomic emission spectroscopy (ICP). This service was provided by Xerox Corporations Analytical Laboratories in Webster NY. Several samples were also sent to Charles Evans East (Plainsboro, NJ) for analysis by Rutherford Backscattering (RBS).

Much information concerning the nature of a thin film can be gained from the suface morphology. We used a scanning electron microscope (SEM) to obtain pictures of the films at magnification up to 15,000X. This work was done primarily on the ISI Super-III in the Mechanical Engineering Department, with some work also done on the Cambridge Instruments 240 in the Institute of Optics. Most recently, SEM photos have been taken at CVC on a Cambridge 90 SEM.

The anisotropic nature and short coherence length of the high T_c materials place stringent requirements on the crystallinity of HTS thin films. Thus an important aspect of this research was structural analysis. Structural analysis of the films was performed using x-ray diffraction which was done primarily at the X-ray spectroscopy laboratory of Kodak Corp. The x-ray diffraction patterns were used to determine phase purity, crystal orientation, and the c axis lattice parameter. Appendix F lists the x-ray powder diffraction lines associated with $YBa_2Cu_3O_7$. The x-ray lines for other compounds containing Y, Ba, and Cu are also available and may be used to identify secondary phases.[48] The x-ray diffraction pattern of c-axis oriented films show only the (00x) lines. The length of the c-axis, which is known to correlate with oxygen stoichiometry,

is most easily measured using the (005) line because there is no interference with the (x00) and (0x0) lines. The degree of orientation is determined by performing a rocking curve analysis on the (005) line. This rocking curve analysis has been shown to correlelate well with critical current densities and microwave surface resistance. Highly oriented films have lines with a full-width-at-half-max (FWHM) of less than 0.5°. It may be noted that other groups have successfully used RBS channeling data to determine the degree of alignment.

3.2.2 Electrical Characterization.

The room temperature sheet resistance was measured using the standard 4-point probe geometry. For a film that is large compared to the probe tip spacing, the sheet resistance may be calculated as $R_s = (V/I)\pi/\ln2$. Bulk resistivity of the film is found from the relation $\rho = R_s \times t$, where t is the thickness of the film. In some cases, particularly in our early work on post-deposition annealed films, the R_s was difficult to measure because of a poorly conducting or insulating layer on top of the film. Improvements were achieved using a large tip radius and a high spring force.

Cryogenic measurements were done in a custom made probe that could be inserted directly into a He storage dewar, avoiding the need to transfer He (Fig. 3.7). The probe consists of an outer 1.5-inch diameter stainless steel tube, which held a vacuum, and an inner 1-inch diameter tube, which contained instumentation wires. Vacuum sealing, which was necessary both to protect the HTS sample from moisture damage and provide thermal isolation, was accomplished with a room-temperature o-ring seal at the top of the probe. The sample was mounted on a temperature controlled copper block equipped with a wire-wound heater which was supported at the bottom of the inner tube by a teflon rod for thermal isolation. The outer tube could be backfilled with He to regulate the heat transfer between the Cu block and the liquid cryogen. For testing to 77 K the probe was immersed in liquid N_2, while liquid He was used to

reach 4.2 K. The temperature was measured by a Si diode thermometer connected to a Lakeshore 405 temperature controller. For routine R vs. T curves, the evacuated probe was backfilled with approximately 100 mTorr of He, immersed in liquid N_2, and allowed to cool passively. Critical current measurements were done by stabilizing the temperature at each desired level using the Lakeshore controller.
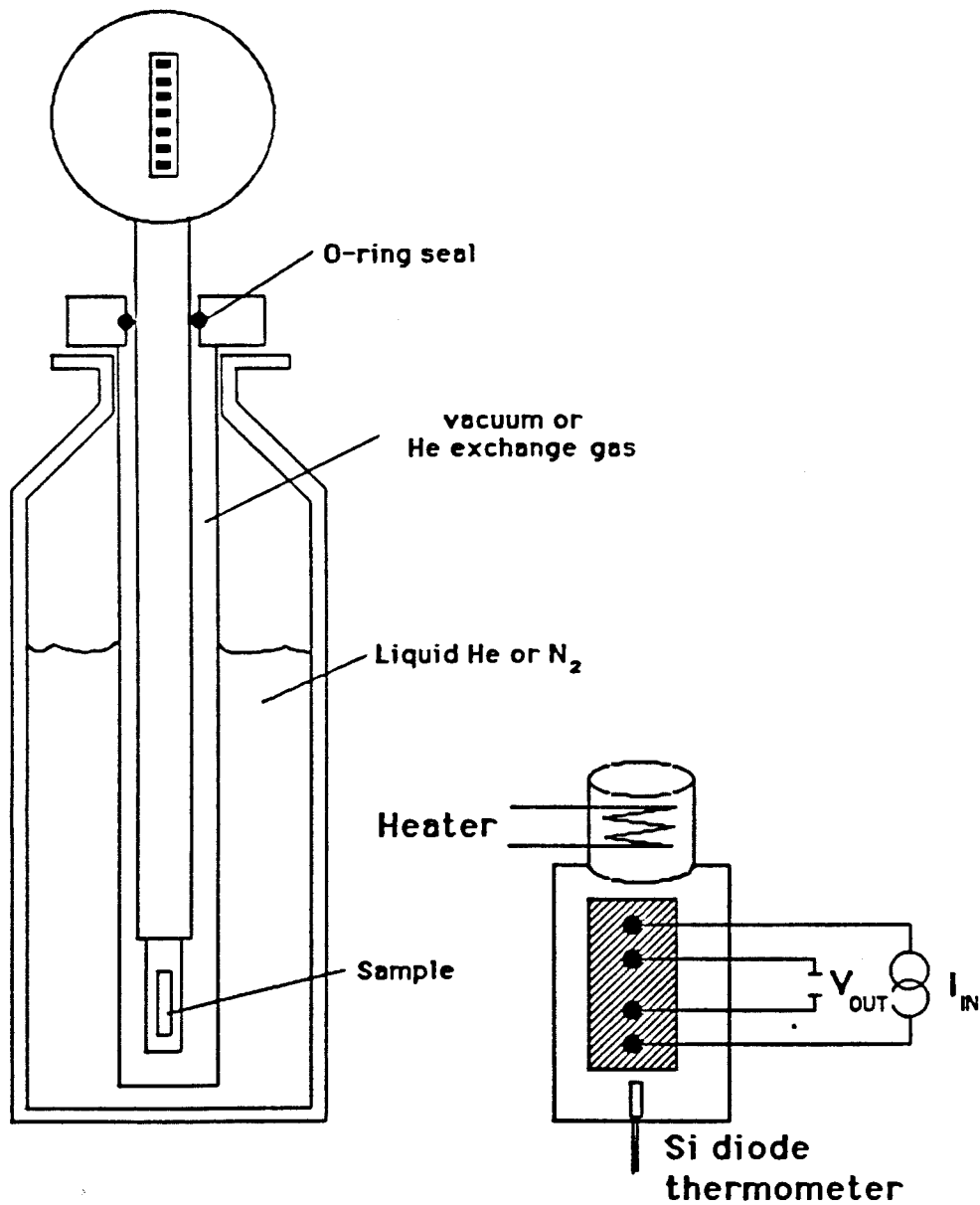
Fig. 3.7. Schematic of the cryogenic probe used for measuring R vs. T and J_c vs. T of HTS films.

In taking electrical measurements of the superconducting films, we used true four-probe measurements. This was essential because the contact resistances tended to be high, nonlinear, and temperature-dependent. Silver paint and pressed indium (with contact areas ≈ 2 mm^2) were found to be effective, although not ideal, contacts, with typical low-temperature resistances under 100 Ω (specific resistance ≈ 10 Ω-cm^2). In contrast, gold-plated spring-loaded copper pins, which normally would work quite well for metallic or semiconducting samples, yielded contacts that someimes became practically insulating at low temperatures. This contact behavior may reflect a surface semiconducting layer in combination with the brittle ceramic nature of the films. For measurements of higher critical current densities, and for fabrication of the fast opening switch (Chapter 4), we used evaporated Ag contacts with wire-bonded leads.[49] Further reduction in the contact resistance to below 10^{-5} Ω-cm^2 was achieved by annealing the films with contacts in an oxygen furnace at 500 °C for about 1 hour.

The voltage was measured by a Keithley 177 Microvolt DMM. Current was supplied either by a Lakeshore model 120 current source with selectable current settings for R vs. T curves or a Keithley programmable current source for J_c vs. T curves. Alternatively, a low frequency (> 1 Hz) triangle wave from a voltage signal generator was used in series with a decade resistance box to sweep out I-V curves. The critical current was defined using a 1 microvolt criterion.

During the course of this research the automated data aquisition package Labview by National Instruments was installed on an Apple Macintosh SE to automatically run the R vs. T and J_c vs. T curves and to record the data on file. This program communicates via the IEEE-488 bus with the temperature controller, voltmeter, and programmable current source.

3.3 Process Development

In this section, the results that led to the optimization of the UR/CVC process for sputtering high-quality YBCO films are described. This work began in 1987, soon after the discovery of this high-temperature superconducting material. At this time, standard methods for depositing YBCO were not yet developed, and we had to develop them ourselves. The properties of the early films were not particularly good, particularly in comparison with what is now available. Nevertheless, we have included this work here because it shows how the research progressed, and because it made clear some of the parameters that would have to be better controlled in the optimized process.

3.3.1 RF Diode Sputtering

As described in section 3.1, the early work used rf sputtering inside a standard production-model CVC-601 system, which is configured so as to permit sputtering up from a horizontal 8-inch diameter target, permitting the use of a semi-loose powder target of unique design, described earlier. We had to use rf (vs. dc sputtering), since a loose powder target is not a good electrical conductor. And we initially chose the diode mode (with the magnets removed from the target assembly) in order to distribute the power uniformly over the target so as to minimize thermal stresses.

Through most of the sputtering runs, the sputtering gas was maintained at about 10 mTorr of an Ar/O_2 mixture (10% O_2) by pumping a continuous flow of gas through a throttle valve to the cryopump. The use of a partial pressure of oxygen appeared to help stabilize the target surface, and was not systematically varied at this stage of the work. Typical rf powers were about 750 W for these 8-inch targets, with an induced dc cathode bias of about 1400 V. The substrates were mounted facing down on an assembly located about 3 inches above the target surface. Substrates in the earlier part

of the study were primarily single-crystal sapphire (c-plane orientation). Later, cubic zirconia crystals (9.5% yttria stabilized) were used. Depositions were carried out on substrates that were either unheated, water-cooled (mounted using an In-Ga eutectic solder which is liquid at room temperature), or heated using a quartz lamp. A typical deposition run of about 2 hours yielded a film of order 1 μm thick, measured after deposition using a Sloan Dektak stylus profilometer, corresponding to a deposition rate of 50 - 100 Å/min.

Compositional control was a problem in this early work with diode sputtering. We were aiming towards films with compositions close to that of $YBa_2Cu_3O_{\approx 7}$, the "1-2-3" stoichiometry with T_c=93 K in bulk. Here and below, metallic element concentrations are normalized so that the sum of the three elements equals unity. In this convention, the stoichiometric compound would be $Y_{.167}Ba_{.333}Cu_{.50}O_x$.

As pointed out earlier, a relatively simple understanding of the sputtering process of a homogeneous compound would lead one to anticipate that the composition of a film should be close to that of the bulk target. Unfortunately, this agreement was frequently not observed, and in some cases the shift was quite dramatic. In making this comparison, it was important to ensure that the composition of the surface of the target (discounting the thin altered layer) accurately reflected the overall bulk composition. In some of our earlier work we used a slurry of YBCO powder and isopropyl alcohol to make the target. This method, however, appeared to result in a drift in film composition from run to run. It was postulated that the slurry resulted in a segregation of particle sizes and composition through the depth of the target, although this could not be confirmed. In any case, this method was discontinued. Targets prepared from dry powder did not exhibit this problem - films made using the dry target gave consistent and repeatable compositions over dozens of successive runs from the same target.

With the composition of the target surface under control, it became apparent that the composition of the films was frequently still different from that of the target, and that temperature of the substrate appeared to be a key parameter. For a substrate water cooled so as to remain close to ambient temperatures, the composition of the film was normally close to that of the target, with perhaps a slight excess of Cu. For example, a 1-2-3 target with 50% Cu (metallic fraction) yielded about 60% Cu in the film, uniformly across the film. A similar relation was observed for a film deposited at low sputtering power, and correspondingly low deposition rates. In contrast, films that were either heated or not cooled effectively exhibited drastic lowering of the Cu content. For example, the same 1-2-3 target might yield 20% Cu in the film.

We were able successfully to counteract such a depletion in Cu in the film by enriching the target in CuO. However, if there are temperature gradients in the substrate, this approach will lead to substantial compositional gradients in the resulting film. A problem of this sort was simulated by using a sapphire substrate that was well cooled on one end only, giving rise to a temperature gradient (not measured). The composition ranged from 70% Cu at the cool end to 20% at the hot end.

The origin of the relative Cu depletion was never fully explained, but it appears to reflect several interrelated phenomena. First, the surface of the substrate is heated substantially by radiation from the target, by the sputtered atoms, and by electrons in this diode geometry. In addition, subsequent work revealed the importance of negative ion bombardment, in which negative oxygen ions near the target are accelerated away from the target and bombard the substrate at high energies. This will produce resputtering of the component atoms at different rates, and this resputtering appears to be temperature-dependent. Other reseachers have also seen this temperature-dependent compositional shift under conditions of substrate bombardment and have attributed it to radiation enhanced surface diffusion[50].

The YBCO sputtered films were not superconducting as deposited, even for compositions close to 1-2-3. These smooth, black films tended to exhibit room temperature sheet resistances of order 10 kΩ to 10 MΩ, which increased sharply at lower temperatures, and never went superconducting. X-ray diffraction scans (not shown) indicated an amorphous or highly disordered structure instead of the desired 1-2-3 perovskite crystalline phase. We annealed the films at high temperatures in oxygen in order to create the proper crystal structure and resultant superconductivity.

Samples were heated in a quartz tube furnace in pure flowing oxygen, and were allowed to cool for several hours to < 150 °C before removing them from the furnace. Samples with the right stoichiometry, after being heated to 500 - 650 °C for about an hour, exhibited significantly lower room temperature resistance than as-deposited films, and in addition showed some x-ray evidence of the proper 1-2-3 polycrystalline phsae. However, they too increased their resistance substantially at low temperatures. It was necessary to go to about 850 °C for one hour in order to obtain superconducting films.

The heat treatment profiles shown in Fig. 3.8 were adapted in part from procedures used elsewhere,[58] and various other combinations of time and temperature were not all systematically examined. However, different procedures appeared to yield significantly different microcrystalline morphologies. Higher temperature (T > 900 °C) was found in several cases to result in films that became agglomerated or otherwise discontinuous. In addition, some films, particuarly those deposited on cooled substrates, exhibited adhesion problems on heating. This "blistering" (small circular flakes $\approx$ 5 μm) was substantially alleviated by reducing the initial rate of heating (curve b in Fig. 3.8). Fig. 3.9 is an SEM photograph of one of our rf diode sputtered YBCO films annealed at 850 °C. The rough surface was typical for our post annealed films on sapphire and zirconia. EDXA revealed the surface grains to be mainly CuO.
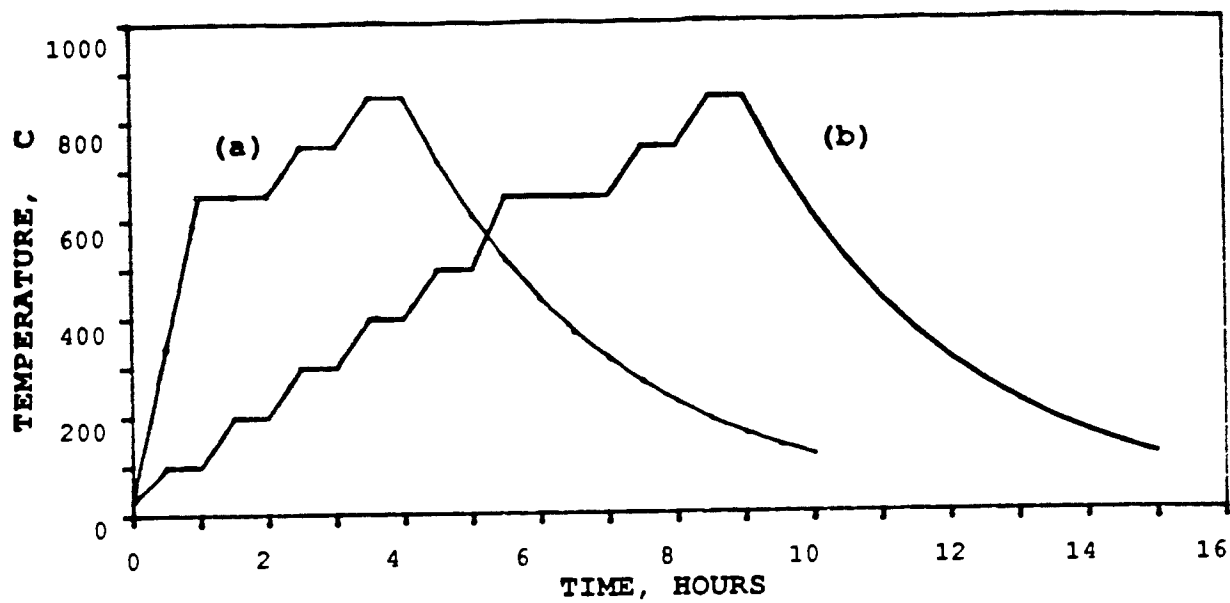
Fig. 3.8. Tube furnace temperature profiles used to anneal HTS films.
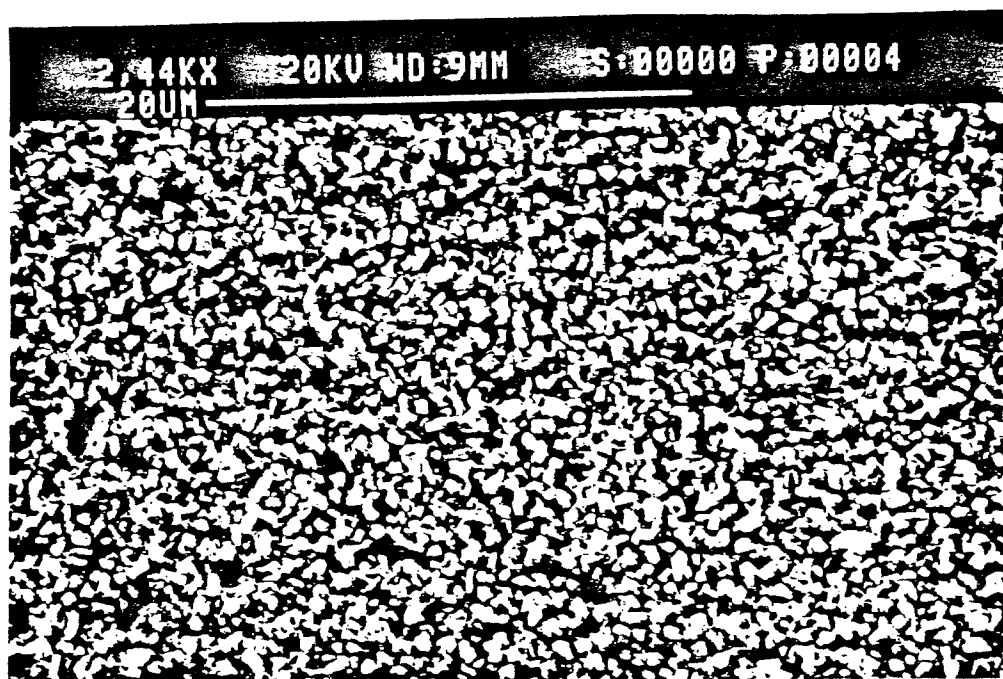
Fig. 3.9. SEM photograph of a granular YBCO film deposited on randomly oriented ZrO_2 by rf diode sputtering at 300 °C and annealed at 850 °C .

Several films were deposited on sapphire and zirconia substrates using this low temperature rf diode process with post annealing. Table 3.1 summarizes the deposition conditions and superconductive transitions for three of these films, and Fig. 3.10 shows the R vs. T curves. The measuring current was 100 μA. Curves a and b are for films on sapphire. Although sapphire is normally considered inert, it apparently reacts somewhat with YBCO, particularly at the high annealing temperatures. Only very thick films ($\approx$ 2 μm) on sapphire went fully superconducting (curve b). Thinner films (curve a) exhibited behavior indicative of superconducting grains separated by insulating tunnel barriers. The best sample on zirconia, which did not show evidence of substrate interaction, showed metallic-type behavior, with a resistance drop of 25% from room temperature down to about 87 K (the "upper" critical temperature T_u). Following this, there was a sharp knee followed by a drop to R=0 at the true critical temperature T_l = 50 K. The intrinsic transition in these films is probably much sharper, and limited here by sample inhomogeneity. These R vs. T transitions should be compared to out later work (see section 3.3.4) in which we were able to produce films in which the normal portion of the curve extrapolates through the origin. For temperatures below 50 K, the critical current of this film was also measured. A narrow constriction in the film was created, and the I-V curves were measured. An estimate of the critical current density at 4 K, probably a lower bound, is in excess of 2000 A/cm^2.

Table 3.1: Parameters for YBCO films deposited by rf diode sputtering

Run #	Composition (%Y,Ba,Cu)	Substrate	Thickness (μm)	T_u,T_l (K)	Temp. Profile (Fig. 3.8)
83	15,27,58	sapphire	0.7	75,0	curve a
43	16,32,52	sapphire	2.2	80,40	curve a
112c	19,23,58	zirconia	1.0	87,50	curve b

It is notable that all of these films on sapphire and zirconia were polycrystalline. Some other groups were finding preferential orientation in post-annealed films on single-crystal $SrTiO_3$, but these substrates were very expensive even for very small sizes (several hundred dollars for 1 cm^2). Our approach (which was initially not funded externally) attempted to use more common substrates and obtain coverage over larger areas.
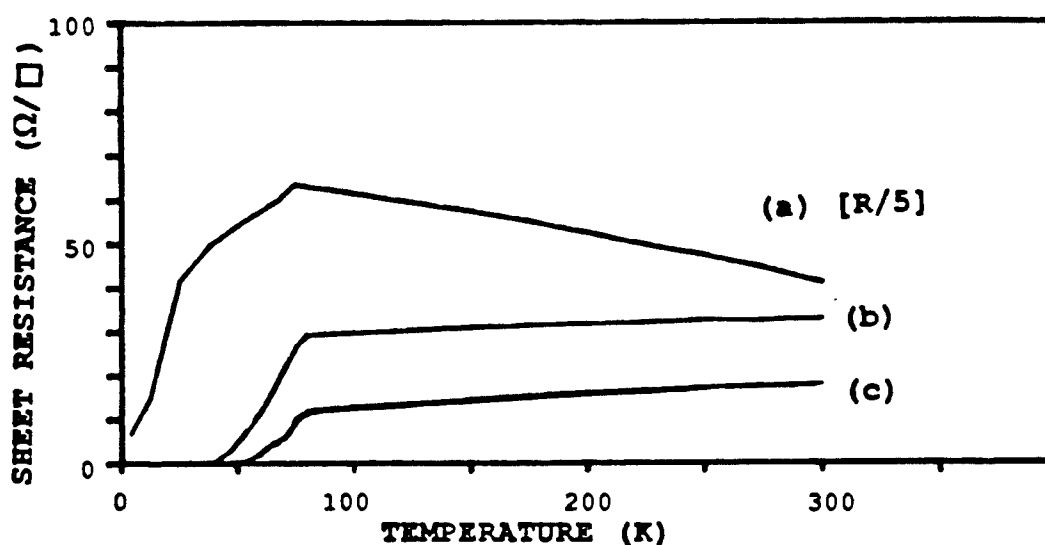
Fig. 3.10. Resistance vs. Temperature curves for three YBCO films deposited by rf diode sputtering. Curves a, b, and c, are for samples 83, 43, and 112c respectively.

3.3.2 Magnetron Sputtering

Given the difficulties in maintaining compositional reproducibility and uniformity using the rf diode mode, we decided to install the magnets in the target assembly and operate in the rf magnetron mode. As will be described below, this greatly improved the compositional control in the region above the center of the target. In addition, it also provided a rather direct indication of the effects of negative ion bombardment in the region directly above the magnetron racetrack. (see Fig 3.5).

The sputtering gases, rf power, and the powder target were exactly the same as in the magnetron mode. However, the target and substrate self-biases observed using the rf magnetron mode were quite different than those seen earlier for identical conditions in the diode mode. The rf-induced cathode potential was typically 55 V for the magnetron mode, as compared with a much larger 1400 V in the diode mode. This striking difference between the two modes is likely to be related to the confinement of the secondary electrons that generally occurs in the magnetron mode.

As for the diode case, there is a period for a new target associated with the formation of an altered layer on the surface. For films grown near the center of the target, the composition is initially copper-rich, but after a period of 10 - 15 hours of sputtering, a stable ratio of 3/2 = 1.5 was reached for a stoichiometric target. Fig. 3.11 shows the development of the altered layer as evidenced by the Cu/Ba ratio of the deposited films. As long as the powder target was not physically disturbed, it could then be used multiple times without such a long pre-sputter.

Fig. 3.11. Ratio of Cu:Ba in rf magnetron sputtered YBCO thin films vs. sputtering time as altered layer develops in surface of a new powdered target.

Effects attributable to negative-ion bombardment and resputtering are clearly evident in the magnetron geometry. Figure 3.12(a) is a plot of the measured thickness of YBCO films as a function of position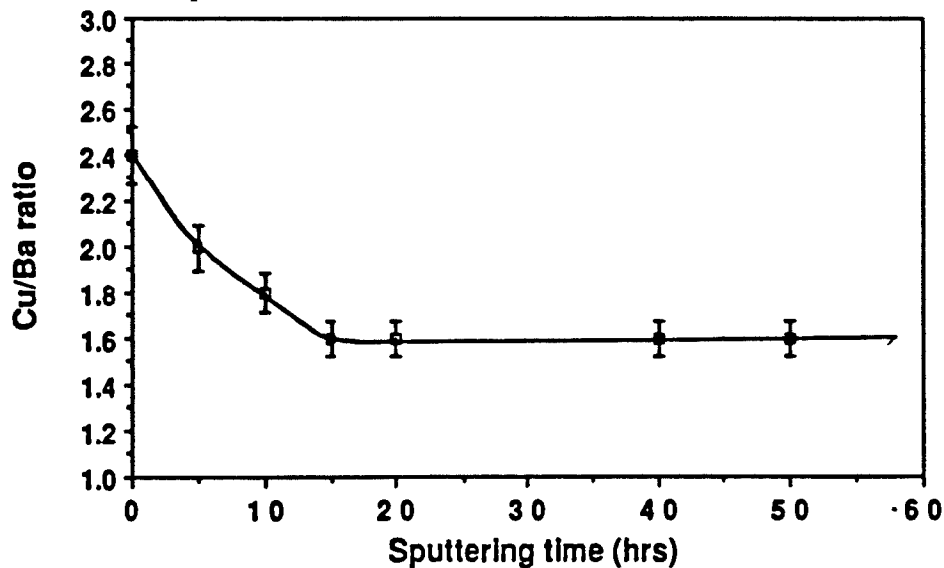 along a cross section of the target. Without resputtering effects, one would expect the thickness in the center to be a bit less than that directly over the racetrack, where the sputter rate is greatest. In contrast, the film is actually much thinner over the racetrack. This is consistent with resputtering due to negative ions that are accelerated perpendicular to the target surface at the racetrack. The negative ions are highly energetic with velocity vectors perpendicular to the target. The sputtered atoms, on the other hand, are ejected with a cosine distribution and coat the entire substrate plane. Fig. 3.12(b) shows the spatial dependence of the film composition, and indeed it is substantially off stoichiometry in the same place where the film is thinnest - directly opposite the racetrack. Even though the exact compositional shift above the magnetron racetrack may be uncertain, due to the aformentioned problems with calibration of EDXA when film thickness is not held constant, it is evident there is a loss of Ba and, to a lesser extent, Cu in this region. Note, however, that given the large size of this target, there is still a region about 2 inches across in the center where the composition is fairly uniform and close to proper stoichiometry. This is the region that we subsequently deposited all of our films. As discussed in Section 2.2.2, the negative ions are actually neutralized in the plasma, and so it is not possible to avoid ion bombardment by placing a negative bias on the substrate.

This ability to reproduce the target stoichiometry in the film appeared to be largely independent of substrate temperature over the range studied (eventually up to 800 °C). This is in contrast to our earlier work in the rf diode mode, where it was necessary to actively cool the substrate in order to maintain uniform stoichiometric composition. The reduction in secondary electron and negative ion bombardment in the present case may be contributing to the improved situation.
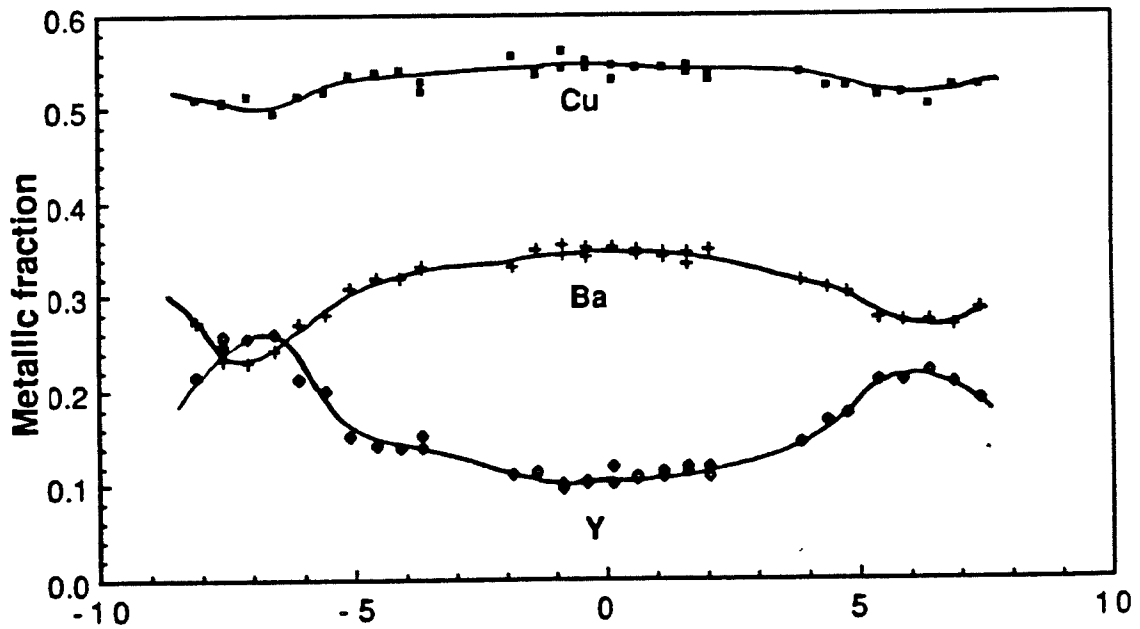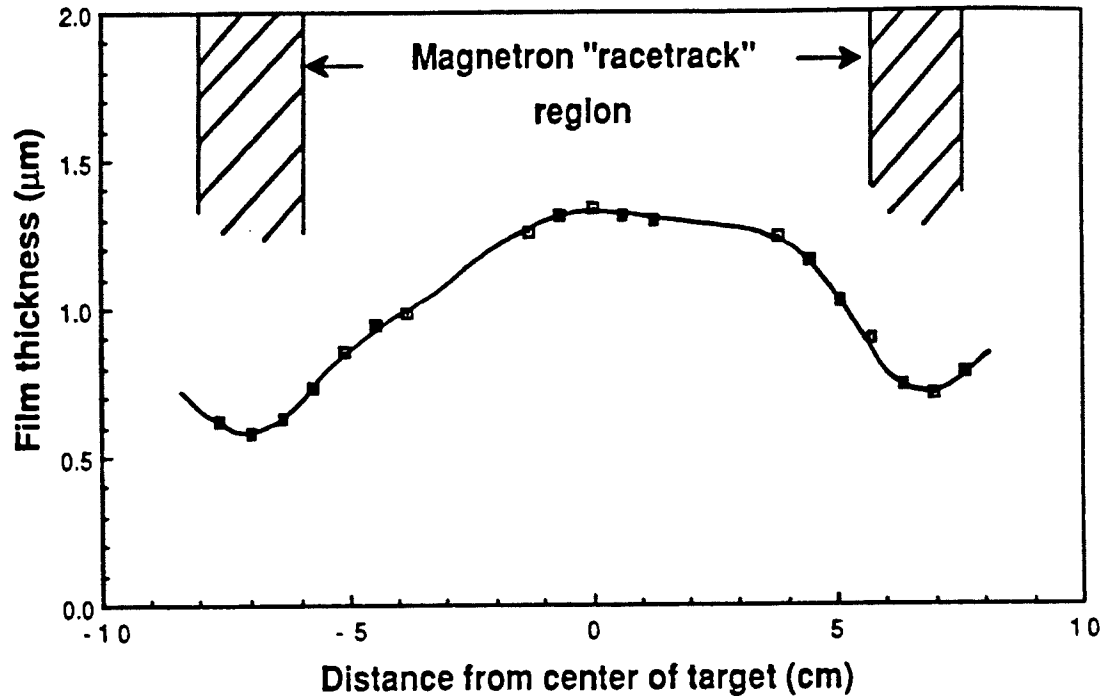
Fig. 3.12. Spatial variation of thickness and composition of magnetron sputtered YBCO film. (a) Film thickness. (b) Metallic fraction of Y, Ba, and Cu.

Using this magnetron sputtering arrangement, together with the post-annealing procedure described above, we were able to obtain more consistent results and improved superconducting properties. Films had compositions that were within a few percent of that of the target, which was within the accuracy of our EDXA method. Some were deposited at ambient temperatures, some were heated as high as 300 °C using quartz lamps. Substrates used included ZrO_2, MgO, and $SrTiO_3$. Films deposited on ZrO_2 and MgO and annealed at 850 °C consisted of randomly oriented polycrystals, with platelets and needle-like crystallites. An SEM micrograph for one film on random cut ZrO_2 is shown in Fig. 3.13 and the x-ray diffraction scan is shown in Fig. 3.14. Both the SEM and XRD data show randomly oriented $YBa_2Cu_3O_7$ with very little secondary phases present.
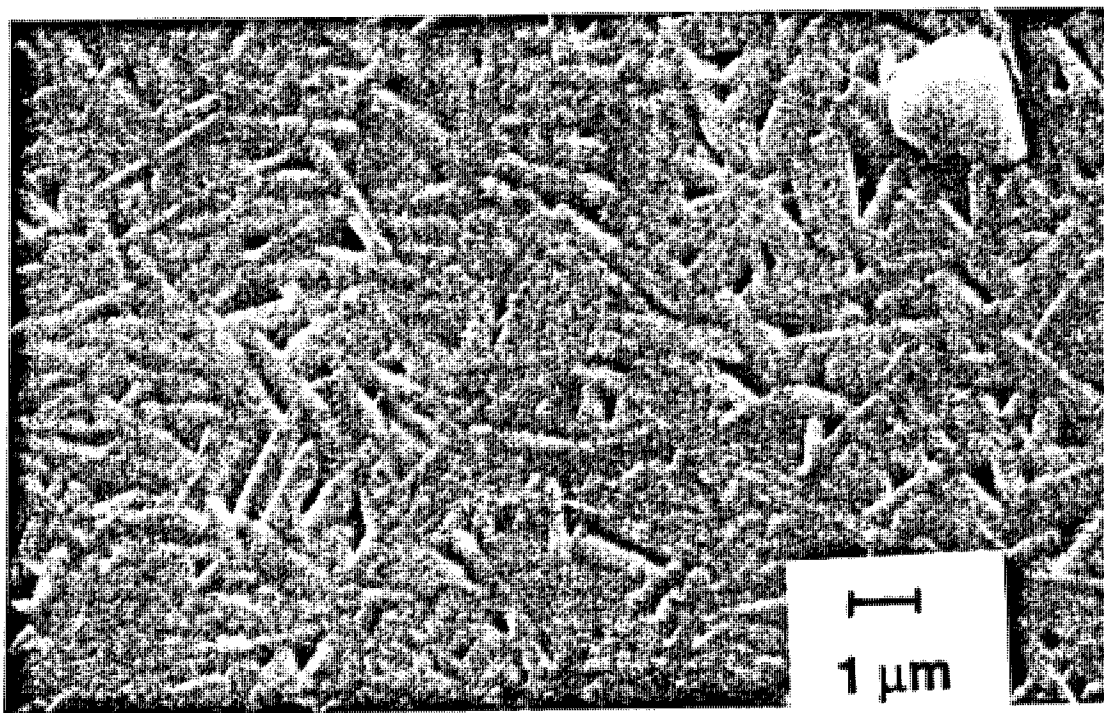
Fig. 3.13. SEM micrograph for YBCO film deposited by rf magnetron sputtering on random cut ZrO_2 at 300 C and annealed at 850 °C in O_2.
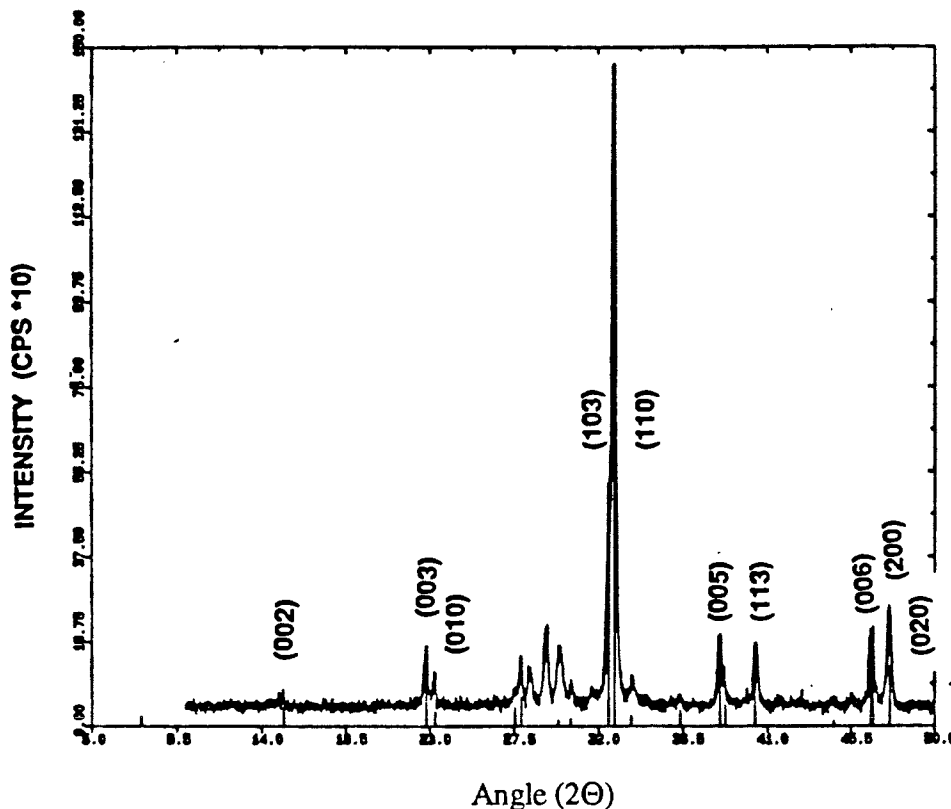
Fig. 3.14 X-ray diffraction curve and SEM micrograph for a rf magnetron sputtered film deposited on random cut zirconia at 300 °C and annealed at 850 °C.

Table 3.2 is a summary of deposition conditions and superconducting properties of selected films deposited at temperatures up to 300 °C and subjected to post deposition anneals at 850 °C. Fig 3.15 shows R vs. T and J_c vs. T curves for one of these films (#167). All of the YBCO films showed onsets of superconductivity around 93 K. There were, however, differences in the zero resistance temperature T_c, the slope of the curve above T_c, and in the critical current densities. Critical temperatures up to 89 K were observed, with critical current density J_c at low temperatures approaching 10^4 A/cm^2. Substantially greater values of J_c were obtained by depositing on (100) SrTiO$_3$. The critical temperature was 87 K, J_c(77 K) was 4 x 10^4 A/cm^2, and J_c(4 K) was extrapolated to almost 10^6 A/cm^2. It is believed that the sample on

$SrTiO_3$ was highly oriented, at least near the bottom of the 1.3 μm film, and this is the reason for the greatly enhanced value of J_c.

Table 3.2: Deposition conditions and superconcuting properties of YBCO films deposited by rf magnetron sputtering at temperatures up to 300 °C.

Run #	Comp. (%Y,Ba,Cu)	Substrate	$T_{deposit}$ (°C)	Res. Ratio R(300)/R(93)	T_c (K)	J_c@77 (A/cm^2)
167	17,33,50	ZrO_2	300	1.69	83	100
170	17,33,50	$SrTiO_3$	ambient	1.35	87	40000
175	15,35,50	ZrO_2	300	2.10	89	1000
176	15,35,50	MgO	ambient	1.10	70	-
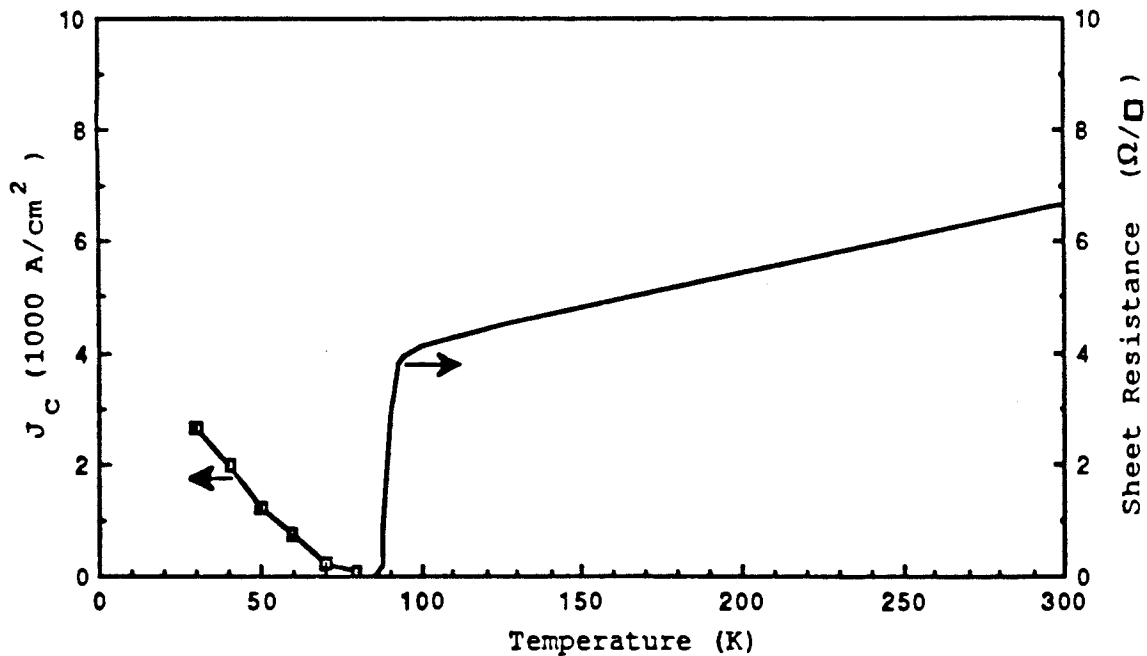
Fig. 3.15. R vs. T and J_c vs. T curves for sample #167.

Early on we used sapphire crystals as the substrate for YBCO, but it soon became clear that film-substrate reaction, mostly during the 850 °C post-anneal, was acting to depress the zero-resistance temperature. Since reaction with zirconia is apparently minimal, a 0.5 μm-thick layer of zirconia was deposited on sapphire in a CVC-601 (the same machine used for the YBCO) by reactive sputtering of metallic zirconium in an argon-oxygen atmosphere. A 1.3 μm YBCO film was deposited on the coated substrate, and exhibited R=0 at 82 K, a substantial improvement over 60 K without the buffer. Figure 3.16 shows the R vs. T curve for a YBCO film on sapphire with a ZrO_2 buffer layer. Other researchers have demonstrated that a similar buffer layer also permits deposition of YBCO on Si.[19]
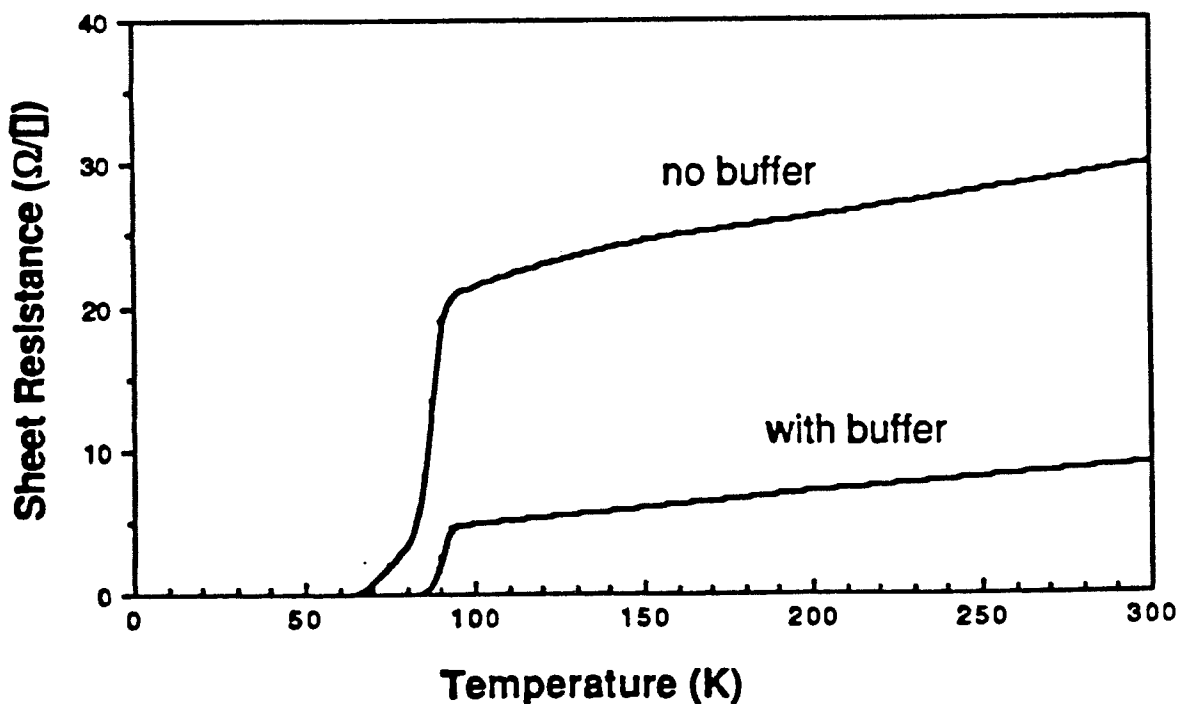
Fig. 3.16 R vs. T for YBCO films on Al_2O_3 with and without a ZrO_2 buffer layer.

Finally, we mention that this same rf magnetron sputtering system was used to prepare a film of another high-temperature superconductor, Bi-Sr-Ca-Cu-O. A loose

powder of composition $BiSrCaCu_2O_x$ was made in the same way as YBCO powder, and spread on a copper plate as a loose powder target. The estimated film composition was $BiSr_{1.2}Ca_{1.5}Cu_{2.7}O_x$, although the target altered layer may not have fully developed. These films were annealed for 1 hour at 770 °C, followed by 5 minutes at 865 °C. Fig. 3.17 shows the R vs. T curve for one such film on (100) MgO. The sample started to go superconducting at 85 K, although with a tail down to 50 K. We saw no evidence of the presence of the higher-T_c phase with a critical temperature of 110 K.[51] This work was not pursued further, since it soon became evident from other researchers that this higher-T_c phase is very difficult to obtain. We returned to concentrating on YBCO.
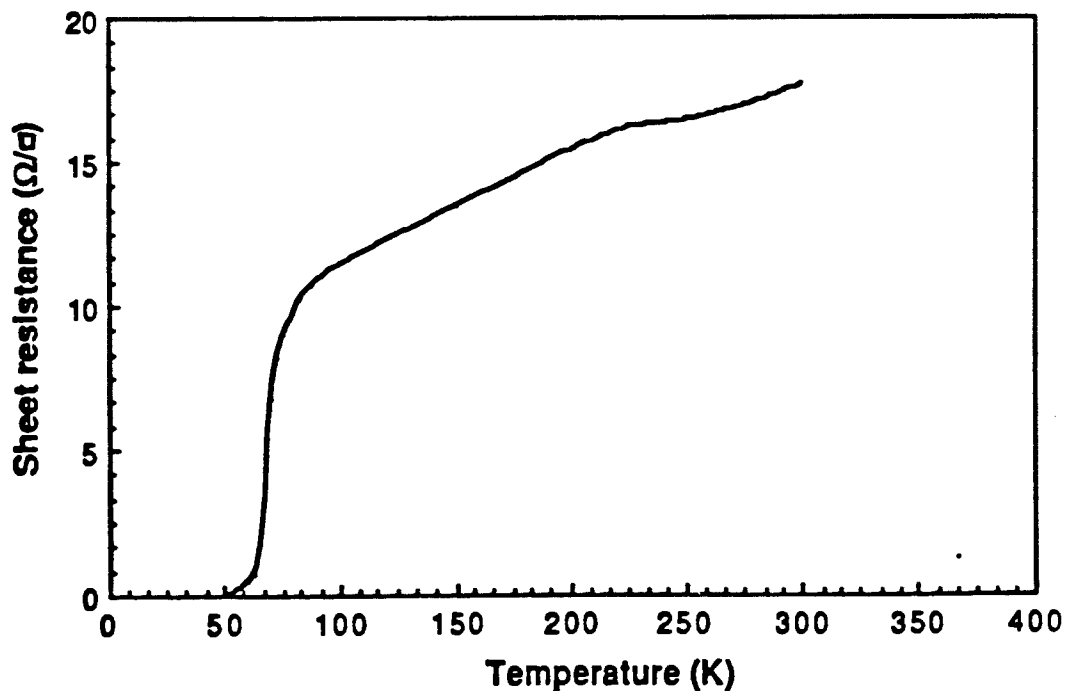
Fig. 3.17. R vs. T curve for a $B_1Sr_{1.2}Ca_{1.5}Cu_{2.7}O_x$ film on (100) MgO annealed up to 865 C.

3.3.3 In-Situ Sputter Deposition of YBCO

For most potential applications of high-T_c superconductors, a critical current density of order 10^6 A/cm^2 is necessary. This requires growth of highly oriented

films, rather than the randomly oriented films we had been obtaining using substrates other than $SrTiO_3$. It had been suggested in the literature that heating to intermediate temperatures, of order 600 - 700 °C, should permit deposition of oriented YBCO films on a wider range of substrates, without the need for an 850 °C post-anneal.[14] This would also reduce the tendency for substrate reaction and film roughening that tend to occur during the post-anneal.

Substrate temperature was measured using a thermocouple, clamped between two substrates, mounted in the sample holder next to the sample being deposited. Unfortunately, the maximum temperature with the quartz heater at full power was about 640 °C, and this also led to excessive heating of the chamber lid. Nevertheless, several runs were carried out at this temperature. The heater was turned on and presputtering started about half an hour before the shutter was opened. Temperatures of 600 - 640 °C appeared to be sufficient to grow the basic perovskite phase on zirconia substrates, although perhaps with defects that would depress the superconducting properties.

A temperatures in excess of 600 °C, however, there is unlikely to be sufficient oxygen in the films for them to be superconducting as deposited. One approach is for additional oxygen to be added during an external 500 °C anneal in one atm. of oxygen. Alternatively, we had increased the oxygen pressure to 1 Torr just after stopping sputtering, and incorporated the oxygen right in the vacuum chamber. It is important, however, not to cool down through the crucial 400 - 500 °C range too fast - at lower temperatures, oxygen diffuses too slowly to be of use.

These films were smooth and fairly shiny as deposited, although there was some haze in most films. Figure 3.18 shows a SEM micrograph of one film deposited on (100) ZrO_2 at 640 °C from a stoichiometric target. The film shows long range crystalline order indicating some sort of epitaxy with the substrate is taking place. This

is somewhat surprising as the lattice mismatch between YBCO and ZrO_2 is 35%. Upon closer inspection of the SEM one can identify at least two crystalline orientations. Figure 3.19 shows the x-ray diffraction pattern for this film. There is a high degree of c-axis aligned material and some randomly oriented material (as evidenced by the (110) peak) as well. This film was cooled after deposition in the absence of oxygen, so that its initial behavior was highly semiconducting. However, a 1-hour anneal in oxygen followed by a slow cooldown was enough to make it fully superconducting at 75 K. Figure 3.20 shows the R vs. T and J_c vs. T curves for the sample shown in Fig. 3.18. We have obtained similar behavior in other samples cooled slowly immediately after deposition in 1 Torr of oxygen. Although the critical temperature was somewhat depressed relative to the best post-annealed samples, the critical currents were substantially increased. In addition, films as thin as 0.4 μm prepared in this way had comparable superconducting properties, in contrast to those deposited on zirconia at low temperatures which had depressed T_cs.
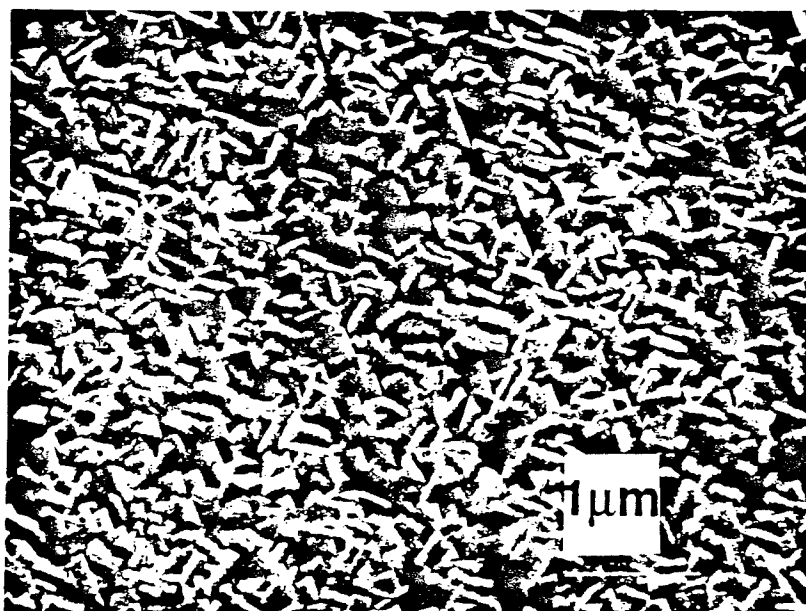
Fig. 3.18. SEM micrograph for YBCO film on (100) ZrO_2 deposited at 640 °C by rf magnetron sputtering.
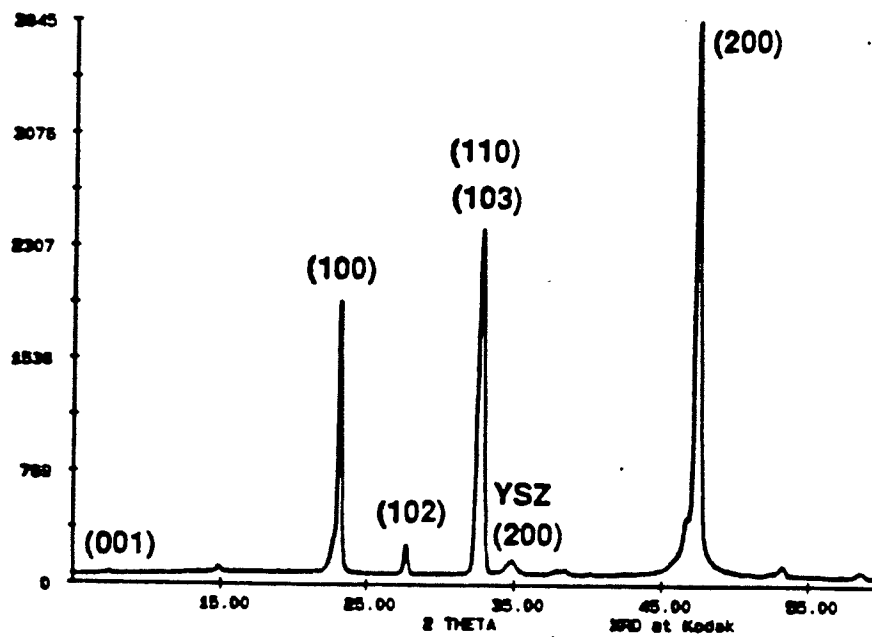
Fig. 3.19 X-ray diffraction curve for film shown in Fig. 3.18.
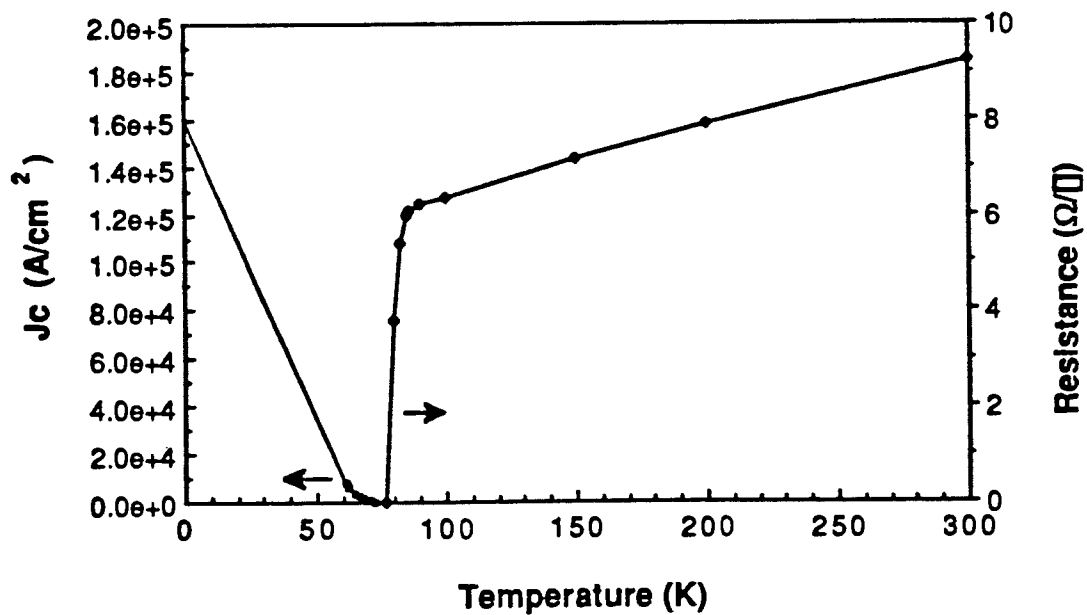
Fig. 3.20. R vs. T and J_c vs. T for YBCO film shown in Fig. 3.18.

Some of the superconducting as-deposited films were subjected to the high-temperaure 850 °C post-anneal used earlier. The films retained the same smooth, crystalline morphology as deposited, and did not develop the rough randomly oriented features as did the low-T deposited films. In addition, the zero-resistance temperature improved from 75 K to 85 K, implying that defects or impurities that depressed T_c were largely being annealed out.

Introduction of the inconel substrate heater described in Section 3.1.4 (and Appendix C) allowed the deposition temperature to be increased up to 800 °C. Films deposited on MgO, $LaGaO_3$, and $SrTiO_3$ substrates at 675 C showed sharp superconducting transitions with T_cs of 72 - 78 K and J_cs on the order of 10^5 A/cm^2 @ 4 K. While these results were encouraging, they still fell short of our goal of T_c = 90 K. X-ray diffraction curves revealed the c-axis lattice parameter of these films was approximately 11.8 Å, as compared to the bulk value of 11.67 Å. Such an extended c-axis is often associated with an oxygen deficient $YBCO_{7-\delta}$ structure. However, post-deposition anneals at temperatures up to 700 °C did not significantly constrict the c-axis nor raise the T_c. Other groups[52] have also seen this behavior and have attributed it to non-oxygen defects. Some further improvement in T_c was achieved by changing the target composition from $Y_{.167}Ba_{.333}Cu_{.500}$ to $Y_{.143}Ba_{.286}Cu_{.571}$, although the superconducting properties was still less than ideal and there were significant numbers of CuO particles on the surface of the film. Further discussion of compositional effects of magnetron sputtered films are given in section 3.3.5.

3.3.4 Negative Ion Shield.

To further minimize any remaining structural defects and/or compositional shifts caused by negative ion bombardment, we developed and installed a grounded shield which was placed directly opposite the substrate and just above the center of the

magnetron target (Figure 3.21). The resistive transitions for two films sputter-deposited on MgO with and without the ion shield are shown in Fig. 3.22. Both of these films were deposited in separate runs using a Cu rich $(Y_{.143}Ba_{.286}Cu_{.571})$ powdered target with a substrate temperature of 675 °C and a sputtering gas consisting of 20 mTorr Ar and 10 mTorr O_2. After deposition, the high vacuum valve was closed and the Ar/O_2 gas flow was continued until the total pressure reached 2 Torr. During this time (about 1 hour) the substrate cooled to 360 °C. Without the negative ion shield, $\rho(300K) = 1700$ $\mu\Omega$-cm, T_c was about 80 K, and the c-axis lattice parameter was found to be extended from the ideal 11.67 Å to 11.86 Å. With the shield in place, $\rho(300K) = 550$ $\mu\Omega$-cm, T_c was increased to 85 K, and c=11.67 Å was observed. The ion shield did not appear to affect film composition or deposition rate as it was placed inside the target dark space shield and did not block the sputtered flux. In addition to further reducing the ion and/or electron flux to the substrate, it is possible that the ion shield helps to improve temperature control of the substrate by reflecting some of the heat back onto the film.

It should be noted that the basic sputtering configuration we have developed is essentially the same as other "off axis sputtering"[37] reported in the literature, in which the substrates are placed off to the side of a small area magnetron source. In our arrangement, however, the sputtered flux originates from a complete ring around the substrate and can thus be considered an integrated off-axis approach. Thus our method leads to higher deposition rates and better thickness uniformity without the need to rotate the substrate holder. Another variant of our geometry which has been used successfully is the inverted cylindrical magnetron[50] in which the YBCO target forms the inside diameter of a hollow cylinder.
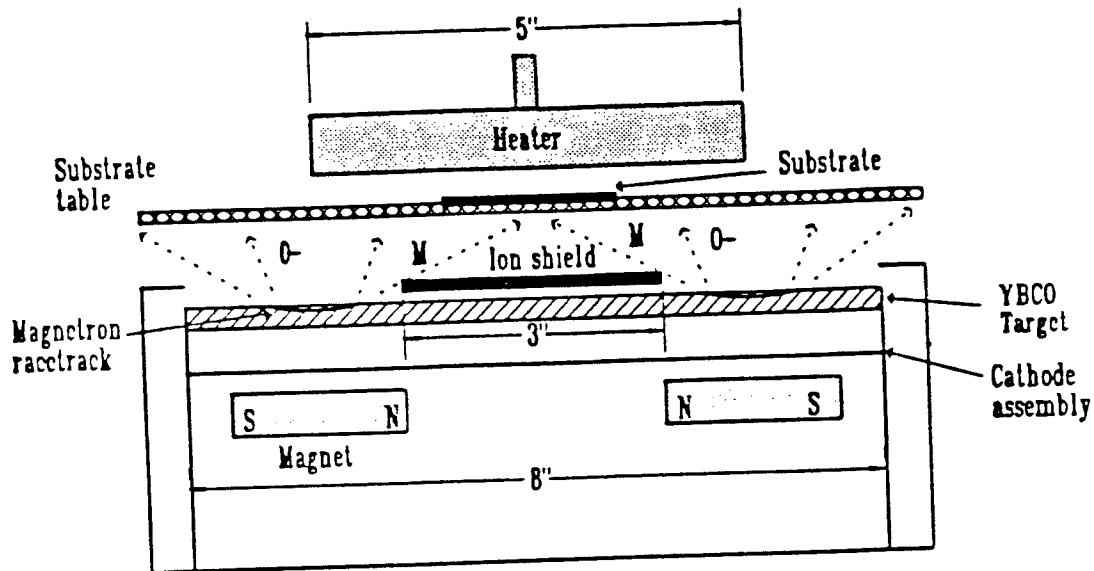
Fig. 3.21. Schematic of rf magnetron sputtering arrangement with negative ion shield.
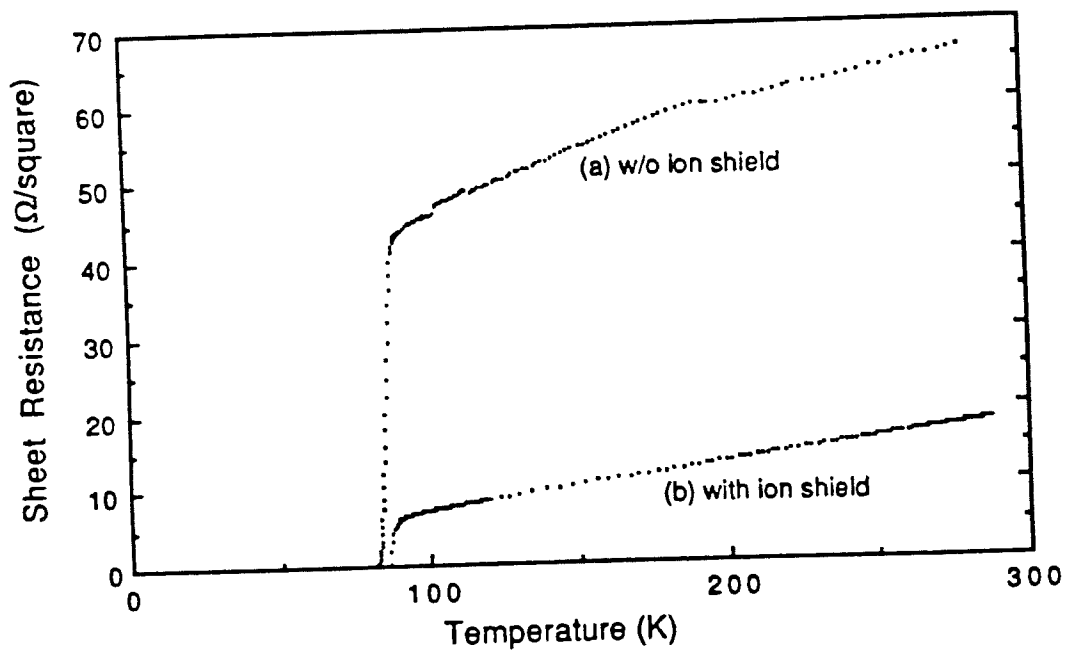
Fig. 3.22. The R vs. T curves for two YBCO films deposited from a Cu-rich target (a) with and (b) without the negative ion shield.

3.3.5 Process Optimization

Having created the proper geometry for YBCO deposition, we began to optimize the deposition conditions. Table 3.3 lists the parameters we varied, the ranges over which they were varied, and the optimum conditions we established. In this portion of our research we used mainly MgO and LaAlO$_3$ substrates because these were becoming available in the larger sizes (2 -inch diameter and up) and because these materials have relatively low dielectric constants and loss tangents, making them useful for high frequency applications.

Table 3.3. Range of process parameters invesigated and optimum conditions derived for *in-situ* YBCO deposition with negative ion shield.

Parameter	Range	Optimum
Target composition	see Table 3.4	$Y_{.189}Ba_{.301}Cu_{.509}$
Substrates	LaAlO$_3$, MgO	LaAlO$_3$
T-S spacing	2.5 - 5 cm	2.5 cm
Target power	450 W	450 W
Total Pressure	5 - 100 mTorr	30 mTorr
O$_2$:Ar ratio	1:10 - 1:1	1:3
Anneal pressure	30 mTorr - 100 Torr	10 Torr
Substrate temperature	600 - 800 °C	740 °C (MgO)
		780 °C (LaAlO$_3$)
Film thickness	1000 Å - 1 μm	4000 Å
Growth rate	10 - 60 Å/min	35 Å/min

The parameter with the most dramatic effect on superconducting properties is composition. Even though there is only a slight shift in composition between the film and the target with our integrated off axis approach, the effect is still enough to cause formation of secondary phases which can alter superconducting properties and create

surface roughness. Table 3.4 lists the target compositions used and the resulting composition for films deposited on MgO substrates. Target compositions were calculated from the weight of the starting component powders. Film compositions were measured either by ICP or by Rutherford Backscattering (RBS) and are believed to be accurate to within 1 atomic %. Figure 3.23 is a portion of the Y-Ba-Cu-O phase diagram showing target compositions (closed circles) and resulting film compositions (open circles) along with values of T_c for these films.

Table 3.4. YBCO target and resulting film compositions for final optimization

Target #	Target composition (%Y,Ba,Cu)	Film composition (%Y,Ba,Cu)	T_c (K)	$\rho(300)$ ($\mu\Omega$-cm)	$\rho(300)/\rho(100)$
1	17,33,50	14,36,50	50	1700	1.5
2	15,28,57	14,24,63	86	550	2.2
3	20,30,50	18,33,49	83	650	3.5
4	18,31,51	17,33,50	88	350	2.4
5*	19,30,51	17.5,32.7,49.1	90	200	3.1

*Preferred composition.

Films deposited from a stoichiometric target (#1) were Ba-rich. These films had smooth surfaces but had depressed T_cs (50 - 80 K) and extended c-axis lattice parameters of 11.8 Å. Films deposited from a Cu-rich target (#2) were further enriched in Cu and had very rough surfaces with granular Cu-rich material (probably CuO) on top of a highly c-axis oriented underlying film. The T_cs of these films, however, were significantly higher, around 85 - 86 K, and the c-axis was 11.68 Å. Films deposited from a Y-rich target (#3) were only slightly Y-rich with T_cs around 83 K and a c-axis lattice parameter of 11.70. Although the films were smooth and featureless to 0.1 μm under SEM inspection, there was some difficulty in making metallic contact to these

films, caused perhaps by the extreme smoothness and hardness of the film surface. Films deposited from a slightly Y-rich target were within 1% of stoichiometric metallic content and had T_cs of 84 - 88 K. Finally, films deposited from targets with composition halfway between (#3) and (#4) were slightly Y-rich and had T_cs of 85 - 91 K. By following the above iterative process, we arrived at an optimum target composition (#5) of $Y_{.189}Ba_{.301}Cu_{.509}$ which gave films of $Y_{.175}Ba_{.327}Cu_{.491}$.
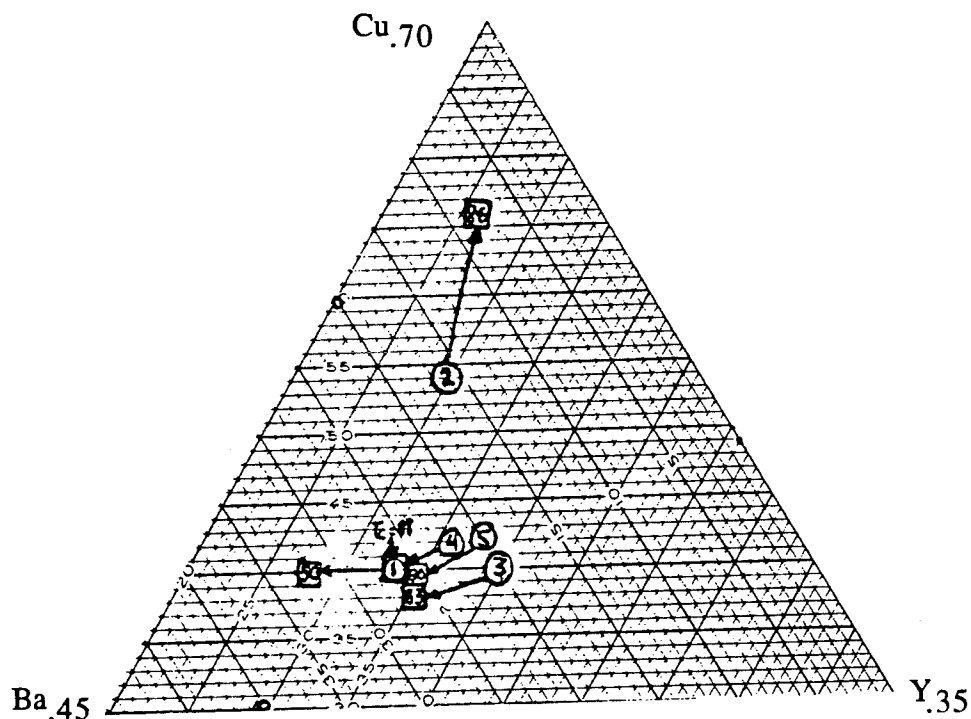
Fig. 3.23 YBCO phase diagram showing composition of the targets we tried (cricles) and resulting film compositions (squares). The critical temperatures of the films are given in the squares.

While the accuracy of our compositional measurements was limited to about 1 atomic %, several observations can be made. The compositional shift between target and film does not always seem to follow the same "path", particularly for the Cu rich films. This may be a result of the large difference in surface morphology of these Cu-rich films. For most of the targets (1,3,4, and 5) the films tended to be enriched in Ba relative to the target. This is in contrast to most other groups doing sputtering of

YBCO[29] and is a result of our geometry. The Ba is preferentially sputtered from the racetrack region and ends up accumulating on the substrate. It appears that films which are slightly Y-rich have better superconducting properties than films that are stoichiometric. This finding is in agreement with Matijasevic et al.[53] who used TEM to determine the excess Y is incorporated as epitaxial precipitates within the $Y_1Ba_2Cu_3O_{7-\delta}$ matrix. Finally, there are definite differences in superconducting properties among films differing in composition by only a few atomic %, which emphasizes the requirement for strict compositional control.

Having obtained the optimum target (and therefore film) composition, we next detemined the optimum substrate temperature. A series of films deposited between 600 and 820 °C showed the optimum to be around 740 °C for MgO and closer to 780 °C for $LaAlO_3$. It is not suprising the optimum deposition temperature depends on the substrate material, as there are various competing conditions present during growth, shuch as lattice match, differential thermal expansion, and chemical interaction.

Sputtering gas total pressure and $Ar:O_2$ ratio were also varied to further optimize film properties. While our investigation was not exhaustive, we found 10 mTorr O_2 and 20 mTorr Ar to be near optimum. It is interesting to note this partial oxygen pressure is significantly less than the 100 - 200 mTorr used by most groups doing either off-axis sputtering or laser ablation. It is also less than what one would expect from the stability map of pressure vs. temperature for the YBCO system. Figure 3.24, taken from Ref. 54, shows the stability line for forming $YBa_2Cu_3O_{7-\delta}$. Our process falls below that line. We explain this by noting the relevant pressure may be that of atomic oxygen, not molecular oxygen. And our process, because the substrate lies in the center of a large plasma ring, provides a high fraction of atomic oxygen.
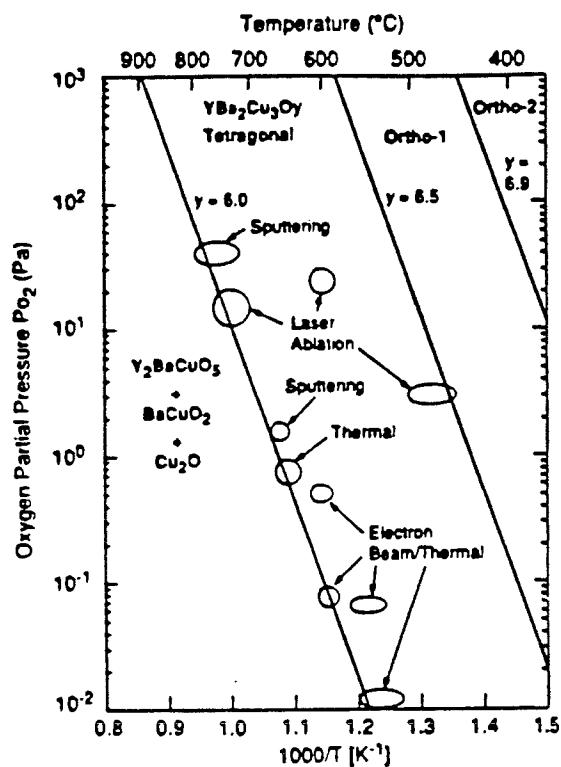
Fig. 3.24. Stability diagram for YBCO (Ref. 54).
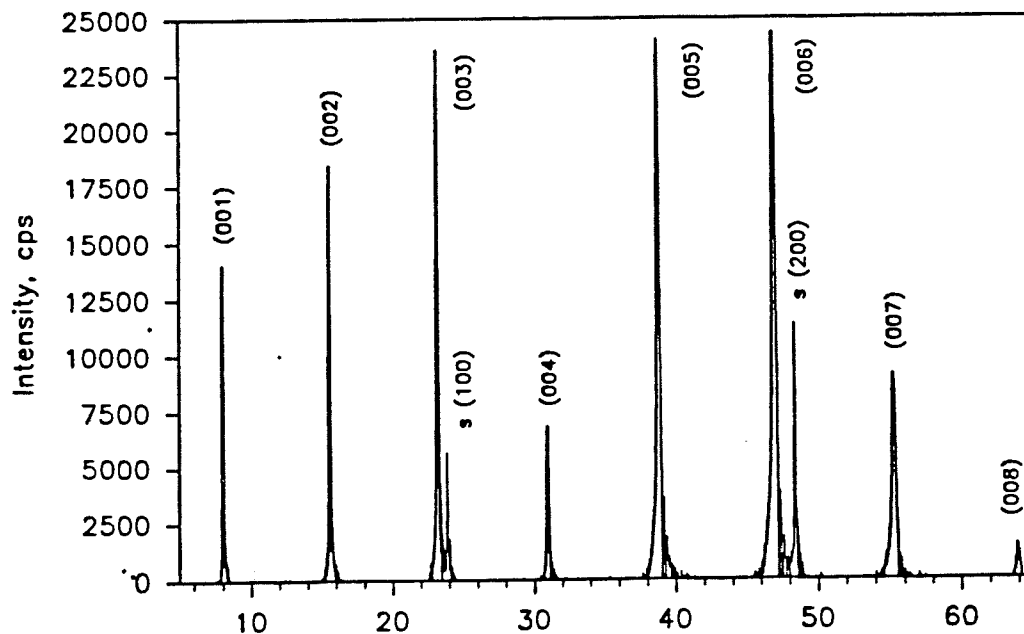
Fig. 3.25 X-ray diffraction curve for YBCO film on LaAlO$_3$ deposited at optimized conditions.

Figure 3.25 shows the x-ray diffraction curve for a 1.2 μm YBCO film on LaAlO₃, showing excellent c-axis alignment and no secondary phases present. Figure 3.26 shows the (004) rocking curve to be 0.16° full width at half max, again indicative of excellent c-axis orientation.
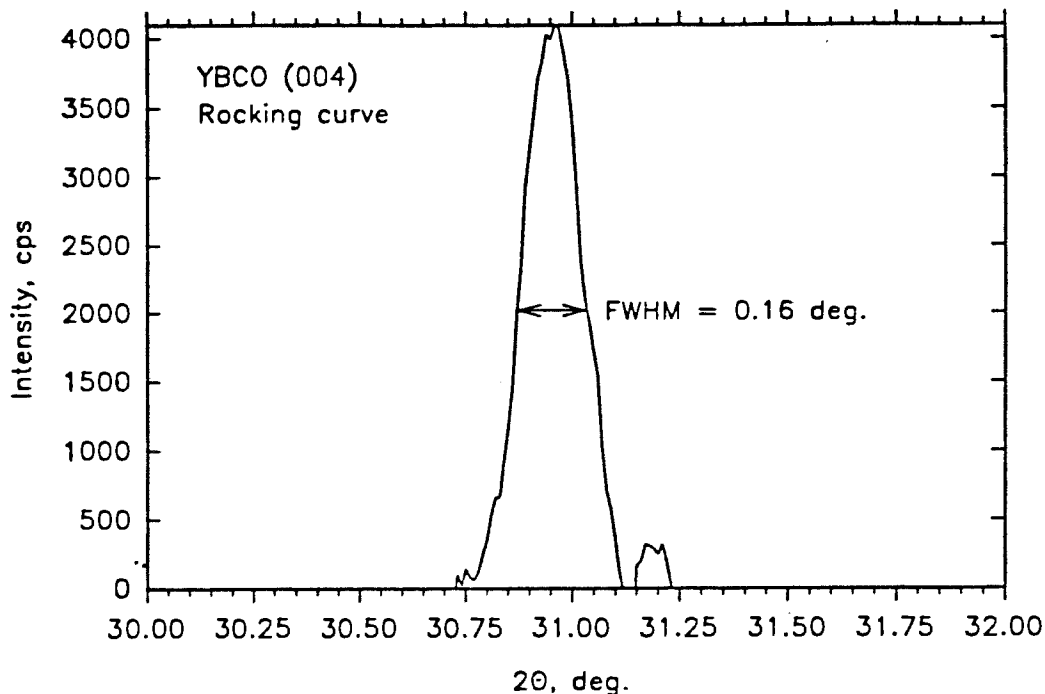
Fig. 3.26 Rocking curve of (004) peak for YBCO film on LaAlO₃ showing FWHM of 0.16°.

Figures 3.27(a) and (b) show the R vs. T curves for YBCO films deposited on MgO and LaAlO₃ respectively using the optimized conditions listed in table 3.3. For a series of tens of films deposited over a two year period, the T_c for films on MgO varied from 85 to 91 K while for LaAlO₃ it was 88 to 91 K. These results were in keeping with most other reseachers who find the repeatability of the process is not as good on MgO as it is on LaAlO₃, possibly due to variations in substrate preparation. The room temperature resistivity of these films was 180 - 200 μΩ-cm. Figure 3.28 shows the critical current vs. temperature for one of our YBCO films on LaAlO₃. The J_c is in excess of 10^6 A/cm² at 80 K.
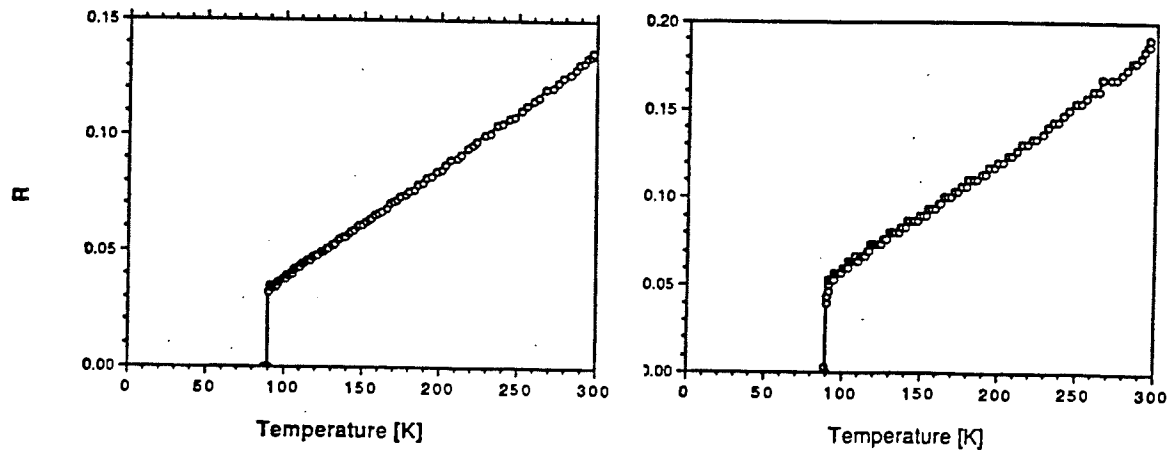
Fig. 3.27 R vs. T curves for YBCO films deposited on (a) MgO and (b) LaAlO$_3$ using optimized conditions listed in Table 3.3.
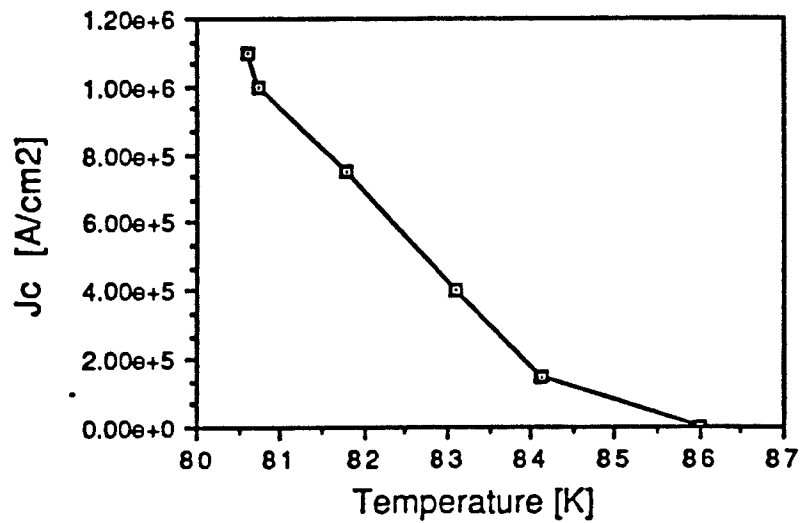
Fig. 3.28. J$_c$ vs. T for YBCO film on LaAlO$_3$ deposited at optimum conditions.

In addition to optimizing superconducting properties, we were also attempting to obtain smooth films which could be patterned into useful devices. While film composition had the most dramatic effect on surface morphology, we also found the electrical potential of the substrate during deposition to have an effect. If the substrate was allowed to contact the grouned support, the films tended to be dull in appearance and rough under the SEM, with CuO particles on the surface. Films that were electrically floating, on the other hand, tended to be shiny and free of surface defects down to the 0.1 μm level.

Good uniformity, in both thickness and superconducting properties, over large areas (relative to what is currently being achieved) is another property we were aiming to optimize. Figure 3.29 shows the thickness plot for films deposited at three different pressures. The uniformity is better than +/- 5% across a 5 cm diameter. Figure 3.30 shows the uniformity in room temperature resistivity for films deposited at 30 mTorr. Note the average value is higher than the 180 μΩ-cm we achieved because this data was taken with an earlier target composition (target #4). Further improvements in uniformity may be possible by adjusting the target-to-substrate spacing and increasing the diameter of the magnetron racetrack and/or negative ion shield.

3.4 Microwave Measurements

Although passive microwave applications are not the central focus of this thesis, we review in this section some work on the measurement of microwave surface resistance of the films we deposited. We do this first because films developed by this process may be used for microwave applications in the future and second because the surface resistance is a very sensitive probe of the quality of superconducting films.
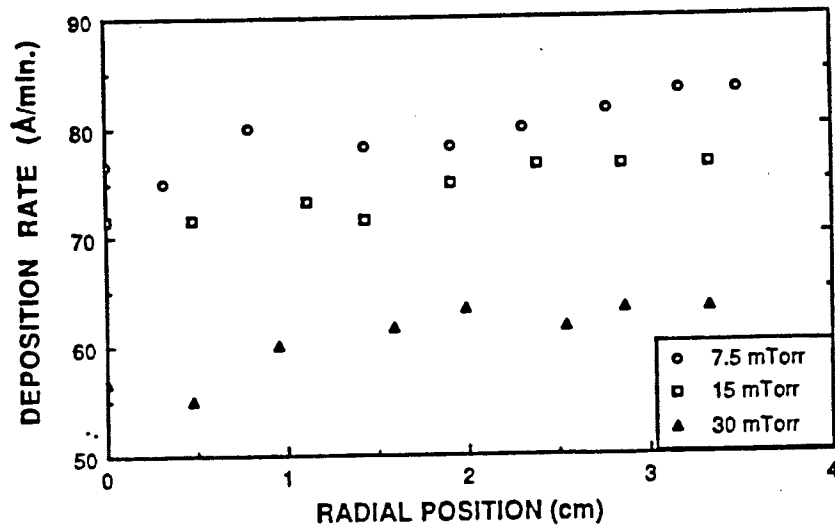
Fig. 3.29 Thickness uniformity for YBCO deposited at optimized conditions.
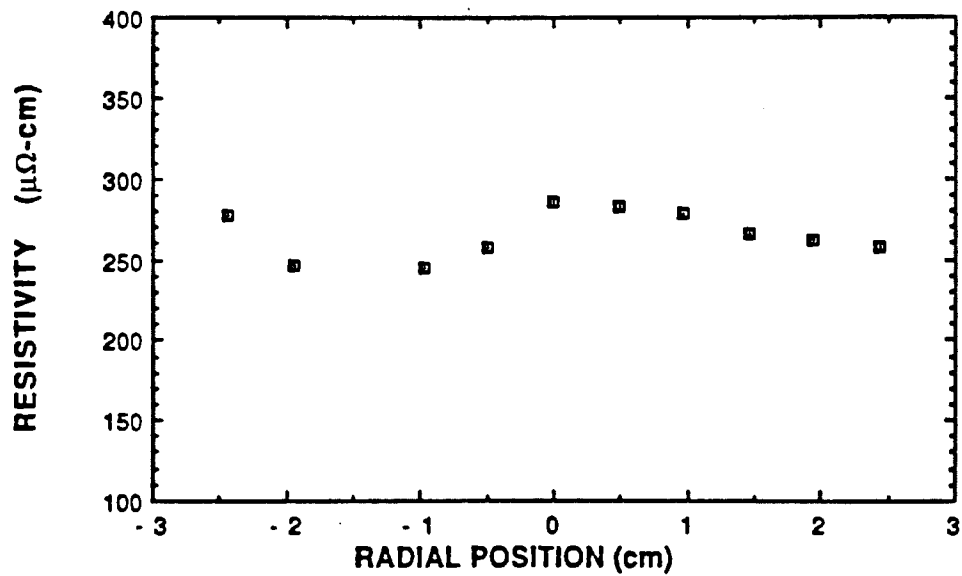
Fig. 3.30. Uniformity in room temperature sheet resistance for YBCO.

Superconductors have true zero resistance only for dc current. At high frequencies, the inductance of the Cooper pairs creates a voltage which causes normal electrons to oscillate and therefore absorb energy. Figure 3.31[3] shows the surface resistance vs. frequency for a normal metal (Cu at 77 K) as well as for high qality YBCO films also at 77 K. It can be seen that for frequencies below 100 GHz, the YBCO films can have significantly lower surface resistance. This feature permits higher performance and/or smaller sizes in a variety of microwave devices, such as high-Q resonators, narrowband filters, and high-performance antennas.
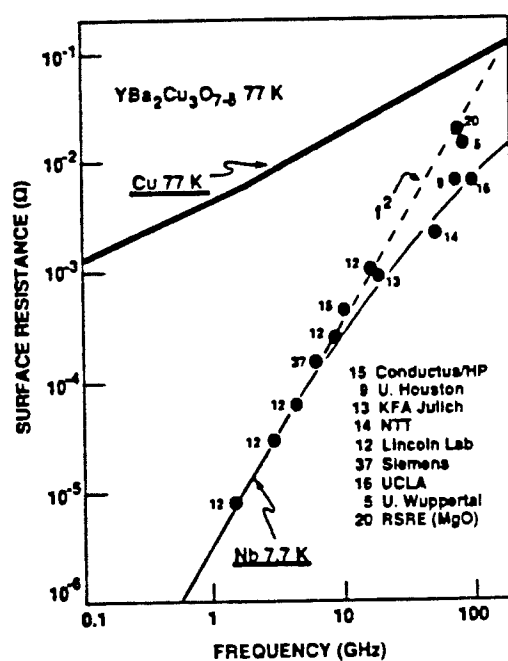
Fig. 3.31 Surface resistance vs. frequency for Cu and YBCO thin films at 77 K. (From Ref. 3)

The microwave surface resistance of the films deposited by the UR/CVC collaboration has been characterized by several groups, including an in-house effort at the U of R.[55] Using the two-port parallel resonator techniqe[56], we measured the

surface resistance at 12.4 GHz from 4.2 to 80 K (Fig. 3.32). At 77 K, we see R_S
equal to 0.45 mΩ. When extrapolated to 10 GHz using a ω^2 dependence, the results
are found to be consistent with the best results achieved to date (see Fig. 3.31). Films
deposited on 2-inch diameter LaAlO$_3$ were sent to J. Martens at Sandia National
Laborotory for characterization using a confocal resonator technique[57] (Fig. 33). This
method is unique in that it provides spatial resolution in measurement of R_S. The
average R_S at 77 K and 10 GHz is 0.6 mΩ, and the uniformity of R_S is better than +/-
5% across 2 inches.
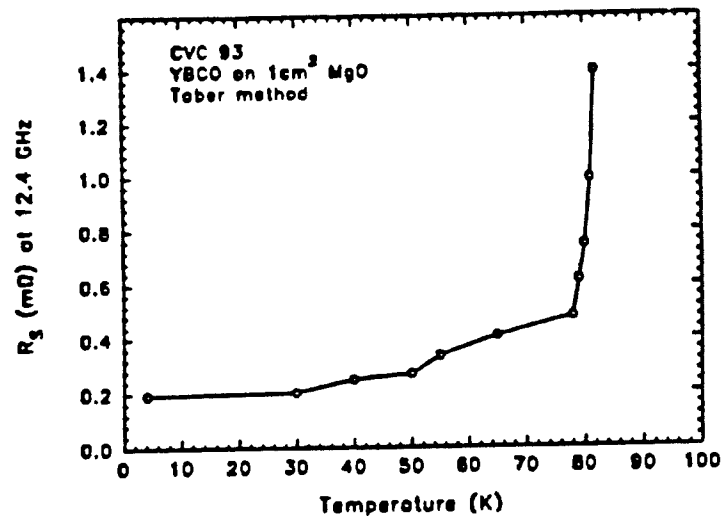
Fig. 3.32. Surface resistance vs. temperature for UR/CVC HTS film at 12.5 GHz measured with
parallel plate resonator technique at the U of R (From Ref. 55).

3.5 Summary

In this chapter we have discussed the development of our sputtering process for superconducting YBCO thin films. We have shown that loose powder targets may be used to provide high quality films provided the proper precautions are taken. RF magnetron sputtering can be used to avoid negative ion bombardment by placing the substrate above the center of an 8-inch diameter target. Further improvement in performance is obtained with use of the negative ion shield. *In-situ* formation of the HTS phase with excellent crystalline orientation can be obtained by heating the substrates to 740 - 780 °C during deposition. Films deposited in this manner are smooth and uniform across 2-inch diameter substrates. We can regularly deposit films with T_cs close to 90 K, J_cs in excess of 10^6 A/cm^2 at 77 K, and a microwave surface resistance of ≈ 0.3 mΩ at 10 GHz and 77 K.
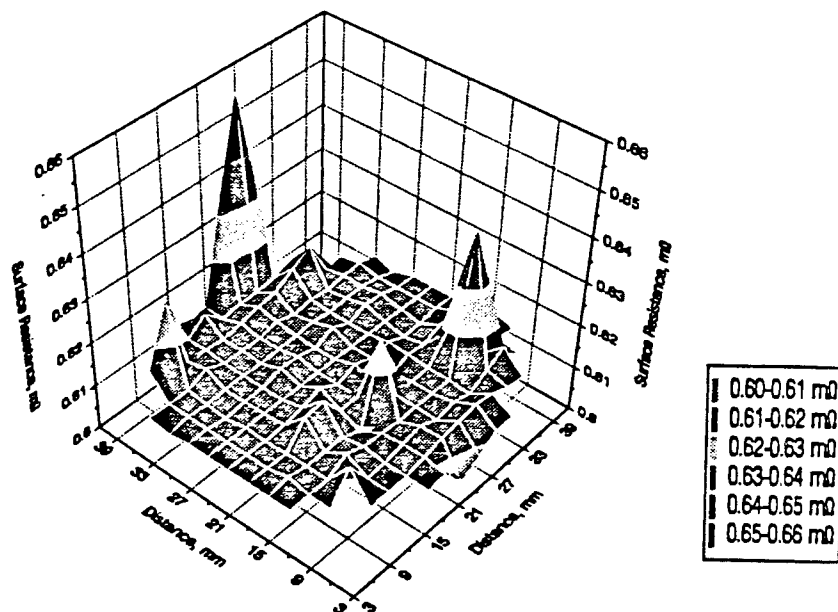
Fig. 3.33. Uniformity of R_s at 77 K and 10 GHz for 0.6 μm thick YBCO on 2-inch diameter LaAlO$_3$ measured using the confocal resonator technique.

Chapter 4

Fast Optoelectronic Response of YBCO Films

Having developed the ability to make good YBCO films, we wanted to explore a possible optoelectronic device application for these films. Dr. William Donaldson at the UR Laboratory for Laser Energetics was interested in the possibility of applying superconducting films to a fast, optically triggered, high current opening switch (Fig. 4.1). In such a switch, a superconducting shunt would pass a large current with little or no resistance in the initial off state. When the superconductor is illuminated by a fast laser pulse, this would be expected to quickly drive the film (possibly by heating) into the highly resistive normal state. This, in turn, would permit the current in the shunt to be quickly diverted to a load down the line. As the superconductor cooled, the switch would close again, allowing the switch to be used repetitively.
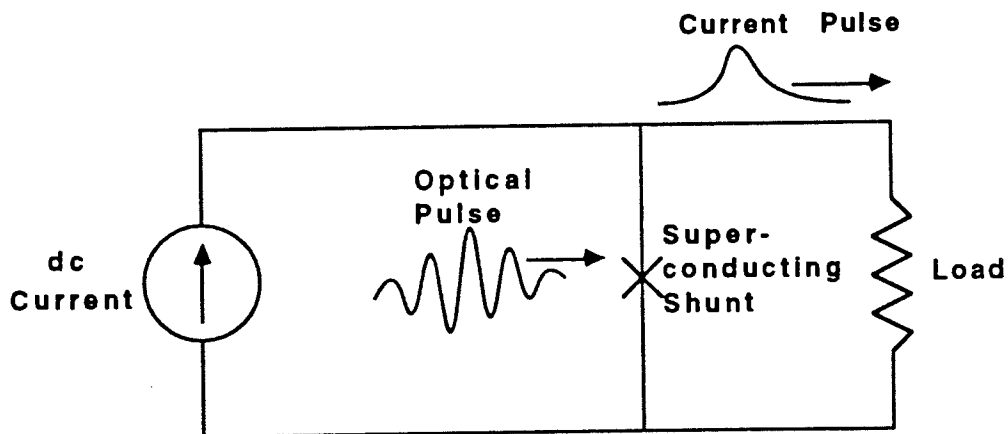
Fig. 4.1. Schematic representation of superconducting fast opening switch .

Such a superconducting opening switch is directly analogous to a semiconducting closing switch that Dr. Donaldson had previously investigated[59]. In this application, a large voltage is initially applied across a high-resistance, intrinsic semiconductor. A fast laser pulse incident on the semiconductor produces excess carriers, thus lowering the resistance and sending a fast voltage pulse down the line. While such fast, repeatable, high-performance closing switches are now well established with pulsewidths on the picosecond timescale, no equivalent fast opening switches have been available.

There had earlier been some work using conventional low-temperature superconducting films (NbN) in an optically triggered opening switch[60], which had not led to any practical applications. However, the new high-T_c superconductors have three potential advantages:

1) They can operate at liquid nitrogen temperatures instead of liquid helium temperatures.

2) They have a somewhat higher resistance in the normal state than typical low-T_c superconductors, increasing the on-off contrast.

3) They are black and highly absorbing in the visible and near-infrared, as compared with more conventional high metallic reflectivity in the low T_c materials.

With this in mind, we set out to determine whether these advantages could be translated into a real device using YBCO thin films, and to understand the basis for the fast optoelectronic response that would determine the performance of such a device. Before describing the experiments done to test the fast photoresponse, we will review the nature of the optical response in both HTS and LTS materials.

4.1 Overview of Superconducting Optical Response

The key question that repeatedly comes up in the study of the optical response of superconductors is this: *Is it bolometric or non-bolometric?* In this context, a bolometric response is one that can be characterized in terms of heating of the superconductor, in thermal equilibrium. A non-bolometric response is one that is non-equilibrium in some important respect, and may involve excess numbers of electron and hole excitations (also referred to as superconducting "quasiparticles") or possibly quantized vortices.

A comparison to a photoconductive semiconductor may be useful here. An intrinsic semiconductor at low temperatures is an insulator, with virtually no electron or hole excitations to carry current. The energy gap E_g is typically of order 1-2 eV, which is also the energy of a photon in the visible to near infrared. If a photon with energy greater than the energy gap is incident on the semiconductor, it can be absorbed to create two excitations, an electron in the conduction band and a hole in the valence band (we are assuming a direct-band semiconductor here). These excitations will continue to exist in the semiconductor until they are either swept out of the material or recombine, and can be relatively long-lived. They are non-equilibrium in the sense that these two excitations do not represent the thermal equilibrium distribution at any temperature, and the lattice in the semiconductor is not heated up to any significant degree.

A superconductor is somewhat more complicated. There is an energy gap 2Δ, but it is much smaller than that in a semiconductor; of order 1 meV for LTS, and 10 meV for HTS materials. In the two-fluid representation of a superconductor, there are two classes of carriers:

1) Superconducting electrons, which can be considered to be bound together in "Cooper pairs" with energy gap 2Δ, and which can carry current with no resistance.

2) Normal electrons and holes, or quasiparticles, which can also carry current but exhibit the usual resistance. At dc, their effects are shunted out by the pairs, but the loss is evident at microwave frequencies and above.

In thermal equilibrium, the energy gap 2Δ is determined by a self-consistency equation with the quasiparticles, which have a thermal distribution, maintained at the lattice temperature by interactions between phonons and quasiparticles. The phonons in the superconductor, in turn, are in thermal equilibrium with the phonons in the substrate and sample holder which support the superconducting film.

What happens when a photon with energy $E >> 2\Delta$ is incident on a superconductor [61]? The first thing that happens is the creation of a single electron-hole pair, but these very quickly (on the fs scale) spread their energy among a large number of quasiparticles, breaking a lot of Cooper pairs in the process. This increases the effective electron temperature T_e in the superconductor, and decreases Δ. This is not yet in thermal equilibrium, however, since T_e may still be elevated above the effective temperature T_l of the lattice. The excess quasiparticles can recombine fairly quickly, typically on the order of an electron-phonon collision time on the picosecond timescale, and equilibrate with the lattice. However, it takes a somewhat longer time (typically on the nanosecond timescale) for this heated superconductor to cool down to the ambient substrate temperature (or "bath temperature") T_b. And it may take even longer, on the microsecond timescale, for the excess heat in the substrate to be conducted through to the sample holder.

This cascade of cooling is summarized in Fig. 4.2. In this context, "electron heating" is generally considered a non-bolometric response; whereas film heating or sample heating is bolometric.

Photon

Pairs	Quasiparticles		Phonons in Film		Substrate
Electrons T_e			T_l		T_b

	Timescale	Temperatures
Electron Heating	fs	$T_e > T_l = T_b$
Film Heating	ps	$T_e = T_l > T_b$
Sample Equilibrium	ns	$T_e = T_l = T_b$
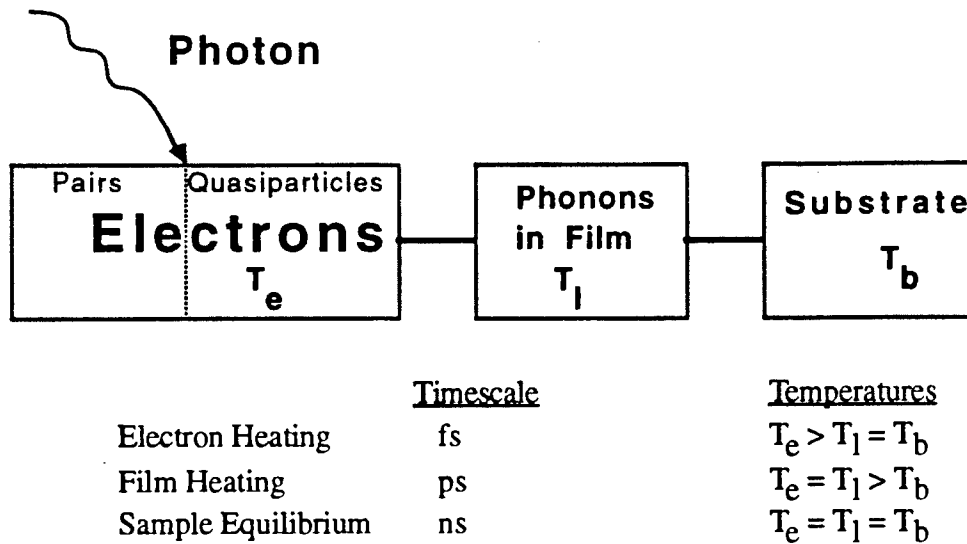
Fig. 4.2. Transient energy balance in a superconductor. The photon energy heats up the electrons on a fs timescale, is transferred to the phonons in the film (T_l) on the ps scale, and to the substrate (T_b) on the ns scale.

There has been great interest in possible application of HTS thin films to fast, sensitive optical detectors, particularly for infrared radiation.[62-64] One type of broad-band infrared detector is a bolometer, which depends on sample heating, measured by a thermometer, to determine the level of incident radiation. For a superconducting bolometer, the most common such thermometer is the resistive transition of the superconductor itself. If the superconductor is held at a temperature in the middle of its resistive transition (typically 85 - 90 K for YBCO), then for a very small temperature rise, the resistance change will be proportional to dR/dT, so that a fairly sharp transition is preferable. Bolometers have a reputation for being very slow, but this is not necessarily the case; it depends on the thermal coupling between the film (or the film-substrate combination) and the thermal bath. YBCO microbolometers have been fabricated that exhibit sensitive performance with a response time below a ms.[65]

Still, a non-bolometric detector offers the possibility of a much faster detector.

There have been a large number of observations of the photoresponse of YBCO and related HTS thin films 66-74. In most cases, a bolometric effect is identified, but in some cases an additional non-bolometric effect is identified is certain regimes. This has been a continuing subject of debate for a number of years. How does one unambiguously distinguish a bolometric from a non-bolometric effect? There is no single feature, but a bolometric response has a number of general characteristics:

1) If the film is biased within the resistive transition, then the response should be proportional to dR/dT in the limit of small incident power. If it is biased below the resistive transition, then there should be a threshold power below which no response is seen.

2) A bolometric response may roll off at high frequencies. However, several bolometric responses with different response times are possible in complicated systems with several thermal couplings.

3) A bolometric response should be largely independent of the wavelength of the radiation, as long as the absorption efficiency remains constant.

A second debate in the field of the superconducting photoresponse has been over whether granular films behave differently than homogenous superconducting films. In this context, a granular film is often viewed as a random array of Josephson junctions, and it is well known that Josephson junctions are very sensitive detectors of electromagnetic radiation, at least below the energy gap. A number of researchers have seen evidence of a nonbolometric photoresponse in granular HTS films, but not in epitaxial HTS films. Other researchers, looking at similar samples of either type, see only a bolometric response.

Probably the clearest examples of a non-bolometric response are those which use an optical excitation of a few ps or less, and see evidence which can be interpreted as fast electron heating and cooling, followed by a slower cooling of the film via the

substrate .[75,76] It was concluded that the electron-phonon relaxation time is of order a few ps at high temperatures, rising to perhaps a hundred ps at 4 K. Everything happening at slower time scales is essentially simple heating.

There is another class of explanations for photoresponse of YBCO and other superconducting films, involving vortices or fluxons, each with quantized flux $\Phi_0 =$ h/2e. These are normally associated with an external magnetic field, and motion of vortices across a superconductor leads to resistance. However, vortices are often immobilized by being "pinned" on impurities or other defects in the superconductor; in that case, they do not cause resistance. If an optical pulse causes transient depinning of vortices in a superconductor, then a voltage pulse could result. Some evidence of ths response been seen in YBCO films .[77] This effect cannot be described in terms of any simple heating, so that it is clearly non-bolometric. However, it is unclear whether it is fast enough to be the basis of an opening switch or a fast IR detector.

Another related non-bolometric mechanism for optical detection in a superconductor was recently proposed by Kadin, et al..[78] In a sufficiently thin superconducting film, the energy of a vortex may become comparable to a photon energy, and then a vortx-antivortex pair can in principle be excited by a photon, even in the absence of an external magnetic field. In the presence of a large transport current, these vortices move transversely to the current, and can create a rather fast voltage pulse in a narrow superconducting line. Such a mechanism could lead to a sensitive detector; preliminary evidence in ultrathin NbN films gave good agreement with the theory and indicated a response 1000 times larger than a bolometric response. There is not yet any evidence that this also holds for HTS superconductors, although the theory should be fairly general.

4.2 Fast Laser Switching Experiments

Optically triggered fast switching of YBCO thin films was demonstrated using 150 ps infrared pulses from a Nd:YAG laser (λ = 1.06 μm). Both granular and epitaxial films were tested, both optically thin and optically thick, prepared using either single target sputtering, or alternatively, co-evaporation (see Table 4.1). Our key result [79], which we will explain below, is that all effects for all samples appear to be bolometric on the ns timescale, with some indirect evidence of fast nonequilibrium effects happening on a shorter timescale.

Sputtered YBCO samples were prepared by single target sputtering, either at CVC or UR, by the methods described in Chapter 3. Early sputtered samples were deposited cold followed by a high-temperature post-anneal, and were granular. Later samples were deposited in-situ without a post-anneal and were oriented or epitaxial. In addition, some samples (#4 and #5 in Table 4.1) were fabricated by Prof. John Scofield of Oberlin College. These were prepared by coevaporation of Y, Cu, and BaF_2 onto epitaxial perovskite substrates ($SrTiO_3$ and $LaGaO_3$), and post-annealed to obtained fairly smooth, high quality, epitaxial YBCO films.[80]

Table 4.1. YBCO samples used for laser switching experiments.

Sample	Dep. Method	Substrate	Morph.	Thickness (μm)	$T_c/\Delta T_c$ (K)	J_c @ T (kA/cm^2)
#1	Sputter/Anneal	YSZ	Granular	0.7	60/20	1 @ 18 K
#2	Sputter/In Situ	MgO	Epi	0.5	50/30	5 @ 40 K
#3	Sputter/In Situ	MgO	Epi	0.2	55/20	12 @ 45 K
#4	Coevap/Anneal	SrTiO$_3$	Epi	0.5	89/2	>100 @ 77 K
#5	Coevap/Anneal	LaGaO$_3$	Epi	0.5	75/10	90 @ 60 K
#6	Sputter/In Situ	MgO	Epi	0.7	79/10	>30 @ 75 K

60'K
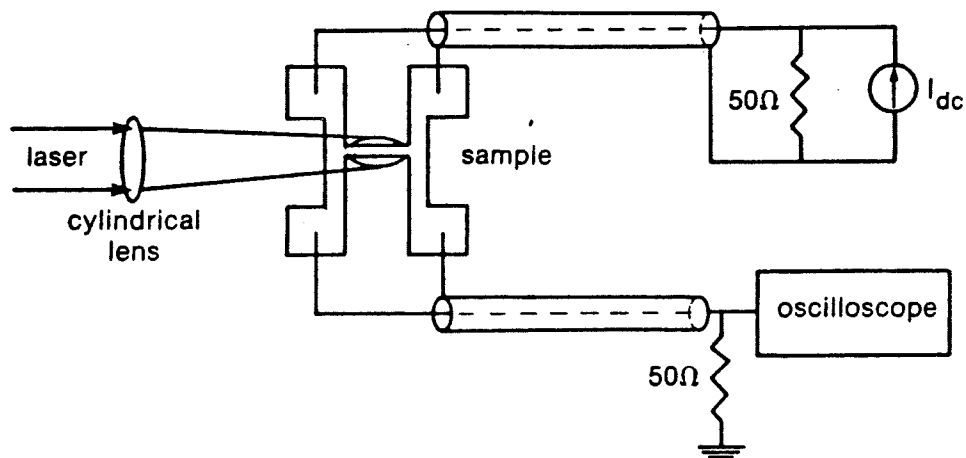
Fig. 4.3. Experimental setup for pulsed laser excitation of superconducting samples.

A schematic of the experimental setup is shown in Fig. 4.3. The films were patterned into an H-shaped structure using laser ablation[81], with a central bridge region 2 mm long x 60 - 250 μm wide acting as the switch. The patterning was carried out using a pulsed Nd:YAG laser with regenerative amplification, with 150 ps pulses at a repetition rate of order 1 kHz. With 10 μJ/pulse, focused down to a 20 μm spot (a fluence $\approx$ 3 J/cm^2), the laser could etch a line through a 1-μm-thick film scanned at 1 mm/s using computer controlled stepper motors.

Evaporated silver contacts were used to reduce contact resistance and heating, with Al wire bonds to terminated 50 Ω coaxial lines to minimize noise and dispersion. The sample was mounted inside an evacuated optical access dewar, and the temperature could be controlled from 10 to 100 K. A dc current bias was applied to the top of the structure, and could be varied from 0.1 to 100 mA.

The same Nd:YAG pulsed laser as for the patterning was used to illuminate the sample for photoresponse measurements, but with a fluence/pulse of a few mJ/cm^2 rather than a few J/cm^2. The pulses, each with up to 100 μJ of energy, repeated at a rate that could be varied from 50 Hz to 1 kHz. The switch was illuminated (from the top) through a quartz window with a 3 mm-wide beam that was focused down with a cylindrical lens so as to completely illuminate the bridge region. The voltage was measured using either a fast analog scope (350 MHz) or a digital sampling scope (200 MHz). Care was taken to avoid possible transmission line reflections in the circuit.

As an example of a granular film, consider the resistive transition of sample #1, shown in Fig. 4.4. This 0.7 μm film had been patterned into a bridge that was 2 mm long by 200 μm wide. This exhibited zero resistance at about 60 K for a small measurement current of 10 μA, but T_c was further depressed to 40 K for a measurement current of 1 mA, more typical of the current level in the photoresponse experiments. The critical current was only of order 1 mA even at lower temperatures, which works out to a current density of order a kA/cm^2 for this granular film.

An example of the transient response of sample #1 to a 150 ps pulse is shown in Fig. 4.5, on the 10 ns timescale. Since the full normal-state resistance of the switch was about 500 Ω, much greater than the 50 Ω line impedance, a parallel combination of the two was measured. The data were taken for T = 17 K, for a current I = 2 mA and incident fluences of 0.53, 2.1, and 6.7 mJ/cm^2. In this case, the switch was biased slightly above the critical current so that the initial voltage is nonzero. Also, there was not significant delay on this scale between the laser pulse and the voltage; the zero on the time axis is arbitrary. When the laser pulse is incident, there is a sharp rise in voltage in about 2 ns, a slower rise in voltage on the scale of 10 - 100 ns (missing in

some cases), and a slow decay back to the background level with a characteristic time of about 1 μs. The fast rise and slow relaxation on these timescales were present for all parameters studied. The measured rise time may be limited by dispersion in the measurement circuit.
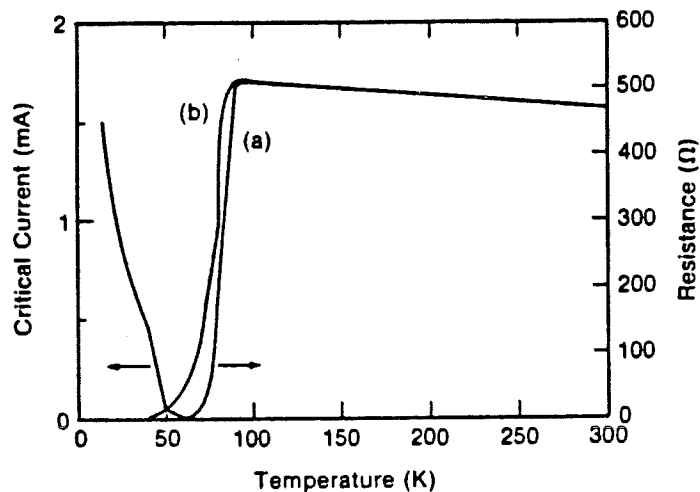
Fig. 4.4. R(T) for granular YBCO film #1 using two measuring currents: (a) I=10 μA, and (b) I=1 mA. Also plotted is the critical current $I_c(T)$.
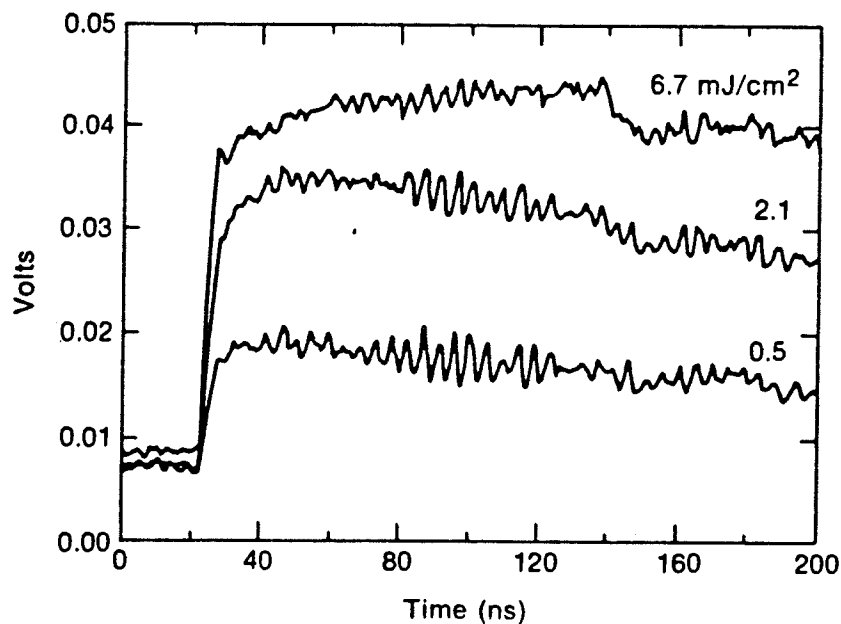
Fig. 4.5. Transient response of sample #1 to a 150 ps Nd:YAG pulse, for several values of laser fluence, for T=17 K and I=2 mA. The zero on the time axis is arbitrary.

The other samples described were all highly c-axis oriented, with somewhat larger low-temperature critical currents. They were morphologically much smoother, and are referred to generically as "epitaxial". The resistive transitions for samples #2 and #3 are shown in Fig. 4.6, together with that of sample #1. Both were sputtered onto heated cleaved MgO substrates, and were superconducting in situ without a high temperature anneal. Sample #2 was 500 nm thick, and exhibited T_c of 50 K and I_c of 5 mA at 40 K ($J_c = 5000$ A/cm^2). Sample #3 was 175 nm, with T_c=55 K and I_c=12 mA at 45 K ($J_c = 10^5$ A/cm^2). These samples were prepared before the in situ sputtering process was completely optimized, but SEM photos showed a smooth surface and XRD patterns indicated a highly c-axis oriented film with no impurity phases.

Fig. 4.7 shows the transient response of Sample #2 at T=28 K, with I_{dc}= 1 mA, and laser fluence F=0.93 mJ/cm^2. In this case, there is an initial fast rise in 1 ns, followed by a slower rise of about 10 ns and a decay time of about 40 ns. Fig. 4.8 shows the corresponding curve for Sample #3 at T=35 K, I=1 mA, and F=0.48 mJ/cm^2. Here again, there is a 1 ns rise followed by a 20 ns decay.
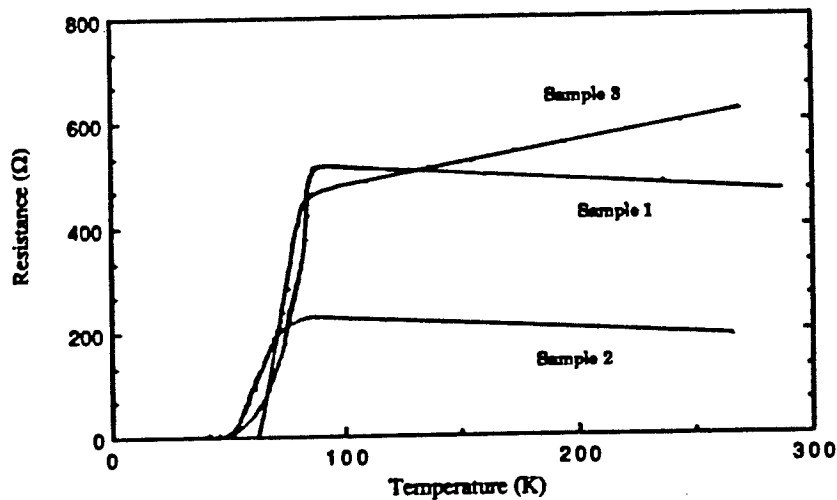
Fig. 4.6. R(T) for YBCO sputtered samples #1, #2, and #3 (see Table 4.1).
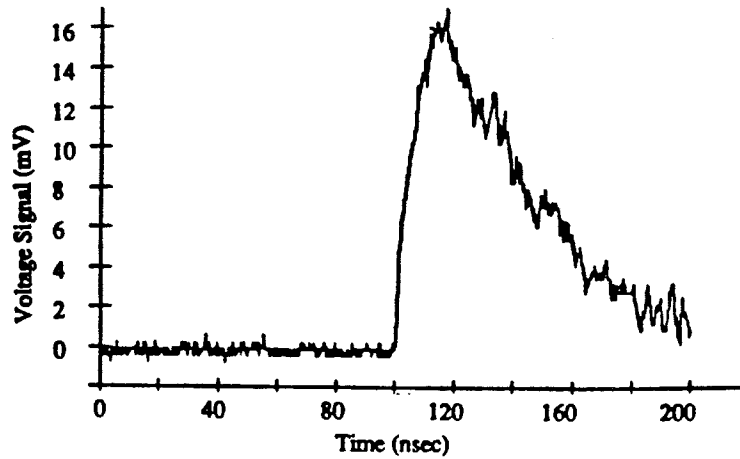
Fig. 4.7. Response of sample #2 to F = 0.93 mJ/cm^2 for T=28 K and I=1 mA.
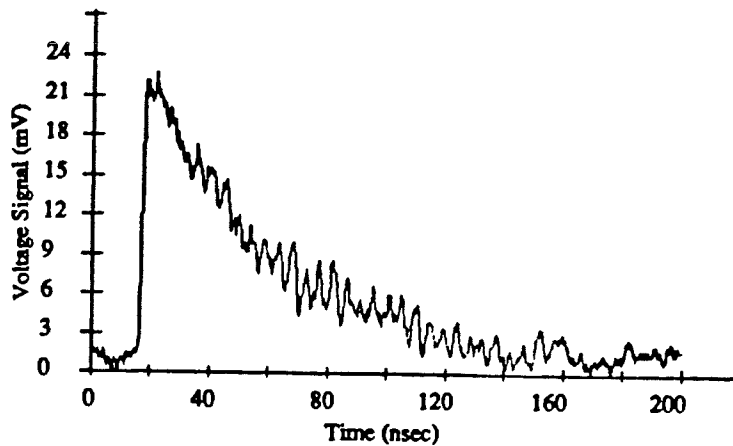
Fig. 4.8. Response of sample #3 to F=0.48 mJ/cm^2 for T=35 K and I = 1 mA.

Samples #4 and #5 were evaporated post-annealed samples from Oberlin College, both 500 nm thick on epitaxial LaGaO$_3$ and SrTiO$_3$ respectively. Sample #4 exhibited T$_c$=75 K and I$_c$(65 K) = 50 mA (J$_c$ = 10 kA/cm^2), and sample #5 showed T$_c$=89 K and I$_c$(77) > 100 mA (J$_c$ > 100 kA/cm^2). Fig. 4.9 shows three transient

response curves for sample #4 at T=60 K, for three different combinations of dc bias and laser fluence. It can be seen that the rise time can be either fast (10 - 90% of rise in 2 ns), slow (≈20 ns), or a combination of both. The relaxation back to the superconducting state took over 50 - 100 ns. At 60 K, the purely slow response occurred only for low values of current and laser fluence. Fig. 4.10 shows the response for sample #5, at T=60 K and I=10 mA. Here, only the slow (20 ns) rise is visible, followed by about a 50 ns cooling.
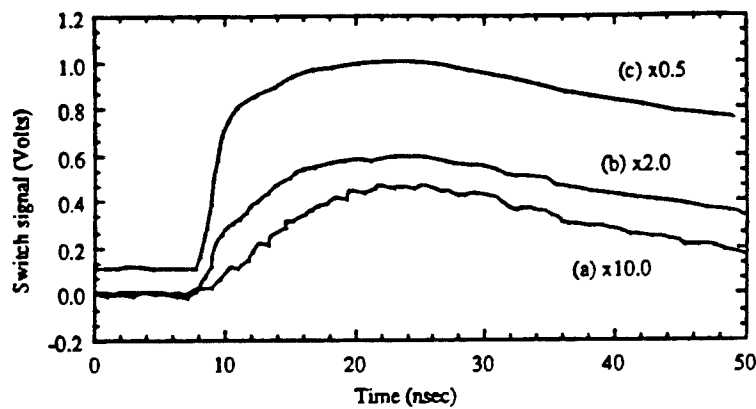
Fig. 4.9. Transient response of sample #4 at 60 K with laser fluence of 0.92 mJ/cm^2, for three different values of current. (a) I=10mA, (b) I=30 mA, and (c) I=100 mA. Note that I_c(60 K) = 90 mA.
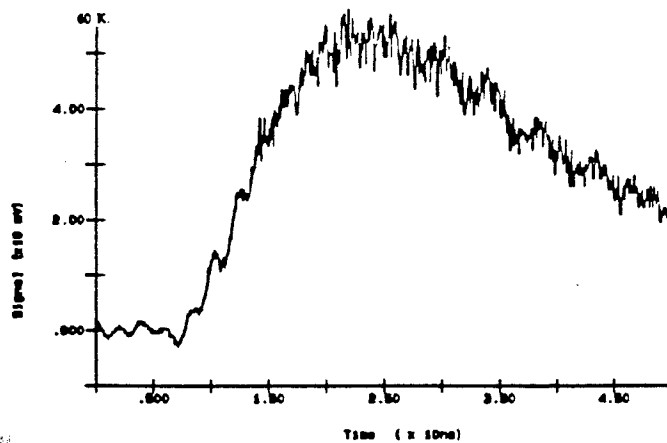
Fig. 4.10. Transient response of sample #5, at T=60 K with I=10 mA.

Finally, large currents can be switched at high temperatures using high-quality sputtered films on polished MgO, as well. Fig. 4.11 shows the resistive transition for an in-situ sputtered YBCO film prepared at UR (sample #6), with $T_c = 79$ K. The transient response of this film is displayed in Fig. 4.12, for I=30 mA and F=8.7 mJ/cm^2, at T=70 K and T=75 K. Note that the rise time is slow ($\approx$ 40 ns) at 70 K, but is much faster ($\approx$ 2ns) at 75 K under otherwise identical conditions.
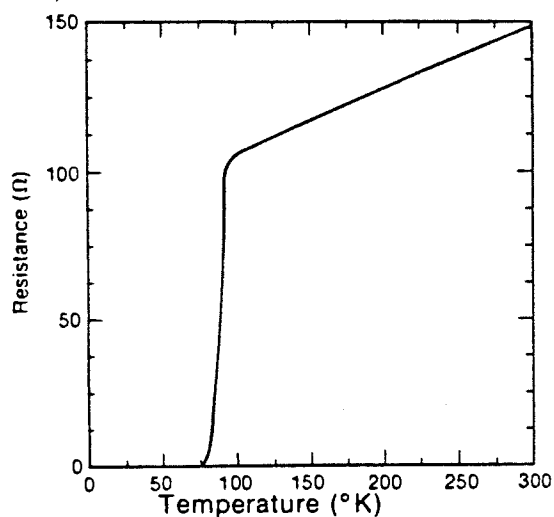
Fig. 4.11. R(T) for YBCO sputtered sample #6, with T_c=79 K (see Table 4.1).
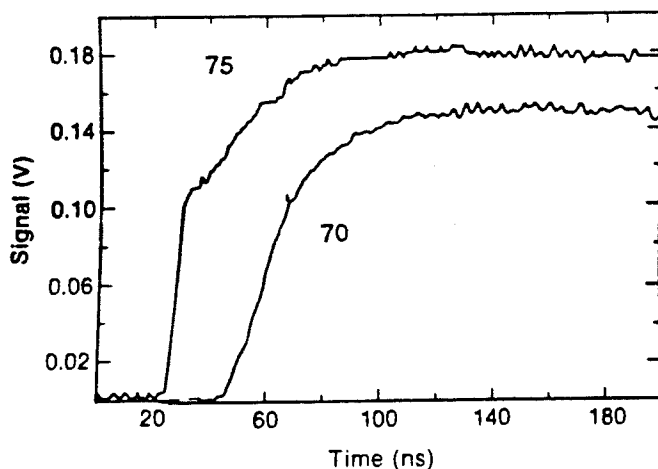
Fig. 4.12. Transient response of sputtered YBCO sample #6 with F= 8.7 mJ/cm^2 with I = 30 mA, at T=70 K and T=75 K.

4.3 Analysis of Results

The previous section presented quite a lot of data from a number of different samples. However, most of it can be understood within the context of a simple heating picture.

We start out by addressing the results for sample #3, which was 175 nm thick. The optical absorption depth for one of our YBCO films was measured using a spectrophotometer and found to be about 120 nm, only weakly dependent on wavelength. This is consistent with other reports in the literature. Sample #3 is a bit thicker than this, but can be considered optically thin. The laser beam then penetrates through the film, heating it fairly uniformly. The ambient temperature is far below T_c, and the bias current is well below I_c. We should then expect to see a fast voltage response if the effective film temperature is raised above T_c. The rise time should be on the order of the optical pulse width, about 0.15 ns. This is consistent with the pulse shape in Fig. 4.8, which exhibits a very sharp onset which is limited by the 1 ns resolution of the measurement.

The fall time would be expected to reflect the time for the film to cool down below T_c again. This will occur primarily through heat diffusion through the film to the substrate. Equilibrium thermal transport is governed by the thermal diffusivity $D = K/C$, where K is the thermal conductivity and C the heat capacity per unit volume. These were not measured for these films, but an upper estimate of K at 25 K (for a single crystal) is of order 0.01 W/cm-K, and the value of C at a similar temperature is 0.1 J/cm^3-K.[82] These correspond to $D \approx 0.1$ cm^2/sec, or diffusion of 300 nm in 10 ns. Furthermore, several groups have pointed out that there is an excess thermal boundary resistance at the interface between HTS films and many substrates, which would tend to slow down the cooloff even further.[83] Together, this is consistent with

the 20 ns decay time for the pulse observed in Fig. 4.8.

Further confirmation of the thermal nature of the response can be obtained by evaluating the magnitude of the response, i.e., the voltage peak in Fig. 4.8. In Fig. 4.13, we plot the magnitude of the voltage peak for sample #3, for a range of laser fluences. We also compare to a simple theoretical model. We make the simplest possible assumption, that all of the optical fluence goes into heating the film uniformly through its thickness, before any conduction to the substrate takes place. (We neglect the small amount of reflection that occurs at this wavelength.) Then, the expected temperature rise of a film of thickness d due to a fluence F, from the initial value T_0 to the peak temperature T_p, can be calculated using the temperature dependent heat capacity $C(T)$:

$$\int_{T_0}^{T_p} C(T)\, dT = \frac{F}{d} \qquad (4.1)$$

For simplicity, we use a linear approximation to the heat capacity,

$$C(T) \approx (T - 17K) \times 16\ \text{mJ/cm}^3 K^2, \qquad (4.2)$$

which is a reasonable approximation between about 20 and 100 K.[81] This in turn provides a simple analytic expression for the fluence needed to heat the film to some value of T_p:

$$F = (d/2) \times [(T_p - 17)^2 - (T_0 - 17)^2] \qquad (4.3)$$

The advantage of such an analytic expression is that it can be calculated on a spreadsheet. We take the array of measured data points from the dc $R(T)$ curve. For each value of T, we substitute in for T_p in Eq. (4.3) to determine the corresponding fluence F. The peak voltage is calculated by multiplying the dc bias current by the resistance R of the switch in parallel with the two 50 Ω transmission lines (Fig. 4.1).

There is clearly excellent agreement between the experimental and theoretical values of the peak voltage, with no adjustable parameters. Both theory and experiment exhibit a threshold fluence, below which no pulse occurs. This represents the minimum fluence needed to heat the film above T_c. Both sets of theory and experiment also exhibit a saturation fluence, above which the film is heated fully into its normal state, so that no further voltage increase should occur.

Note that the threshold fluence in the experiment is somewhat lower than that in the theory curve in Fig. 4.13. This may be due to exceeding the critical current at a temperature just below T_c. It might have been more accurate, therefore, to measure the dc R(T) curve with the same 1 mA current used in the photoresponse measurements. Still the level of agreement is quite satisfactory, particularly given the fairly crude approximations used. There is certainly no need to invoke any kind of nonequilibrium mechanism to obtain better agreement. Evidently, the laser pulse is heating the sample by tens of degrees above its ambient temperature.
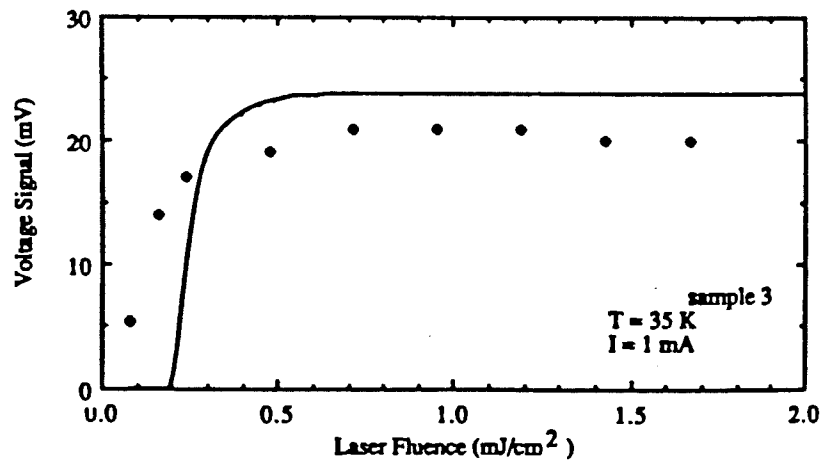
Fig. 4.13. Peak voltage vs. laser fluence for sample #3 with T=35 K and I = 1 mA. The dots are the experimental values and the solid line is a theory curve assuming a model of simple, unform heating.

For optically thick films, it is not at all obvious that this simple thermal model should hold. In particular, one would expect that the heating would be very non-uniform, since it is initially deposited in the top 100 - 200 nm of a film that is 500 - 700 nm thick. We will get back to this issue later. However, if we simply assume for the time being that the voltage peak corresponds to a uniform heat distribution, we can apply the same analysis as was used to obtain Fig. 4.13. These are shown in Fig. 4.14, for samples #1 and #2. In all cases, there is excellent agreement, again with no adjustable parameters. Fig. 4.14 exhibits no threshold since the bias current was already slightly above the critical current at this temperature. Evidently, the magnitudes of the photoresponse corresponds to simple heating even in the optically thick samples.
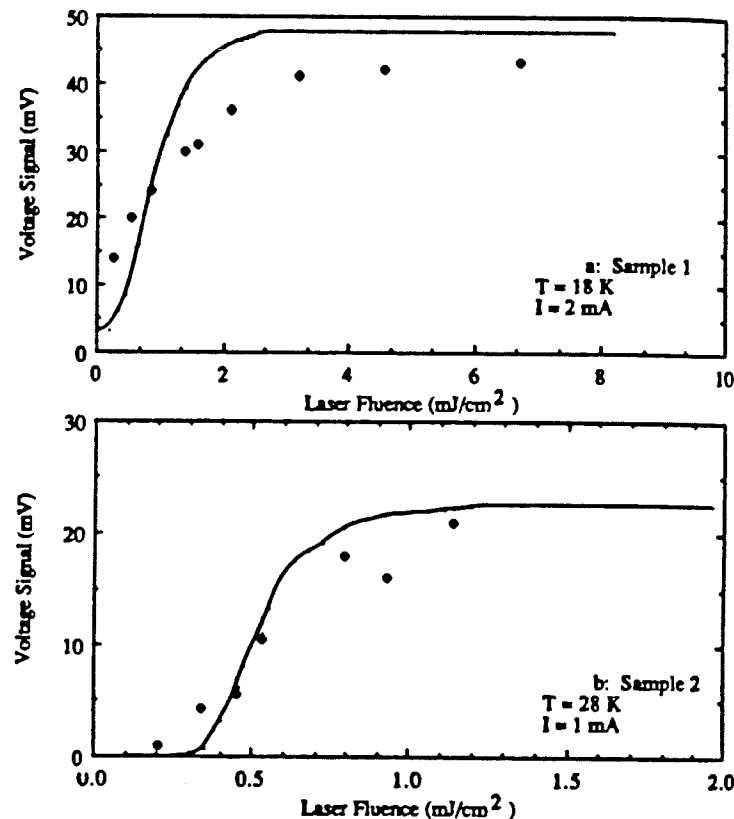
Fig. 4.14. Measured (dots) and calculated (lines) voltage response vs. laser fluence for samples #1 (a) and #2 (b). The calculated response is based on a simple heating model.

The decays of the voltage pulses also make sense in terms of a heating model. The decay time would be expected to get longer for thicker films, essentially as d^2 for heat diffusion, and that generally seems to be the case. The decay time seems to be particularly long for sample #1, where it approaches a μs. However, in this case (one of the first samples tested with an early setup), the substrate may not have been well thermally sunk to the sample holder, which might account for the difference.

The initial voltage rises for the optically thick films are not quite as clear within this heating picture. What we would expect is that initially, just the top 100 - 200 nm would heat up, and that the remainder of the film would remain superconducting until the heat spreads down through the film. The current can very quickly divert into a deeper layer of the film that is still superconducting. This current redistribution should occur much faster than equilibrium heat flow into the film (see below), and prevent any fast voltage rise from occurring.

This can be understood in terms of the characteristic times for the problem (see Table 4.2). A straightforward application of Maxwell's equations shows that field penetration into a conductor (essentially the ac skin depth) occurs by a diffusive process with a characteristic electromagnetic diffusivity $D_{em} = \rho/\mu_0 \approx 10^4$ cm^2/sec, where $\rho \approx$ 100 $\mu\Omega$-cm is the normal resistivity of this film. This corresponds to $t_{em} = d^2/D_{em} =$ 10 fs for current to divert around a normal layer $\approx$ 100 nm thick, much faster the optical pulsewidth.

In contrast, the thermal distribution time should be smaller than but comparable to the cooldown time; $t_h = d^2/D \approx 25$ ns for distribution about 500 nm through the film. What we would expect to see in our optically thick films, then, is a delay time of order

10 - 20 ns, followed by a gradual increase in voltage as the bottom of the sample heats up through the resistive transition. The sharpness of the voltage rise would then be expected to reflect the sharpness of the resistive transition.

Table 4.2. Characteristic Response Times in Pulsed YBCO Films

Physical Process	Time (ps)
Optical Pulsewidth	150
Current Redistribution	0.01
Electrical Risetime	<2000 to >10,000
Heat Flow	>10,000
Electron-Phonon Scattering	1 to 100

A somewhat more quantitative analysis of the heat distribution in an optically thick film was done by numerical simulation. We assumed that the heat was instantaneously deposited in the film by exponential absorption in the optical penetration depth. Following that, thermal diffusion caused the heat to spread down through the remainder of the film via the diffusion equation, using the estimated temperature dependent thermal diffusivity. The resulting temperature profile is shown for various times after the pulse, in Figs. 4.15 and 4.16.

Fig. 4.15 describes a 2 μm film initially at 20 K, subjected to a pulse with fluence 2 mJ/cm^2. This should be similar to the situation of sample #1 in Fig. 4.5, which was 0.7 μm thick. Fig. 4.15 indicates that although the initial temperature at the front surface of the film is very high (150 K!), it would take about 50 ns for the back of the film to reach 40 K, at which point the critical current would be exceeded and a voltage would start to appear. It would take over 500 ns for the back of the film to reach 80 K, which would complete the resistive transition and should correspond to the voltage peak. This was not what was oberved in Fig. 4.5, for which there was a negligible delay followed by a very fast (2 ns) voltage rise.
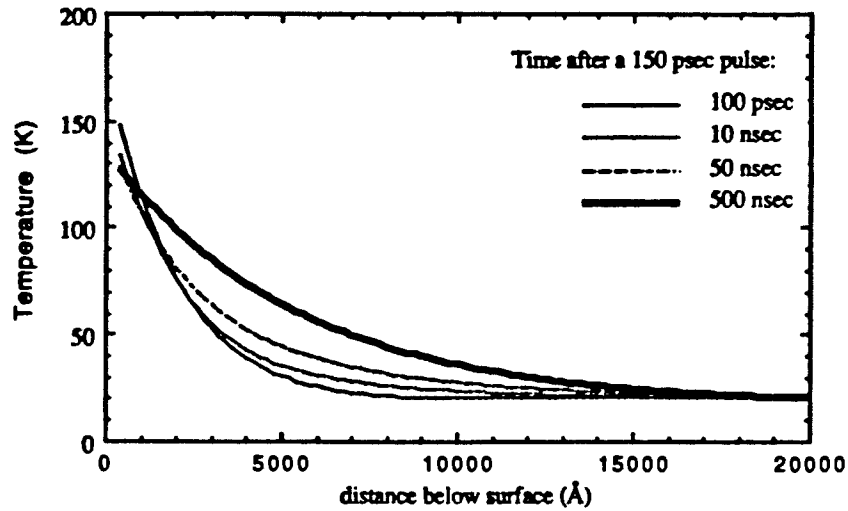
Fig. 4.15. Temperature profile from numerical simulation of optical heating of YBCO film. The optical fluence was 2 mJ/cm^2, and the initial temperature 20 K, corresponding to sample #1 (Fig.5.4).
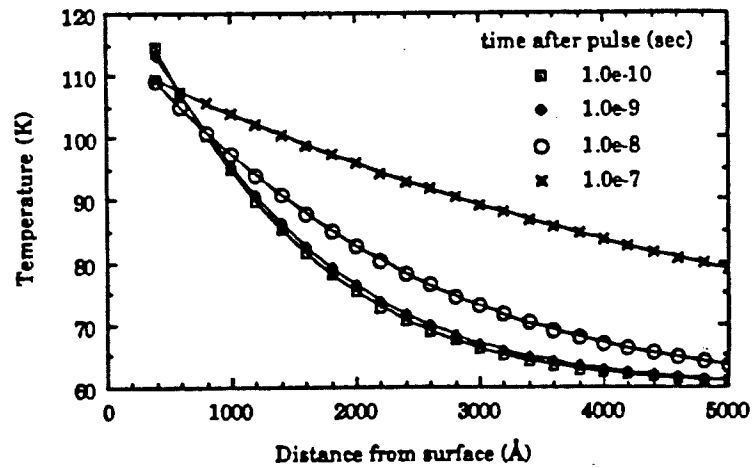
Fig. 4.16. Temperature profile from numerical simulation of optical heating of YBCO film. The optical fluence was 0.92 mJ/cm^2, and the initial temperature 60 K, corresponding to sample #4 (Fig. 4.9).

Similarly, Fig. 4.16 was set up to model the transient effects for sample #4 (Fig. 5.9), which is 500 nm thick, for a laser fluence of 0.92 mJ/cm^2. It would take almost 10 ns to raise the temperature at the back of the film to 75 K, to start the voltage pulse, and probably another 10 - 20 ns to raise it to 90 K, corresponding to the voltage peak. Although the onset delay was not carefully measured for this sample, this is actually similar to the behavior observed for the smallest test current in Fig. 4.9. This does not, however, appear to explain the faster rise for larger currents.

Some other samples also exhibit results consistent with simple thermal diffusion. For example, sample #5 showed only a slow (20 ns) rise, as shown in Fig. 4.10, for all combinations of fluence, temperature, and current tested. In addition, sample #6 also showed this slow rise in certain cases, but a fast (2 ns) rise in other cases (Fig. 4.12). Evidently, thermal diffusion is certainly involved with these results, but something else is also going on as well.

It is noteworthy for these optically thick samples, the evidence for the faster switching occurs only for large currents, relatively close to T_c. Here, we believe that the fast rise results when the current is shifted into the lower unheated portions of the film, exceeding the critical current in the portion of the film that is still superconducting. As pointed out above, this current redistribution is very fast. For example, in Fig. 4.9, the curve showing the fastest rise is the one where the critical current is already exceeded at I=100 mA even before the laser pulse. Heating up the top portion of this 500 nm film permits that current to be redistributed to the bottom 300 nm, rapidly driving that portion into the fully resistive state.

This may also explain the fast rise in sample #6 at 75 K, very near its T_c when the critical current is likely to be relatively small. In contrast, for sample #5 on $SrTiO_3$,

the critical current at 77 K was so large (well above 100 mA) that it was not possible to see a fast component for the temperatures and bias currents that were tested.

Still, there are some optically thick samples, with broad resistive transitions (samples #1 and #2), that exhibit a sharp rise even when the current is not near the critical current. The magnitude of this sharp rise indicates that the heat is fairly uniformly distributed through the film, within a few nanoseconds of the laser pulse. This cannot be explained by equilibrium heat transfer, which is far too slow. These samples were also distinct in having substantially depressed values of T_c, and were tested at temperatures of 40 K or less.

If neither optical absorption nor equilibrium heat flow is capable of distributing this energy, then an alternative non-equilibrium mechanism must be responsible. We suggest that hot-electron transport, which has previously been demonstrated for optically excited metals such as Cu and Au[84], is likely to provide part of the answer. The initial effect of the radiation is to create a number of highly excited electrons and holes in the top 100 nm of the film. These distribute their energy among other highly excited electrons, which spread diffusively into the film. They then thermalize with the lattice due to electron-phonon scattering, in a relaxation time which is expected to be a few ps at 77 K, but almost 100 ps at 4 K.[85] In this way, non-equilibrium effects on the ps timescale can interact with equilibrium thermal effects on the ns timescale.

The electron diffusivity is expected to be much greater than the equilibrium thermal diffusivity, particularly at low temperatures. Estimating a Fermi velocity of 3 x 10^7 cm/s and a mean free path of 10 nm, we estimate $D_e = v_F l/3 = 10$ cm^2/s (in comparison with an equilibrium value $D \approx 0.1$ cm^2/s). In a time of order 100 ps, this

would correspond to a non-equilibrium diffusion length $L_{ne} = \sqrt{(D_e t_{e-p})} \approx 300$ nm. This might well be large enough to explain the low-temperature behavior of samples #1 and #2. Furthermore, this would also explain the absence of the same effect in more optimized samples at higher temperatures; L_{ne} would then be less than 100 nm and would be unable to provide signficant heat redistribution in the film.

Although we feel that these results provide strong indirect evidence that non-equilibrium effects are occurring in some of these samples, there may also be a possibility that sample inhomogeneity might be responsible. Sample #1 was a granular sample, and sample #2 was an off-stoichiometric oriented sample, both with rather broad resistive transitions. If the lower portion of these films consisted of material with a substantially reduced value of T_c or I_c, then a conventional current redistribution effect might explain a fast onset without the need for any nonequilibrium effects. We feel that this is unlikely, but at present we cannot completely rule it out.

A more direct test of the non-equilibrium response would require a faster pulse, together with faster electrical sampling. If an excitation pulse is used which is much shorter than the electron-phonon relaxation time (a few ps at 77 K), it should be possible to heat up the electrons to a transient temperature above that for the phonons. This would be expected to bring about a fast voltage rise (at least for an optically thin film), followed by a fast recovery on the same timescale, as the phonons (which carry most of the thermal mass at high temperatures) cool off the electrons. However, complete recovery will require the excess heat to leave the film, and this will take much longer. This is the subject of another study.

In summary, we have observed the photoresponse across current-biased YBCO films illuminated with a 150 ps optical pulse. These included sputtered and evaporated films, high-quality epitaxial and granular films. For all films, the magnitude of the

response and its slow (>20 ns) decay are fully consistent with a bolometric response, and can be quantitatively understood using a model of film heating. For optically thin films, there is a fast (1 ns) voltage onset, as expected within this picture. For optically thick films, a fast response can be obtained at high temperatures only by biasing the film close to the critical current, in which case rapid current redistribution can account for the observed signal. At lower temperatures, however, a rapid response is achieved even for currents much less than I_c, suggesting that non-equilibrium electron transport may be responsible for energy distribution in the film. We have not seen any evidence of other non-equilibrium effects, such as those related to vortex motion in these films. Such effects may be more pronounced in magnetic fields, or possibly at lower fluence levels.

One potential application of optoelectronic switching of HTS fims is as a fast opening high-current switch. For example, a superconducting current storage loop could be used in combination with such a switch to deliver pulsed power. In order to switch large currents, it is desirable to work with films that have large critical currents and therefore are relatively thick. In addition, an optically thick film would make efficient use of the optical excitation energy. As our results indicate, fast switching of optically thick films may be achievable if the film is biased close to the critical current, and the intrinsic opening time can probably be less than 1 ns. Non-equilibrium effects are probably not important at the operating temperatures of interest, probably around 77 K. However, the closing time is limited by the film thickness, since it is limited by diffusion of heat into the substrate. In addition, one aspect to consider in any high-current design is the amount of self-heating that takes place when the switch is in the open state. For sufficiently high bias currents, self-heating might cause thermal runaway which could destroy the switch. Nevertheless, currents as high as 100 mA were switched in a time of order 1 ns in our experiments, and we see no fundamental reason why this cannot be scaled up to 10 A or higher.

Chapter 5

Summary and Concluding Remarks

In this thesis we have described the development of a process for depositing superconducting $YBa_2Cu_3O_7$ thin films and we have explored the use of these films as the active element in an optically triggered fast-opening switch. The films were deposited using rf magnetron sputtering from a single 8-inch diameter loose powder target. The process was developed in a collaborative effort between CVC Products, Inc. and The Department of Electrical Engineering at the University of Rochester.

Due to the complex chemical and structural nature of these HTS materials and the sensitivity of the electrical (in particular superconducting) properties to the film structure, the deposition process itself became a major focus of this research. By optimizing this process we have been able to produce epitaxial thin films with T_cs above 90 K and J_cs greater than 10^6 A/cm^2 at 77 K. In addition, the microwave surface resistance for 10 GHz is approximately 0.45 mΩ at 77 K, which is a factor of 20 below that of Cu at the same temperature. With these properties, HTS films may be used in a wide variety of applications, including high speed digital interconnects and passive microwave devices.

We have demonstrated that HTS films may also be useful in certain electro-optic applications, due to a unique combination of optical absorption and electrical conduction. The fast opening switch may someday find use in pulsed power applications where inductively stored energy must be switched in the nsec time scale. While there already exists semiconductor-based fast closing switches, the HTS materials may represent the best solution for a fast opening switch. In the

process of investigating this application, we have also looked at the nature of the optical response of HTS materials. Our results show a simple bolometric behavior with some indication of hot electron transport through the thickness of films that are thicker than the optical penetration depth (≈ 2000 Å).

There continues to be a great deal of interest in HTS materials, both from a fundamental point of view and in terms of potential applications. Much work continues to be done in the area of materials processing, particularly thin film deposition for electronic applications. Single layer thin films of YBCO with low microwave losses have been patterned into passive microwave devices on 2-inch diameter $LaAlO_3$ substrates and used as narrow bandwidth filters and chirp filters.[87] Some of these devices have been tested in space communications systems as part of the U.S. Government's High Temperature Superconducting Space Experiment (HTSSE). Currently work is underway to develop advanced multichip modules using high temperature superconductors for high speed interconnects.

There is considerable interest in multilayer structures combining HTS films with insulating layers. Such multilayer structures have been used in making cross overs for multi-turn pickup coils in SQUID circuits. In addition, work proceeds on the formation of Josephson Junctions based on HTS and insulating films. One such structure consists of epitaxial layers of $YBa_2Cu_3O_7$ and $PrBa_2Cu_3O_7$, the latter being an insulator.

The intense world wide efforts on HTS thin film processing over the last several years are likely to provide additional benefits in other areas of technology as well. Other perovskites, which have similar deposition requirements as the HTS materials, are known to exhibit such diverse behavior as ferroelectric, pyroelectric,

and electro optic. The ability to deposit complex oxide thin films and multilayer structures may allow for the development of ferroelectric memory devices and electro optic switches. Recently, a ferroelectirc capacitor consisting of a two layer structure of YBCO and the ferroelectric $PbLa_xZr_{(1-x)}Ti_3O_y$ has been demonstrated at the U of R.[88] Such a material system may find use in a static RAM or high density DRAM IC. In the comong years, other applications and materials systems, perhaps beyond what is currently envisioned, are likely to emerge.

Bibliography

1. J.G. Bednorz and K.A. Mueller, Z. Phys. B **64**, 189 (1986).

2. M.K. Wu, J. R. Ashburn, C.J. Torng, P.H. Hor, R.L. Meng, L. Gao, Z.J. Huang, Y.Q. Wang, and C.W. Chu, "Superconductivity at 93 K in a New Mixed Phase Y-Ba-Cu-O Compound System at Ambient Pressure", Phys. Rev. Lett. **58**, 908 (1987).

3. N. Newman and W.G. Lyons, "High T_c Microwave Devices", J. Superconductivity **6**, 119 (1993).

4. F.S. Galasso, Perovskites and High T_c Superconductors (Gordon & Breach, New York, 1990).

5. A.W. Sleight, J.E. Gillson, P.E. Bierstedt, Solid State Commun. **17**, 27 (1975).

6. M. Beasley, "High-Temperature Superconductive Thin Films", Proc. IEEE **77**, 1155-1163 (1989).

7. T. Hirata and Y. Asada, "A Review of the Size of the Energy Gap in Superconducting Oxides", J. Superconductivity **4**, 171-177 (1991).

8. B.H. Loo et.al, in High Temperature Superconducting Materials, ed. by W.E. Hatfield and J.H. Miller Jr., pp. 345-359 (Marcel Dekker, New York, 1988).

9. I.K. Schuller and J.D. Jorgenson, MRS Bull., XIV, 27 (January 1989).

10. H. Ihara, et al., Physica C **153-155**, 948 (1988).

11. R.J. Cava, B. Batlogg, A.P. Ramirez, D. Werder, C.H. Chen, E.A. Rietman, and S.M. Zahurak, in High Temperature Superconductors, Mat. Res. Soc. Proc. 99, ed. by M.B. Brodsky, R.C. Dynes, K. Kitizawa, and H.L. Tuller, pp. 19-26 (MRS, Pittsburgh, 1988).

12. D. van der Marel, J. van Elp, G.A. Sawatzky, and D. Heitmann, Phys. Rev. B 37, 5136 (1988); M.K. Kelly, P. Barboux, J.M. Tarascon, and D.E. Aspnes, Phys. Rev. B40, 6797 (1989).

13. A.M. Kadin, P.H. Ballentine, and W.R. Donaldson, Physica B **165-166**, 1507 (1990).

14. H. Adachi, K. Hirochi, K. Setsune, M. Kitabatake, and K. Wasa, "Low-Temperature Process for the Preparation of High T_c Superconducting Thin Films", Appl. Phys. Lett. 51, 2263 (1987).

15. D. Dimos, et al., Phys. Rev. Lett, **61**, 219 (1988).

16. R. Sobolewski, et al., IEEE Trans. Mag. **27**, 876 (1991).

17. R.W. Simon, et al., "Low-Loss Substrate for Epitaxial Growth of High-Temperature Superconductor Thin Films", Appl. Phys. Lett. **53**, 2677 (1988); R.L. Sandstrom, et al., Appl. Phys. Lett. **53**, 1874 (1988).

18. H. Nakajima, et al., "Interdiffusion and interfacial Reaction between an $YBa_2Cu_3O_x$ Thin Film and Substrates", Appl. Phys. Lett. **53**, 1437 (1988).

19. A. Mogro-Campero, L.G. Turner, and G. Kendall, "Thickness and Annealing Dependence of the Superconduting Transition Temperature of $YBa_2Cu_3O_{7-x}$ Thin Films on Oxidized Silicon and Polycrystalline Alumina Substrates", Appl. Phys. Lett. **53**, 2566 (1988).

20. R.B. Laibowitz, R.H. Koch, P. Chaudhari, and R. J. Gambino, Phys. Rev. B **35** 8821 (1987).

21. L.I. Maissel and R. Glang, Handbook of Thin Film Technology, (McGraw-Hill, New York, 1970) pp. 1.26 - 1.27

22. A. Mogro-Campero, B.D. Hunt, L.G. Turner, M.C. Burrell, and W.E. Balz, Appl. Phys. Lett. **52**, 584 (1988).

23. M. Naito, et al., J. Mater. Res. **2**, 713 (1987).

24. P.M. Mankiewich, et. al, in ref. 11. pp 119-126.

25. N. Missert, et al., IEEE Trans. Magn. **25**, 2418 (1989).

26. R.M. Silver, A.B. Berezin, M. Wendman, and A.L. de Lozanne, Appl. Phys. Lett. **52** 2263 (1988).

27. D.D. Berkley et. al, Appl. Phys. Lett. **53**, 708 (1988).

28. For a review of sputtering, see Ref. 21 or Thin Film Processes, ed. by J.L. Vossen and W. Kern (Academic Press, New York, 1978).

29. O. Michikami, H. Asano, Y. Katoh, S. Kubo, and K. Tanabe, Jpn. J. Appl. Phys. **26**, L1199 (1987).

30. M. Kawasaki, et al., Jpn. J. Appl. Phys. **26**, L738 (1987).

31. P.L. Reydet et al, Physica C **153-155**, 806 (1988).

32. S.I. Shah and P.F. Carcia, Appl. Phys. Lett. **51**, 2146 (1987).

33. J.J. Cuomo, R.J. Gambino, J.M.E. Harper, and J.D. Kuptus, J. Vac. Sci. Tech. **15**, 281 (1978).

34. S.M. Rossnagel and J.J. Cuomo, "Negative Ion Effects during Magnetron and Ion Beam Sputtering of $YBa_2Cu_3O_x$", p. 106 in Thin Film Processing and Characterization of High-Temperature Superconductors, ed. by J.M.E. Harper, R.J. Colton, and L.C. Feldman, American Institute of Physics Conf. Proc. **165** (AIP, New York, 1988).

35. T. Akune and N. Sakamoto, Jpn. J. Appl. Phys. **27**, L2078 (1988).

36. U. Poppe, J. Schubert, R.R. Aronz, W. Evers, C.H. Freiburg, W. Reichert, K. Schmidt, W. Sybertz, and K. Urban, Solid State Comm. **66**, 661 (1988).

37. R.L. Sandstrom, W.J. Gallagher, T.R. Dinger. R.H. Koch, R.B. Laibowitz, A.W. Kleinsasser, R.J. Gambino, B. Bumble, and M.F. Chisholm, Appl. Phys. Lett. **53**, 444 (1988).

38. W.Y. Lee, J. Salem, V. Lee, C.T. Rettner, G. Gormam, R. Savoy, V. Deline, and T. Huang, Thin Solid Films **166**, 181 (1988).

39. K. Char, A.D. Kent, A. Kapitulnik, M.R. Beasley, and T.H. Geballe, "Reactive Magnetron Sputtering of Thin Film Superconductor $YBa_2Cu_3O_{7-x}$", Appl. Phys. Lett. **51**, 1370 (1987).

40. M. Scheuermann, C.C. Chi, C.C. Tsuei, D.S. Yee, J.J. Cuomo, R.B. Laibowitz, R.H. Koch, B. Braren, R. Srinivasan, and M.M. Plechaty, Appl. Phys. Lett. **51** 1951 (1987).

41. M. Gurvitch and A.T. Fiory, Appl. Phys. Lett. **51**, 1027 (1987).

42. T. Venkatesen, X.D. Wu, A. Inam, and J.B. Wachtman, "Observation of Two Distinct Components during Pulsed Laser Deposition of High T_c Superconducting Films", Appl. Phys. Lett. **52**, 1193 (1988).

43. S. Witanachchi, H.S. Kwok, X.W. Wang and D.T. Shaw, "Deposition of Super-conducting Y-Ba-Cu-O Films at 400 °C without Post-Annealing", Appl. Phys. Lett. **53**, 234 (1988).

44. From AESAR Corp., div. Johnson Matthey, Ward Hill, MA 01835.

45. Superconductive Components, Inc., Columbus, OH 43212

46. Tektronix Inc., Beaverton, OR 97077.

47. A.C. Westerheim, et al., J. Vac. Sci. and Technol. A **10**, 3407 (1992).

48. Powder Diffraction File, Inorganic Volume, JCPDS International Centre for Diffraction Data, Swarthmore, PA, 1987.

49. J.W. Ekin, A.J. Panson, and B.A. Blankenship, "Method for Making Low-Resistivity Contacts to High T_c Superconductors", Appl. Phys. Lett. **52**, 331 (1988).

50. J. Geerk, G. Linker, and O. Meyer, "Epitaxial Growth and Properties of YBaCuO Thin Films", Mater. Sci. Reports, **4**, 195 (1989).

51. W. Kula, R. Sobolewski, J. Gorecka, and S.J. Lewandowski, "Highly Oriented Bi-Based Thin Films With Zero Resistance at 106 K", IEEE Trans. on Magn. **27**, 1581 (1991).

52. C.B. Eom, et al., "Synthesis and Properties of $YBa_2Cu_3O_7$ Thin Films Grown *In-Situ* by 90° off-axis Single Magnetron Sputtering, Physica C **171**, 354 (1990).

53. V. Matijasevic, P. Rosenthal, K. Shinohara, A.F. Marshall, R.H. Hammond, and M.R. Beasley, "Reactive Coevaporation of YBaCuO Superconducting Films", J. Mater. Res. **6**, 682 (1991)

54. R. Hammond and R. Bormann, Physica C **162-164**, 703 (1989).

55. J.K. Truman, W.R. White, P.H. Ballentine, D.S. Mallory, and A.M. Kadin, "Continued Improvement of Large Area *In-Situ* Sputter Deposition of Superconducting YBCO Thin Films", IEEE Trans. on Appl. Superconductivity" **3**, 1679 (1993).

56. R.C. Taber, "A Parallel Plate Resonator Technique for Microwave Loss Measurements on Superconductors", Rev. Sci. Instrum. **61**, 2200 (1990).

57. J.S. Martens, V.M. Hietala, D.S. Ginley, T.E. Zipperian, and G.K.G. Hohenwarter, "Confocal Resonators for Measuring the Surface Resistance of High Temperature Superconducting Thin Films", Appl. Phys. Lett. **58**, 2543 (1991).

58. M.Naito, et al., "Thin-Film Synthesis of the High-T_c Oxide Superconductor $YBa_2Cu_3O_7$ by Electron-Beam Codeposition", J. Mater. Res. **2**, 713 (1987).

59. W.R. Donaldson, "High Speed, High Repetition Rate, High Voltage Photoconductive Switching", pp. 241-244, in *Picosecond Electronics and Optoelectronics II*, ed. by F.J. Leonberger, C.H. Lee, F. Capasso, and H. Morkoc (Springer Verlag, Berlin, 1987).

60. T.L. Francavilla, D.L. Peebles, H.H. Nelson, J.H. Claassen, S.A. Wolf, and D.U. Gubser, "A Laser Quenched Superconducting Switch for Pulsed Power Applications", IEEE Trans. Magn. 25, 1397-1400 (1987).

61. A.M. Kadin, W.R. Donaldson, P.H. Ballentine, and R. Sobolewski, "Nonequilibrium Hot-Electron Transport in Optically Irradiated YBCO Films", Physica C 162-164, 387-388 (1989).

62. P.W. Kruse, "Physics and Applications of High-T_c Superconductors for Infrared Detectors", Semiconductor Science & Technology 5, S229-S239 (1990).

63. A.I. Braginski, M.G. Forrester, and J. Talvacchio, "Progress Toward Understanding the Mechanism of Optical Detection by High Temperature Superconductors", Extended Abstracts of International Superconductivity Electronics Conf. (ISEC '89), Tokyo, June 1989, pp. 482-488 (Japan Soc. of Appl. Phys., Tokyo, 1989).

64. S.A. Wolf, U. Strom, and J.C. Culbertson, "Visible and Infrared Detection Using Superconductors", Solid State Technology, pp. 187-191 (April 1990).

65. T.G. Stratton, B.E. Cole, P.W. Kruse, R.A. Wood, K. Beauchamp, T.F. Wang, B. Johnson, and A.M. Goldman, "High Temperature Superconducting Microbolometer", Appl. Phys. Lett. 57, 99-100 (1990).

66. W.R. Donaldson, A.M. Kadin, P.H. Ballentine, and R. Sobolewski, "Interaction of Picosecond Optical Pulses with High T_c Superconducting Films", Appl. Phys. Lett. 54, 2470-2472 (1989).

67. W.S. Brocklesby, D. Monroe, A.F.J. Levi, M. Hong, S.H. Liou, J. Kwo, C.E. Rice, P.M. Mankiewich, and R.E. Howard, "Electrical Response of Superconducting $YBa_2Cu_3O_7$ to Light", Appl. Phys. Lett. 54, 1175-1177 (1989).

68. A. Frenkel, M.A. Saifi, T. Venkatesan, P. England, X.D. Wu, and A. Inam, "Optical Response of Nongranular High-T_c YBa$_2$Cu$_3$O$_{7-x}$", J. Appl. Phys. 67, 3054-3068 (1990).

69. M.G. Forrester, M. Gottlieb, J.R. Gavaler, and A.I. Braginski, "Optical Response of Epitaxial and Granular Films of YBa$_2$Cu$_3$O$_{7-d}$", IEEE Trans. Magn. 25, 1327-1330 (1989).

70. M. Leung, P.R. Broussard, J.H. Claassen, M. Osofsky, S.A. Wolf, and U. Strom, "Optical Detection in Thin Granular Films of Y-Ba-Cu-O at Temperatures Between 4.2 and 100 K", Appl. Phys. Lett. 51, 2046-2047 (1987).

71. D.P. Osterman, R. Drake, R. Patt, E.K. Track, M. Radparvar, and S.M. Faris, "Optical Response of YBCO Thin Films and Weak Links", IEEE Trans. Magn. 25, 1323-1326 (1989).

72. H.S. Kwok, J.P. Zheng, Q.Y. Ying, and R. Rao, "Nonthermal Optical Response of Y-Ba-Cu-O Thin Films", Appl. Phys. Lett. 54, 2473-2475 (1989).

73. K. Tanabe, Y. Enomoto, M. Suzuki, T. Iwata, and A. Yamaji, "Nonbolometric Infrared Detection in La$_{2-x}$Sr$_x$CuO$_4$ and YBa$_2$Cu$_3$O$_y$ Epitaxial Thin Films", Jpn. J. Appl. Phys. 29, L466-L469 (1990).

74. G.L. Carr, M. Quijada, D.B. Tanner, C.J. Hirschmugl, G.P. Williams, S. Etemad, B. Dutta, F. DeRosa, A. Inam, T. Venkatesan, and X. Xi, "Fast Bolometric Response by High T_c Detectors Measured with Subnanosecond Synchrotron Radiation", Appl. Phys. Lett. 57, 2725-2727 (1990).

75. N. Bluzer, "Temporal Relaxation of Nonequilibrium in Y-Ba-Cu-O Measured from Transient Photoimpedance Response", Phys. Rev. B44, 10222-10233 (1991).

76. A.D. Semenov, I.G. Goghidze, G.N. Gol'tsman, A.V. Sergeev, E.E. Aksaev, and E.M. Gershenzon, "Nonequilibrium Quasiparticle Response to Radiation and Bolometric Effect in YBaCuO Films", IEEE Trans. Appl. Supercond. 3, 2132-2135 (1993).

77. E. Zeldov, N.M. Amer, G. Koren, A. Gupta, "Nonbolometric Optical Response of $YBa_2Cu_3O_{7-\delta}$ Epitaxial Films", Phys. Rev. B39, 9712-9714 (1989).

78. A.M. Kadin, M. Leung, A.D. Smith, and J.M. Murduck, "Photofluxonic Detection: A New Mechanism of Infrared Detection in Superconducting Thin Films", Appl. Phys. Lett. 57, 2847-2849 (1990).

78. P.H. Ballentine, A.M. Kadin, W.R. Donaldson, J.H. Scofield, and L.J. Bajuk, "Laser Induced Swithing of YBCO", pp. 247-255 in *High T_c Superconducting Thin Films: Processing, Characterization, and Applications*, ed. R.L. Stockbauer, et al., AIP Conf. Proc. 200 (AIP, New York, 1990).

80. P.M. Mankiewich, J.H. Scofield, R.E. Howard, A.H. Dayem, and E. Good, "Reproducible Technique for Fabrication of Thin Films of High Transition Temperature Superconductors", Appl. Phys. Lett. 51, 1753-1755 (1987).

81. P.H. Ballentine, A.M. Kadin, M.A. Fisher, D.S. Mallory, and W.R. Donaldson, "Microlithography of High-Temperature Superconducting Films: Laser Ablation vs. Wet Etching", IEEE Trans. Magn. 25, 950-953 (1989).

82. H.E. Fischer, S.K. Watson, and D.G. Cahill, "Specific heat, Thermal Conductivity, and Electrical Resistivity of High Temperature Superconductors", Comments on Condensed Matter Physics 14, 65-127 (1988).

83. M. Nahum, S. Verghese, P.L. Richards, and K. Char, "Thermal Boundary Resistance for $YBa_2Cu_3O_{7-d}$ Films", Appl. Phys. Lett. 59, 2034-2036 (1991).

84. S.D. Brorson, J.G. Fujimoto, and E.P. Ippen, "Femtosecond Electronic Heat Transport Dynamics in Thin Gold Films", Phys. Rev. Lett. 59, 1962-1965 (1987).

85. M. Gershenzon, G.N. Gol'tzman, A.D. Semenov, and A.V. Sergeev, "Mechanism of Picosecond Response of Granular YBaCuO Films to Electromagnetic Radiation", IEEE Trans. Magn. 27, 1321-1324 (1991).

86. R.W. Ralston, M.A. Kastner, W.J. Gallagher, and B. Batlogg, "Cooperating on Superconductivity", IEEE Spectrum Vol. **29**, No. 8, p. 50 (August, 1992).

87. J.C. Ritter, M. Nissenoff, G.Price, and S.A. Wolf, "High Temperature Superconducting Space Experiment (HTSSE)", IEEE Trans. on Magn. **2**, 2533 (1991).

88. P.J. Borrelli, P.H. Ballentine, and A.M. Kadin, "Compositional and Structural Properties of Sputtered PLZT Thin Films", in Ferroelectric Thin Films II, ed. by A.I. Kingon, et al., Proc. Materiasl Research Society, **243** pp. 417-422, (1993).

Appendix A: Publications of P.H. Ballentine

1. J. Argana, R.C. Rath, A.M. Kadin, and P.H. Ballentine, "RF Sputter Deposition of Y-Ba-Cu-O Superconducting Thin Films from an Oxide Powder Target", in **Thin Film Processing and Characterization of High-Temperature Superconductors**, Proc. 1987 American Vacuum Society Topical Conference, ed. by J.M.E. Harper *et al.* pp. 58-65 (American Institute of Physics, New York, 1988).

2. P.H. Ballentine, A.M. Kadin, J. Argana, and R.C. Rath, "Thin Films of Y-Ba-Cu-O by RF Sputtering", in **High-Temperature Superconductors**, Mat. Res. Soc. Symp. Proc. **99**, ed. by M.B. Brodsky *et al.*, pp. 335-338 (MRS, Pittsburgh, 1988).

3. A.M. Kadin, P.H. Ballentine, J. Argana, and R.C. Rath, "Superconducting Properties of Magnetron-Sputtered $YBa_2Cu_3O_7$ Films", in **Superconductivity and its Applications**, ed. by H.S. Kwok and D.T. Shaw, pp. 152-160 (Elsevier, New York, 1988).

4. P. Ballentine, A.M. Kadin, J. Argana, R.C. Rath, and P. McCluskey, "Thin Films of High-T_c Superconductors by RF Magnetron Sputtering from a Single Oxide Target", in **Processing and Applications of High T_c Superconductors**, ed. by W.E. Mayo, pp. 31-41 (The Metallurgical Society, Warrendale, PA, 1988).

5. A.M. Kadin, P.H. Ballentine, J. Argana, and R.C. Rath, "High Temperature Superconducting Films by RF Magnetron Sputtering", Proc. 1988 Applied Superconductivity Conf., in IEEE Transactions on Magnetics **25**, 2437-2440 (1989).

6. P.H. Ballentine, A.M. Kadin, M.A. Fisher, D.S. Mallory, and W.R. Donaldson, "Microlithography of High-Temperature Superconducting Films: Laser Ablation vs. Wet Etching", Proc. 1988 Applied Superconductivity Conf., in IEEE Trans. on Magnetics **25**, 950-953 (1989).

7. W.R. Donaldson, A.M. Kadin, P.H. Ballentine, and R. Sobolewski, "Interaction of Picosecond Optical Pulses with High-T_c Superconducting Films", Appl. Phys. Lett. **54**, 2470-2473 (1989).

8. A.M. Kadin, W.R. Donaldson, P.H. Ballentine, and R. Sobolewski, "Nonequilibrium Hot-Electron Transport in Optically Irradiated YBCO Films", Physica **C162-164**, 387-388 (1989).

9. W.R. Donaldson, A.M. Kadin, P.H. Ballentine, and M. Shoup, "Optically Activated High Temperature Superconductor Opening Switches", in Digest of Technical Papers, 7th IEEE Pulsed Power Conf., ed. by R. White and B.H. Bernstein, pp. 897-901 (IEEE, 1989).

10. A.M. Kadin, D.S. Mallory, P.H. Ballentine, M. Rottersman, and R.C. Rath, "Microwave Loss Measurements on YBCO Films Using a Stripline Resonator", in Proc. Conf. on Superconductivity and Applications, Buffalo NY, 1989, ed. by H.S. Kwok, et al., pp. 757-766 (Plenum, 1990).

11. P.H. Ballentine, A.M. Kadin, and W.R. Donaldson, "Sputtered High-T_c Superconducting Films as Fast Optically Triggered Switches", in Proc. Conf. on Superconductivity and Applications, Buffalo NY, 1989, ed. by H.S. Kwok, et al., pp. 685-693 (Plenum, 1990).

12. P.H. Ballentine, A.M. Kadin, W.R. Donaldson, J.H. Scofield, and L.J. Bajuk, "Laser Induced Switching of YBCO", in **High T_c Superconducting Thin Films: Processing, Characterization, and Applications**, Proc. AVS Topic Conf., Boston MA, 1989, ed. by R. Stockbauer, et al., AIP Conf. Proc. **200**, pp. 247-254 (American Institute of Physics, 1990).

13. P.H. Ballentine, J. Archer, J.P. Allen, and A.M. Kadin, "Reproducible in-situ sputter deposition of superconducting $YBa_2Cu_3O_7$ films", in Proc. 33rd Technical Conf. of Society of Vacuum Coaters, New Orleans, 1990, pp. 303-307 (1990).

14. A.M. Kadin, P.H. Ballentine, and W.R. Donaldson, "Relaxation processes in optically excited high-T_c films", Physica **B165**, pp. 1507-1508 (1990).

15. P.H. Ballentine, A.M. Kadin, W.R. Donaldson, J.H. Scofield, and L. Bajuk, "Optically triggered switching of YBCO thin films", in **High Tc Superconductivity: Thin Films and Applications**, SPIE Vol. 1287, ed. by C.C. Chi and R.B. VanDover, pp. 134-143 (1990).

16. P.H. Ballentine, A.M. Kadin, W.R. Donaldson, J.H. Scofield, and L. Bajuk, "Fast infrared response of YBCO thin films", in **Superconductivity Applications for Infrared and Microwave Devices**, SPIE Vol. 1292, ed. by K.B. Bhasin and V.O. Heinen, pp. 176-186 (1990).

17. A.M. Kadin, P.H. Ballentine, D.S. Mallory, and J.P. Allen, "Preparation and properties of in-situ sputtered YBCO films", Supercond. Sci. Technol. **4**, S175-177 (1991).

18. P.H. Ballentine, A.M. Kadin, and D.S. Mallory, "In-situ sputtering of YBCO films for microwave applications", IEEE Trans. Magnet. **27**, 997-1000 (1991).

19. P.H. Ballentine, J.P. Allen, A.M. Kadin, and D.S. Mallory, "Large-area sputtering of in-situ superconducting YBCO films", J. Vacuum Sci. and Technol. **A9**, 1118-1122 (1991).

20. D.S. Mallory, A.M. Kadin, and P.H. Ballentine, "Performance of stripline resonators using sputtered YBCO films" in Superconductivity Applications for Infrared and Microwave Devices II, ed. by V. Heinen and K.B. Bhasin, SPIE vol. 1477 (SPIE, Bellingham WA, 1991), pp. 66-76.

21. P.H. Ballentine, J.P. Allen, A.M. Kadin, and D.S. Mallory, "Commerical scale production of high temperature superconducting thin films", in Superconductivity and Its Applications, American Institute of Physics Conf. Proc. 219, ed. by Y.H. Kao, P. Coppens, and H.S. Kwok (AIP, New York, 1991), pp. 429-438.

22. W.R. Donaldson, A. Kadin, P. Ballentine, and K. Kortkamp, "An optically triggered superconducting opening switch", Proc. 4th SDIO/ONR Pulse Power Meeting (Los Angeles CA, June 1991), ed. by G.D. Roy (1991), pp. 54-60.

23. J.K. Truman, W.R. White, P.H. Ballentine, D.S. Mallory, and A.M. Kadin, "Continued improvement of large area, in situ sputter deposition of superconducting YBCO thin films", IEEE Transactions on Applied Superconductivity 3, 1679-1682 (1993).

Appendix B. Operating Instructions for CVC SC-4000 Sputter Deposition System at UR-EE

NOTES:

1. Read over CVC instruction manual and OEM manuals before operating system.
2. Never operate the system when you are alone in the building
3. Always keep a log book of depositions and system maintenance.
4. If the system is to be left under high vacuum for more than a few hours, turn off the mechanical pump after the pumpdown procedure

TO VENT THE SYSTEM AND LOAD A SAMPLE

1. Push the vent button on the automatic valve controller (AVC-485) (Make sure the N_2 bottle has gas)
2. Wait for the pressure to rise to atmosphere
3. Raise the hoist.
4. Check the condition of the powder target. Repaire any large disruptions by tamping down.
5. Check operation of the shutter.
6. Place your new sample on the holder. Make sure the holder is electrically isolated from the table.
7. If a sample thermocouple is used make sure it is not shorted out to ground.
7. Make sure there are no hairs or particles on the o-ring or o-ring mating surface
8. Lower the hoist

TO PULL A HIGH VACUUM ON THE CHAMBER

1. Make sure the throttle valve is in the open position.
2. Make sure the mechanical pump is on.
3. Push "start" on the AVC-485 (The AVC 485 will automatically rough down the chamber and open the high vacuum valve)
4. When the pressure falls below 10^{-3} Torr, turn on the ion gauge (GIC-410)
5. Wait for the pressure to fall below 5×10^{-7} Torr (approximately 2 hours) before performing deposition. If pressure does not come down after 8-hours, check for leak with RGA. Also, check to see if cryopump needs regeneration (or more He gas) by looking at regen light (and pressure Gauge)

TO PREHEAT THE SUBSTRATE

1. Wait for base pressure to reach 5×10^{-7} Torr.

2. Make sure cooling water is on and interlocks are met (no red lights on interlock control panel)

3. Turn on the "Start Continuous" switch on the Master Control Panel.

4. Turn on the heater relay on the heater control panel.

5. Press the upper right hand button on the West 3800 Temperature controller until the "P" appears on the readout. This puts the unit in the power control mode with no temperature feedback.

6. Adjust the heater power set point to 28%. **Caution: Do not go above 30% or the heater may burn out**

7. Push the black start button on the heater control panel

TO DEPOSIT A HIGH T_C FILM

1. Close throttle valve and open MKS Nupro valve (make sure Ar and O_2 tanks have pressure)

2. Adjust MKS 250 controller to reach desired pressure (controller will read 1/10 of pressure in mTorr, i.e. 30 mTorr = 3.0) (See MKS Manual for details)

3. Adjust the gas flow ratio between channels 1 and 2 on the 247C mass flow controller (MFC) (See MKS Manual for details)

4. Start the rf power supply by turning on the two bottom breakers.

5. Turn on the matching network and switch it to "Auto" mode.

6. Make sure incident power dial is set to 0, then push "rf on" button on power supply control panel.

7. Increase incident power to 100 W. Plasma should ignite as evidenced by (1) dull glow in chamber, (2) zero reflected power, and (3) red light on matching network control panel is lit. If plasma does not ignite, turn on plasma starter for a few seconds. If this does not work, try opening and closing the shutter. If this does not work, try increasing pressure to 100 mTorr momentarily.

8. Slowly ramp up the rf power to the set point (typically 450 W). This should be done while keeping the pressure below 35 mTorr, (50 W increment every 10 min.). If reflected power goes above 50 W, abort run and check for short in cathode.

9. When the power is at the set point, let the system stabilize for 10 minutes, then open the shutter.

10. Record start time and process parameters in lab notebook.

TO TERMINATE A DEPOSITION AND ANNEAL FILM IN OXYGEN

1. Record final heater temperature
2. Close shutter
3. Turn down rf power to 0 and switch off.
4. Turn off matching network and rf power supply breakers.
5. Hit "stop" button on AVC-485 to close high vacuum valve
6. Switch off Ar MFC in channel 1 and increase O_2 flow in channel 2 to maximum of 100 sccm until chamber pressure reaches 100 Torr (approx. 40 minutes).
7. Close MKS Nupro valves and re-set MFC's to original settings.
8. Turn off heater breaker switch and allow temperature to coast down.
9. When temperature falls below 200 °C, turn off cooling water.
10. Turn off Master Control switch
11. Allow temperature to fall below 100 °C before venting to remove sample

Appendix C. Design of Substrate Heater

Accurate control of substrate temperature is a common problem found in thin film processing. The situation is made more difficult because the substrate is often at reduced pressures or high vacuum in which case convective heat transfer is insignificant. Certain processes, such as plasma etching of a substrate that is partially coated with photoresist, require cooling of the substrate. Other processes, such as thermally driven chemical vapor deposition (CVD), require substrates to be heated, in some cases above 1000 °C. In sputtering, substrates may be need to be cooled or heated.

Thin film deposition of high temperature superconductors requires high substrate temperatures (600 - 850 °C) in order to form the proper crystalline structure, as discussed in Chapter 2. The substrate temperature must be fairly uniform (+/- 10 °C) in order to provide uniform film properties. In addition, the substrate heater must be compatible with the high oxygen partial pressures used during HTS deposition. In sputtering, it is also desirable to have the ability to provide rf or dc bias to the substrate during deposition. As there was no commercially available substrate heater that met all of these specifications, as part of this project we designed a new commercial scale substrate heater for HTS deposition. This Appendix describes the design and construction of the heater.

There are a variety of substrate heater configurations in use today. One common approach is to use lamps which are typically placed outside of the vacuum chamber and radiate through a quartz window. In our application, however, this method has two serious drawbacks. One is deposition on the window. The HTS materials are black and absorbing, and even small amounts of coating (a few 100 Å) can block the lamp light. The coating is difficult to avoid, particularly at the high operating pressures used

for HTS deposition. The second drawback is that the quartz window placed behind the substrate is incompatible with substrate bias. Another common substrate heater configuration is to heat a metal block with resistance heat and place the substrate on or near the block. This is essentially the approach we took for the HTS heater.

Target
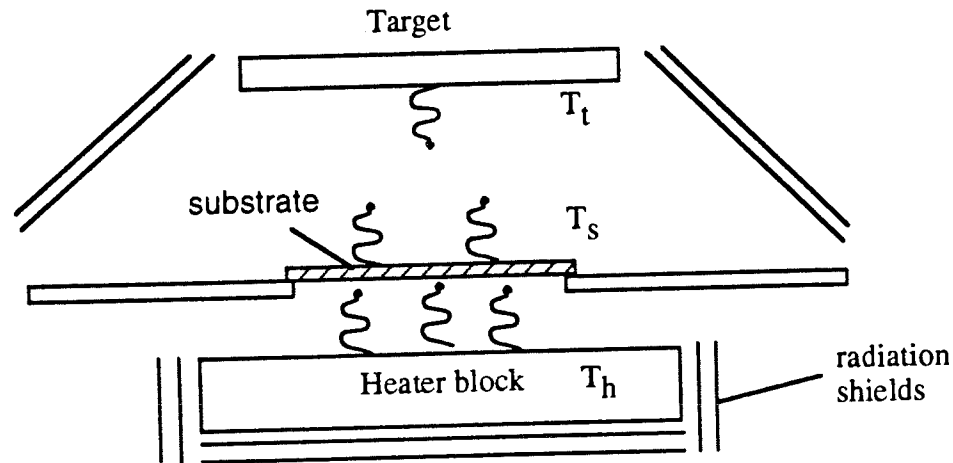
Fig. C.1 Schematic of substrate heater

C.1 Heat Transfer Calcutations

Here we derive the basic heat transfer equations that govern the heater design. Figure C.1 is a schematic representation of the substrate heater geometry. At steady state, the temperature of the substrate is determined by a balance of heat loss and heat gain.

$$Q_{in} = Q_{out} \qquad \qquad (C.1)$$

The three basic modes of heat transfer are convection, conduction, and radiation. The total heat flow into the substrate, expressed in Watts, is given by

$$Q_{in} = Q_{conv.} + Q_{cond.} + Q_{rad.} \tag{C.2}$$

Convective heat transfer is given by

$$Q_{conv} = hA(T_{heater} - T_{substrate}) \tag{C.3}$$

where h is the convection coefficient in $W/m^2\text{-}^\circ C$ and A is the surface area. At atmospheric pressures, convection is independent of gas pressure and can play a major role in determining the temperature of a body. At lower pressures, however, the heat transfer coefficient is greatly reduced and becomes small relative to the conductive and radiative terms. At typical sputtering pressures (10 mTorr), and typical spacings (0.1 mm), the convective heat transfer coefficient is .01 $W/m^2\text{-}^\circ C$. This is insignificant compared to the effective radiative coefficient.

Conduction heat transfer is given by

$$Q_{cond} = kAdT/dx \tag{C.4}$$

were k is the thermal conductivity in $W/m\text{-}^\circ C$. Conduction is only effective when the substrate is well attached to the heater block. A substrate that is simply supported on a heater block in a vacuum is said to be in "three point contact" and the effects of conduction are minimal. Many HTS researchers have resorted to attaching the substrate to a heater block using some type of thermal transfer medium (in many cases silver paint, like that used in mounting SEM samples, is used). We chose not to pursue this approach because it is incompatible with load lock entry of samples and because it is difficult with the large area substrates we were aiming to coat. Therefore conduction was not significant in transferring heat either into our out of the substrate.

Radiation heat transfer between two parallel plates is given by by

$$Q_{rad} = A\sigma(T_1^4 - T_2^4)/[(1 - \varepsilon_1)/\varepsilon_1 + 1 + (1 - \varepsilon_2)/\varepsilon_2] \qquad C.5$$

where ε_n is the emissivity of surface n, T_n is the temperature in degrees K, and σ is the

Stephan-Boltzmann constant (5.667×10^{-8} W/m^2-K^4). The front side of a substrate

can "see" a wide variety of surfaces. The most conservative approach to heater design

is to assume the substrate stares into a room temperature surface with emissivity equal

to 1. Furthemore, if we assume the substrate has an emissivity of 1 we can calculate

the power per unit area required to maintain a given substrate temperature. For a

substrate temperature of 800 C, this gives 7.5 W/cm^2.

At equilibrium, this heat flux must be provided by the heater. Again, assuming unit

emmisivity for both substrate and heater, the required heater temperature is found to be

$T_{htr.} = 1005$ °C.

In order to achieve a uniform substrate temperature across a 4-inch diameter

substrate, we chose to build a 5-inch diameter heater with a substrate-to-heater spacing

of less than 0.25", which should be sufficient to minimize edge effects. The total heat

load out of the front of the heater is then A x Q/A = 950 W.

There are additional losses from the back and sides of the heater. In order to

minimize these losses, we constructed a series of metallic reflector shields that are

placed around and behind the heater. The shields were made from highly reflective

metal in order to have as low of an emissivity as spossible. We estimate the emissivity

of these shields to be less than 0.2. From equation C.5, it can be shown that each shield reduces the radiation heat transfer by a factor of 9. The use of two or more shields reduces the side and back losses to less than 5% of the required power.

The design criteria for the heater, then, are
Temperature = 1005 C
Power = 950 W

For a resistive heater element we chose to use cable heater technology, in which a heater element (usually Kanthal or Nichrome wire) is encased in a metallic sheath packed with MgO powder. The sheath is made of inconel, an alloy of Cr, Ni, and Fe that is compatible with both high temperatures and high oxygen concentrations. The heater element can be obtained in either a coaxial configuration, in which two ends must be passed through a vacuum, or in a "looped" configuration, in which only one vacuum feedthrough is needed. We have used both of these configurations successfully, although the coaxial configuration provides for longer heater life. The length of the heater element was chosen to provide a reasonable resistance while maintaining an acceptable heat flux per unit length. The acceptable levels of linear heat flux are in turn determined by the maximum operating temperatures and voltages. Our final design was to have 5 ft of heater length, with a total resistance of 30 Ω operating at 168 Volts max.

We chose to braze the heater element to an inconel block in order to match the thermal expansion coefficients. The final heater is shown in the photograph in Figure 3.6. This heater has been used at the U of R and at several other labs around the world to deposit HTS films and other perovskite materials as well.

Appendix D.   Patterning of HTS Films

MICROLITHOGRAPHY OF HIGH-TEMPERATURE
SUPERCONDUCTING FILMS: LASER ABLATION VS. WET ETCHING

P.H. Ballentine, A.M. Kadin, M.A. Fisher, and D.S. Mallory
Department of Electrical Engineering
University of Rochester, Rochester, NY 14627

and

W.R. Donaldson
Laboratory for Laser Energetics
University of Rochester, Rochester, NY 14623

Abstract

Narrow lines and microbridge structures have been etched in sputtered superconducting films of Y-Ba-Cu-O by variations of two methods. The first uses standard photolithography followed by wet etching in weak acid. The second uses a maskless process involving a focused pulsed YAG laser together with a computer-controlled x-y stage to produce local ablation of the superconducting film. Issues relating to limits of resolution, annealing of films, and degradation of superconducting properties are critically discussed for the two approaches.

Introduction

A wide variety of microelectronic applications have been proposed for high-temperature superconducting films, from electronic interconnects to SQUIDs to fast switches. In addition to optimizing the properties of the films themselves, it will also be necessary to develop the technology for patterning these films into device structures, probably on the μm scale. One class of approaches has been based on conventional photolithography, combined with either wet etching,[1,2] dry reactive ion etching,[3] or ion-implantation passivation of the exposed regions.[4] Alternatively, a number of groups have explored the use of scanned focused laser beams either to etch[5-7] or to passivate[8,9] parts of the films. We have chosen a dual approach which focuses on photolithography and acid etching on the one hand, and on pulsed laser ablation on the other. In the present paper we examine patterns prepared in superconducting YBCO films by the two methods and discuss advantages and disadvantages of each. Important considerations include uniformity of etching, edge resolution, and possible degradation of superconducting properties near the edge.

Fabrication and Properties of Superconducting Films

The films used in this study were fabricated by rf magnetron sputtering by R.C. Rath and J. Argana at CVC Products, Inc. of Rochester, NY. A companion paper that describes fabrication methods and superconducting properties of these films in more detail is also included in this Conference Proceedings.[10]

In brief, these films were sputtered from a stoichiometric YBCO powder target in an Ar/O_2 gas mixture, and were essentially single phase $YBa_2Cu_3O_7$. Typically, 0.5-1.5 μm-thick films were deposited on yttria-stabilized cubic zirconia substrates (YSZ) 1-inch square, and yielded uniform composition across the film, as determined by energy-dispersive x-ray analysis (EDXA) in a scanning electron microscope (SEM). Films deposited at moderately low substrate temperatures below ≈400°C were black and shiny as deposited, but were amorphous or highly disordered and required a high-temperature (850°C) anneal to become superconducting. After annealing, the films were much rougher, with morphology consisting of a randomly oriented mixture of needle and platelet crystallites ≈1-5 μm in size (Fig. 1a).

Fig. 1. Microscopic morphology of YBCO films on zirconia substrates. a) Low temperature deposition followed by 850°C anneal (Type II). b) Medium-T (650°C) deposition (Type III).
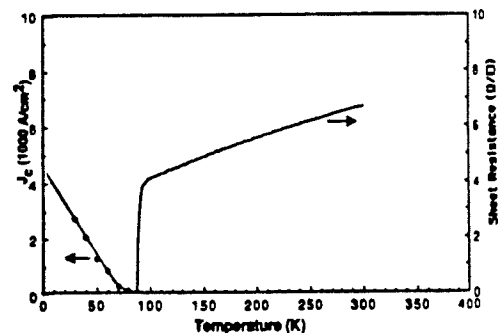

Fig. 2. Superconducting properties of YBCO film (Type II) on zirconia.

A superconducting transition of one such film is shown in Fig.2. The critical temperature is fairly high (zero resistance at 85 K), but the critical currents are limited by grain boundaries and random orientation of the crystallites.

An alternative approach that we have recently been developing involves depositing films at somewhat elevated temperatures (600-650°C) to yield films that are already crystalline and superconducting as deposited, without requiring an 850°C anneal. The morphology of these films consisted of a densely packed array of partially oriented crystallites on the 0.1μm length scale (Fig. 1b).

Three different classes of YBCO films were included in this study of patterning:
Type I - "amorphous" films deposited at low temperatures, before annealing. These then had to be annealed after patterning.
Type II - Class I films after annealing to 850°C.
Type III - Medium-T deposited films.
Given that the physical and morphological properties of these classes were so different, it was important to establish to what extent this affected their etching characteristics.

Patterning using Photolithography

Photolithography with resolution down to the micron level and beyond is a standard technique in the semiconductor industry. We have adapted a standard set of procedures using AZ-1350J positive photoresist and contact-printing a photomask using ultraviolet exposure. Generally speaking, films can be photolithographically patterned either by etching off those areas of a film unprotected by resist, or alternatively by depositing the film on top of a developed resist layer and using lift-off. Since we are using heated substrates, the latter method is impractical, and we have chosen to etch away the exposed YBCO film with a weak acid.

Sections of two different photomasks used to investigate are shown in Fig. 3. The first is designed to measure critical currents in a 100μm-wide strip in each of two orthogonal directions; the second consists of patterns for potential use as microbridges and SQUIDs.

The procedures used in transferring the pattern to the superconducting film are as follows:
1. Spin on photoresist (=1μm thick) at 4300 rpm
2. Bake at 95°C
3. Insert in mask aligner and expose for 13 sec.
4. Develop the pattern in Microposit MF351 developer
5. Stop the developer in deionized water.
6. Bake to dry.
7. Dip in the acid etch (see below for more information).
8. Stop etch in deionized water.
9. Dissolve off remaining photoresist in acetone.

Although virtually any kind of acid will etch YBCO, we tested two in particular, phosphoric (H_3PO_4) and hydrochloric (HCl).

To obtain an etch rate that is not unreasonably fast, the HCl must be diluted to a far greater degree than the phosphoric acid. For a typical etch rate of order 1 μm/minute, 1:320 HCl is equivalent to about 1:50 phosphoric (see Table I). These dilution ratios correspond to the dilution of commercially available concentrated acids: 38% HCl by weight (density 1.2) and 86% H_3PO_4 (density 1.7). For example, 1:320 HCl is more precisely 0.039 M HCl (with pH 1.4).

One might anticipate that etch rates might be significantly different for the three types of YBCO films, but they are really rather similar. As indicated in Table 1, however, there appeared to be more variation in etch rate for the crystalline films, even within the same film.

Table 1
Etch Rates of YBCO Films

	Type 1	Type II	Type III
H_3PO_4 (1:40)	1.2	0.5-0.7	0.6-0.8
HCl (1:320)	0.6	0.6-0.8	0.3-0.6

The edge resolution of the three types of films were of order 2μm or better. Although the annealed large-grain films (Type II) gave slightly rougher edges (=2μm) corresponding to the grain size, the sharper lines of the Type I films were degraded substantially (=5μm) during the subsequent high-T anneal. In contrast, Type III films showed sharp edges (=1μm) and were already superconducting without annealing (see Fig. 4).

However, measurements on Class II films patterned into microbridge structures (=10μm wide) indicated a substantial depression in T_c (from 83K to 50K), suggesting degradation of superconductivity near the patterned edge. Annealing after patterning may heal this, but at the cost of additional roughening. There appears to be a trade-off between resolution and superconducting properties, which we have not yet completely optimized. Type III films appear to exhibit less roughening even on annealing to 850°C, and offer promise for μm scale high-quality superconducting features.
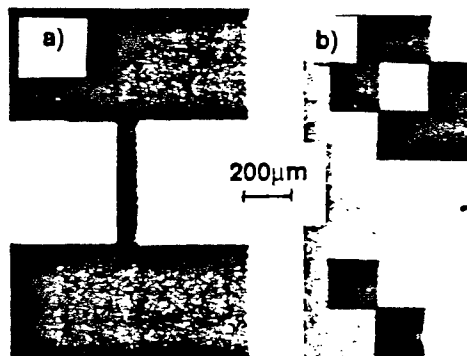

Fig. 3. Two patterns used in photolithography of YBCO films.
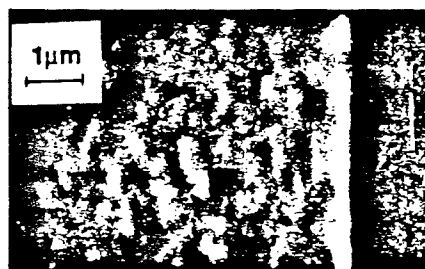a) 100μm strips for critical current measurement.
b) 5μm microbridges and SQUIDs.

Fig. 4. Electron micrograph of patterned Type III YBCO film exhibiting 1μm edge resolution.

In evaluating superconducting properties of lines 100μm wide and 500μm long patterned from the films, the resistive transition frequently shows a drop of =2 K in the temperature at which the resistance goes to zero, compared to the unpatterned film. This may be a reflection of a small degree of inhomogeneity in T_c, thather than degradation by the photoresist. A long, narrow region is relatively more likely to include a spot with a lower T_c, whereas in the wider film the current will just flow around it.

Patterning using Laser Ablation

Since soon after the discovery of YBCO, lasers have been used both for deposition and patterning of thin films. These have taken advantage of the combination of strong optical absorption and low thermal conductivity of YBCO, that permit local evaporation or ablation of material with very little heating just a few microns away. Both cw and pulsed lasers have been used, corresponding to two quite different regimes. The effects that have been seen with cw lasers are probably due to simple heating, and melting, evaporation, and passivation (by oxygen elimination) have all been explored. Pulsed lasers, on the other hand, deposit huge peak powers in short times, and appear to "ablate" the material by a process that may have a non-thermal component.

We have chosen to investigate laser etching using a pulsed Nd-YAG laser with regenerative amplification, with 120 psec pulses at wavelength 1.064 μm in the infrared and a repeat rate of order 1 kHz. The schematic of the relatively simple setup is given in Fig. 5. The sample was mounted on a x-y stage controlled by computer-driven stepper motors with step-size 6μm. Typical scan rates involved shifting by 6μm every 4 msec, for an average macroscopic rate of 1.5 mm/sec. Power could be varied over a wide range, but levels of 2-20 mW average powers were typical. In addition to the fundamental line in the infrared, the second harmonic at 532 nm in the green was produced using a KTP nonlinear crystal and also used for etching.
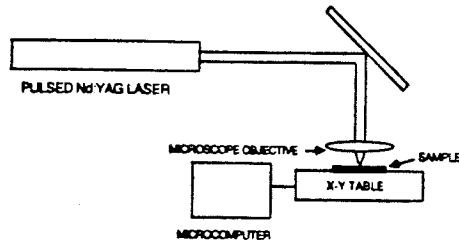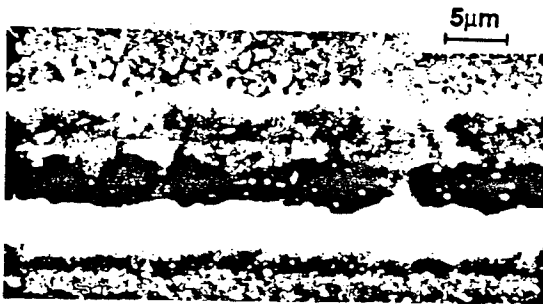
Fig. 5. Schematic of setup for laser patterning.

Fig. 7. Laser patterned line in 1.4μm film using frequency-doubled YAG (532 nm), 3.2mW average power, 1kHz rep. rate.

Fig. 6. Line patterned in 1.4μm film using YAG laser fundamental (1.064μm), 10mW average power, 500 Hz rep. rate.

For either wavelength, the beam was focused down through a 10X microscope objective (5 mm focal length) onto the film. For the infrared line, focusing was obtained by visually observing the glowing ablation plume and optimizing brightness for minimum power. This technique was more difficult for the green line, since the direct laser spot itself was very bright. In either case, the focus may not have been completely optimized. Estimates of the width of the beam made from the etch pattern itself suggest values in the range of 5-15μm, depending on the focus.

Several examples of lines etched in YBCO films are given in Fig. 6 and 7. Lines as narrow as about 6μm were achieved. Even for the 1.5μm-thick films, it was generally possible to etch entirely through the film with no more than a few pulses at a given point. In general, this process threw a fair amount of "rubble" out over the surrounding film. This rubble sitting on top of the films did not appear to degrade their superconducting properties. Typical ablation parameters for a 1.6μm-thick film were 10mW average power with a repeat rate of 1kHz; for a thinner 0.4μm film, 2mW @ 500Hz. For an estimated 10μm-wide spot, this corresponds to a fluence of order several J/cm^2 in each pulse. This is orders of magnitude smaller than the fluences used in cw laser etching, indicating the dramatically different regimes of operation.

Finally, it was also possible to produce a superconducting microbridge with length and width ~10 μm (Fig. 8). From the micrograph, there appears to be some damage to the film several μm on each side of the edge. The effect of this on superconducting properties is still being evaluated.

Since the stepper motors in this setup are computer controlled, one can make more complicated structures as well. Fig. 9 shows a pattern (with a 200μm wide line in the center of the "H") that is being used both to measure critical currents and to investigate fast switching in the superconducting films.

In general, we believe that apart from possible damage near the edge, the superconductivity in the film is unaffected by the laser patterning. Apart from slight decreases in T_c that reflect minor inhomogeneities, superconducting properties from patterns such as those of Fig. 9 accurately reproduce those of the unpatterned films.
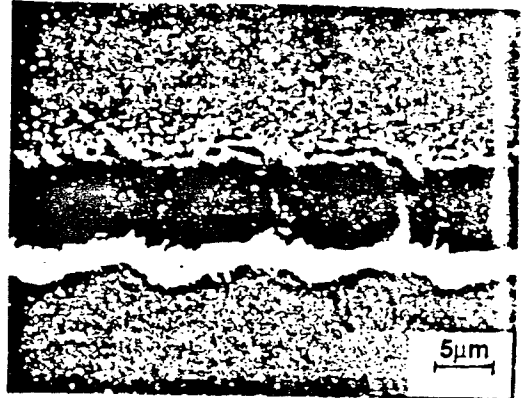
Fig. 8. Thin-film microbridge patterned using ~10μm-wide YAG beam. The beam has ablated the film on the left and right, leaving a region ~8μm wide in the center.

Fig. 9. Laser-patterned YBCO film for critical current and transient response studies. The bright spots on the corners are evaporated Ag contact pads.

Discussion and Conclusions

At this point in our study, we have been moderately successful using both patterning methods, and neither holds a clear-cut edge over the other. Photolithography requires a photomask to be made, which can take a day. Once that is available, the 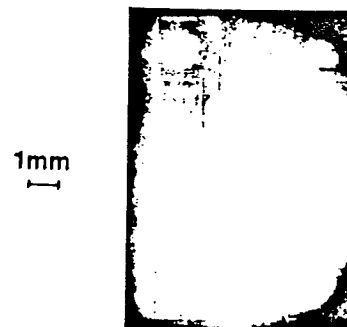entire patterning process takes several hours with standard equipment. For a simple pattern, the laser patterning can be much faster, particularly at the scan rate of ≈1mm/sec that we have used.

With respect to resolution, the major limitation in our laser etching was in the degree of focus that could be maintained. The optimum focus depends on the wavelength and the f-number of the optics used. We have used 1.06 and 0.53μm, and therefore excimer lasers with 0.25μm have a slight advantage. Lowering the f-number of the optics is also possible, although moving a lens closer makes it more likely to get coated with material ablated from the film. Still, we should be able to achieve somewhat narrower lines using this setup, perhaps ≈2-5μm. The resolution achieved in photolithography appears to be comparable to the limits given by our mask aligner (≈2μm) and grain size. In both cases, the degree of local damage on the scale of 1μm from the edge has to be better quantified.

Finally, we plan to pursue further the implications of the very short 120 psec pulsewidth produced by our YAG laser. Although the average powers are only a few mW, the peak power approaches a TW. During such a pulse, there is virtually no time for heat deposited by the beam to spread. Since the optical penetration depth is 100-200 nm, only the top portion of our films is directly heated, but the ablation process for a given pulse appears to go significantly deeper. A more complete understanding of this process may permit us to better optimize the etching process. Even apart from ablation, the use of these short pulses should allow us to explore nonequilbrium and transient responses of YBCO on sub-nsec time scales.

Acknowledgements

References

[1] Y. Yoshizako, M. Tonouchi, and T. Kobayashi, "Chemical Etching of High-T_c Superconducting Y-Ba-Cu-O Films in Phosphoric Acid Solution", Japan. J. Appl. Phys., vol. 26, pp. L1533-4, Sept. 1987.

[2] I. Shih and C.X. Qiu, "Chemical Etching of Y-Ba-Cu-O Thin Films", Appl. Phys. Lett., vol. 52, pp. 1523-4, May 1988.

[3] J.W.C. de Vries, et al., "Preparation, Patterning, and Properties of Thin $YBa_2Cu_3O_{7-\delta}$ Films", Appl. Phys. Lett., vol. 52, pp. 1904-6, May 1988.

[4] G.J. Clark, A.D. Marwick, R.H. Koch, and R.B. Laibowitz, "Effects of Radiation Damage in Ion Implanted Thin Films of Metal-Oxide Superconductors", Appl. Phys. Lett., vol. 51, pp. 139-41, July 1987.

[5] J. Mannhart et al., "Micropatterning of High T_c Films with an Excimer Laser", Appl. Phys. Lett. vol. 52, pp.1271-3, 1988.

[6] A. Inam et al., "Pulsed Laser Etching of High T_c Superconducting Films", Appl. Phys. Lett., vol. 51, pp. 1112-4, October 1987.

[7] G. Fisanick et al., "CW Laser Etching of $Ba_2YCu_3O_7$ Films", in Thin Film Processing and Characterization of High-Temperature Superconductors, AIP Conf. Proc. No. 165, ed. by J.M.E. Harper et al., pp. 189-196. New York: American Institute of Physics, 1988.

[8] M. Rothschild, et al., "Laser Patterning of Metal Oxide Superconductor Films by Reactive Solid-State Transformation", IEEE Electron Device Lett., vol. 9, pp. 68-70, Feb. 1988.

[9] H. Koinuma et al., "Reversible Resistitivy Control of $Ba_2YCu_3O_{7-\delta}$ Thin Films by Laser Annealing", Japan. J. Appl. Phys., vol. 27, pp. L652-4, April 1988.

[10] A.M. Kadin, P.H. Ballentine, J. Argana, and R.C. Rath, "High Temperature Superconducting Films by RF Magnetron Sputtering", this Conference Proceedings.

Appendix E.   EDXA Compositional Analysis

A good introductory treatment of EDXA is given by Goldstein *et al.*[1].

What follows is a brief description. Figure E.1 shows a schematic diagram of the EDXA process. High energy electrons from the SEM column (in our case the energy is kept at 25 keV) strike the sample and cause tightly bound inner shell electrons to be ejected. As outer shell electrons drop in energy, x-rays are emitted which are characteristic of the atomic species. These x-rays are collected by a detector, in this case a Li-drifted Si detector cooled by liquid nitrogen. The output from the detector is sent to a multi-channel analyzer and is recorded as number of counts versus x-ray energy. The output spectrum for a YBCO thin film with a composition close to 1-2-3 is shown in Fig. E.2. The principle x-ray lines used for YBCO in this study are given in Table E.1
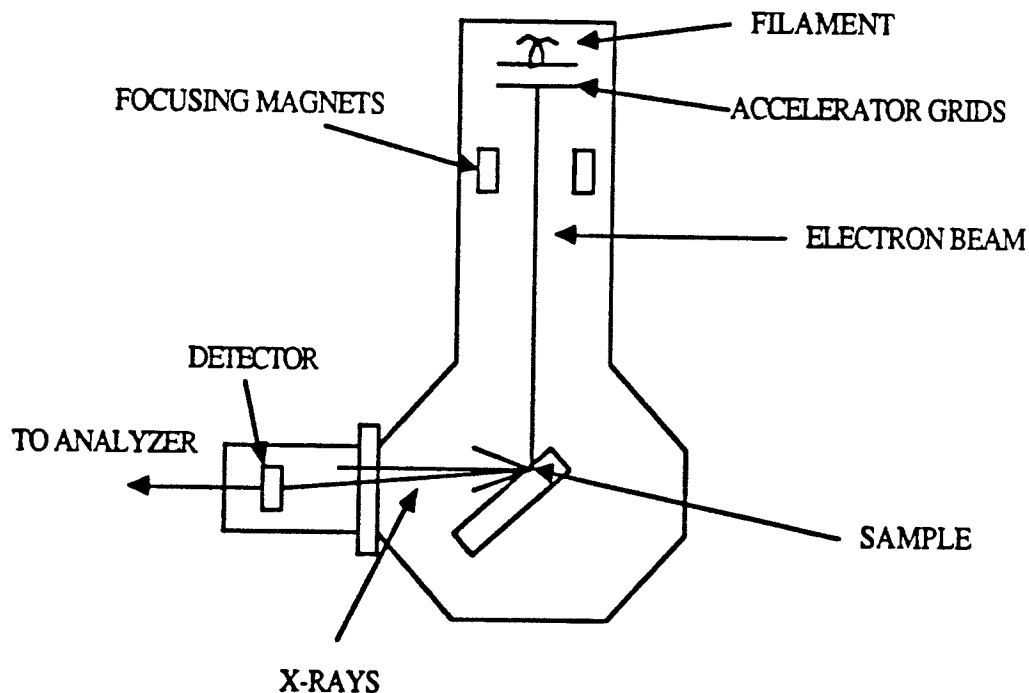
Fig. E.1 Schematic of SEM with Energy Dispersive X-ray Analysis

[1] J.I. Goldstein, et al., "Scanning Electron Microscopy and X-ray Microanalysis: A Textbook for Biologists, Materials Scientists, and Geologists (Plenum Press, New York, 1981)
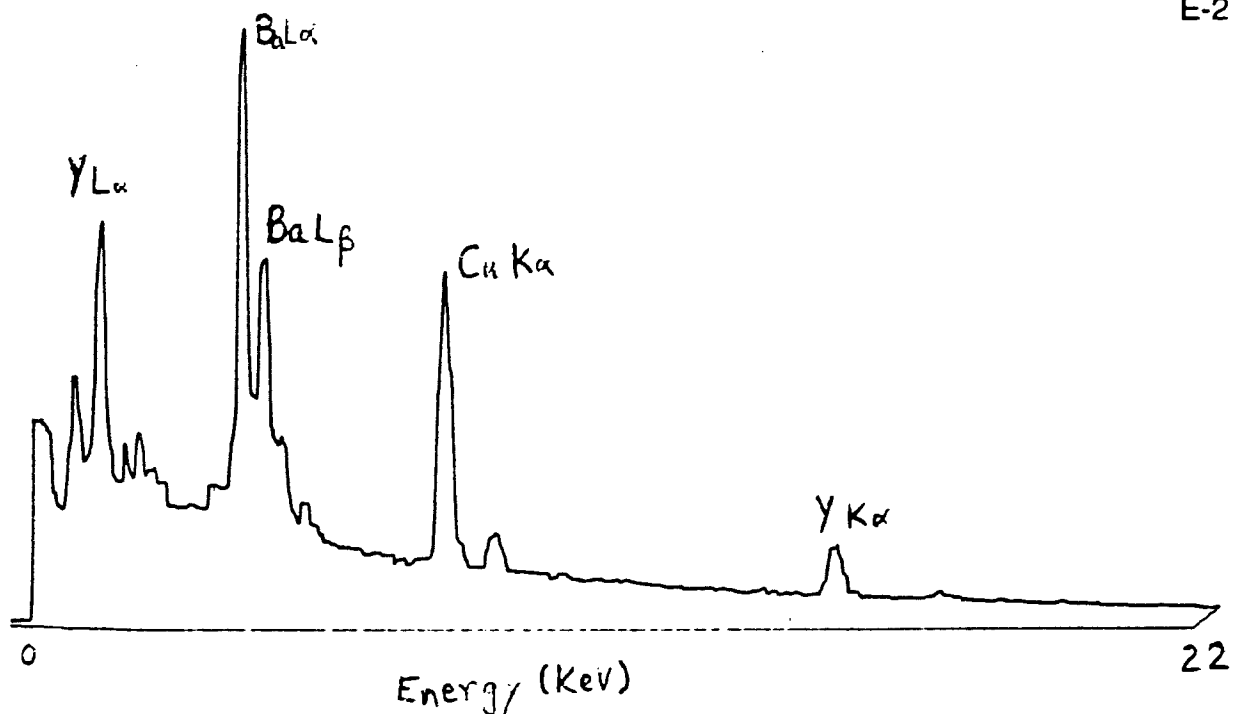
Fig. E.2. Sample X-ray spectrum output from $YBa_2Cu_3O_7$.

Table E.1 Characteristic x-ray lines for EDXA of YBCO

Element	Line	Energy (keV)
Y	$L\alpha_I$	1.922
Ba	$L\alpha_I$	4.467
Ba	$L\beta_I$	4.828
Cu	$K\alpha_I$	8.047
Y	$K\alpha_I$	14.957

The intensity of a given x-ray line is, in general, proportional to the concentration of the element and the cross section for electron stimulated x-ray emission. There are a number of other factors that affect the x-ray spectrum as well such as surface roughness and the sample-to-detector geometry. For thin film analysis, film thickness and substrate type also play an important role. The composition can be calculated from the measured x-ray intensities either by using a

standard of known composition or by using a computer program (such as ZAF) which is a standardless method. In our case we use thin film standars for which we collect sufficient EDXA data and then have analyzed by an outside lab using the method of iductively coupled plasma atomic emission spectroscopy (ICP). The concentration of an element in the sample can be expressed as

$$C_i = x_i\frac{C_{si}}{x_{si}}/\Sigma\left(x_j\frac{C_{sj}}{x_{sj}}\right)_j \qquad \text{E.1}$$

where

C_i = concentration of element i in the sample

x_i = intensity of the x-ray line from element i in the sample

C_{si} = concentration of element i in the standard

x_{si} = intensity of the x-ray line from element i in the standard

Originally we used a bulk pellet with the 1-2-3 composition as a standard but quickly realized the significant error (>10%) introduced by this practice. We also ran into trouble when measuring the composition of films on yttria-stabilized zirconia (YSZ) substrates because Y x-rays from the substrate were adding to the signal and the x-rays from the Zr were fluorescing more x-rays from the Y in the film, resulting in measurements that were too high in Y concentration. By keeping the film thickness constant and by always using smooth (i.e. un-annealed) films on Al_2O_3 substrates we have found EDXA can be accurate to within 2 atomic %. Later on we obtained callibration of the EDXA by having our "standard" films measured by Inductively Coupled Plasma Atomic Emmision Spectroscopy (ICP) at Xerox Corp. in Webster NY. It should be pointed out that EDXA can only provide information on elements with atomic number greater than 11 (Na), so we could not say anything about the oxygen concentration using this technique.

Appendix F. X-Ray Diffraction Lines for YBa$_2$Cu$_3$O$_7$

Barium Copper Yttrium Oxide, Ba$_2$Cu$_3$YO$_7$

Sample
The sample was obtained from F. Beech of the Reactor Radiation Division, NBS. A stoichiometric mixture of CuO, Y$_2$O$_3$ and BaCO$_3$ was intimately mixed and fired at 500°C overnight. Reaction with container was avoided by placing the pellet on a support of the same material. The resulting powder was ground and pressed into pellets and re-fired at 900°C overnight. The pellets were reground, repressed, and fired at 950°C overnight. Final annealing took place at 750°C for 27 hours under oxygen.

Color
Black

Symmetry classifications
Crystal system   Orthorhombic
Space group   Pmmm (47)
Pearson symbol   oP13
Structure type   Distorted perovskite

Data collection and analysis parameters
Radiation   CuKα_1
Scanned to   5° 2θ
Wavelength   1.5405981 Å
Mean temperature   25.5°C
2θ standards   Silicon, FP

Crystallographic constants
a = 3.8856 (3) Å
b = 11.6804 (7)
c = 3.8185 (4)

a/b = 0.3327
c/b = 0.3269

V = 173.30 Å^3
Z = 1
Density (calc.) = 6.383 g/cm^3

Figures of merit
F$_{30}$ = 66 (0.0091, 50)
M$_{20}$ = 71

Comments
The structure was determined by T. Siegrist and S. Sunshine *et al.*[1]. The sample was characterized by neutron Rietveld refinement technique by A. Santoro at NBS. Superconductor with Tc of 92K. The compound was first reported by Cava and Batlogy[2].

References
1. Siegrist, T. *et al.* (1987). Phys. Rev. Lett., to be published.
2. Cava, R. *et al.* (1987). Phys. Rev. Lett., to be published.

d(Å)	I^{rel}	h	k	l	2θ (°)
11.69	11.	0	1	0	7.557
5.890	4	0	2	0	15.119
3.891	10	0	3	0	22.835
3.819	4	0	0	1	23.274
3.235	3	1	1	2	0	27.554

(continued)

Barium Copper Yttrium Oxide, Ba$_2$Cu$_3$YO$_7$ *(continued)*

d(Å)	I^{rel}	h	k	l	2θ (°)
3.196	5	0	2	1	27.893
2.918	11.	0	4	0	30.618
2.750	55	1	3	0	32.558
2.725	100	1	0	1	32.842
2.653	2	1	1	1	33.757
2.441	3	1	2	1	36.770
2.336	13	0	5	0	38.512
2.319	5	0	4	1	38.799
2.2317	14	1	3	1	40.384
1.9909	2	1	4	1	45.524
1.9461	22	0	6	0	46.633
1.9425	21	2	0	0	46.725
1.8295	12	0	0	2	47.500
1.7732	4	1	5	1	51.495
1.7408	3	1	6	0	52.526
1.7345	4	0	6	1	52.733
1.7144	2	0	3	2	53.400
1.6683	2	0	7	0	54.979
1.6595	1	2	2	1	55.313
1.5817	20	1	6	1	58.207

d(Å)	I^{rel}	h	k	l	2θ (°)
1.5695	13	1	1	2	58.826
1.5534	11.	1	7	0	60.307
1.5272	1	0	7	1	60.494
1.4939	2	2	5	0	62.000
1.4880	2	2	4	1	62.262
1.4783	3	0	5	2	62.659
1.4225	2	1	7	1	65.571
1.3751	5	2	6	0	68.134
1.3666	5	1	8	0	68.618
1.3635	13	0	8	1	68.797
1.3619	12	2	0	2	68.908
1.2978	1	0	9	0	72.820
1.2951	11.	3	0	0	72.995
1.2865	2	1	6	2	73.561
1.2657	1L	2	7	0	74.977
1.2566	1	0	7	2	75.615
1.2141	11.	2	4	2	77.247
1.2187	4	1	9	0	77.480
1.2286	6	0	9	1	77.654
1.2263	5	3	0	1	77.827

d(Å)	I^{rel}	h	k	l	2θ (°)
1.2099	5	0	3	3	79.068
1.2015	3	2	7	1	79.749
1.1164	1	1	2	3	81.141
1.1763	2	2	5	2	81.812
1.1702	1L	3	3	1	82.335
1.1683	1	0	10	0	82.498
1.1551	1	1	3	3	83.650
1.1188	3	1	10	0	87.028
1.1161	6	2	8	1	87.287
1.1114	4	1	8	2	87.748
1.0861	1	3	5	1	90.751
1.0792	1	2	9	0	91.089
1.0734	1	0	9	2	91.722
1.0617	1	0	11	0	93.027
1.0551	1	2	7	2	93.786
1.0377	4	3	6	1	95.853
1.0333	4	3	5	2	96.394
1.0273	4	1	6	3	97.145